A comprehensive review on the output voltage/power of wearable thermoelectric generators concerning their geometry and thermoelectric materials

Zohreh Soleimani[a,*], Stamatis Zoras[a], Boris Ceranic[a], Yuanlong Cui[a], Sally Shahzad[b]

[a] Department of Built Environment, College of Engineering and Technology, University of Derby, DE22 3AW, Derby, UK
[b] Sheffield School of Architecture, University of Sheffield, S10 2TN, Sheffield, UK

Abstract: Wearable thermoelectric generators (TEGs) are considered as a promising power supply for low power wearable electronics. To obtain high thermoelectric (TE) generation, the focus should be on two main factors, including TE materials and the configurations of TE legs. Concerning these two factors, this paper provides a comprehensive review of recent studies on wearable TEGs. In general, TE materials can be classified into three categories, including inorganic, organic, and hybrid (inorganic-organic). In addition, the TE legs can be prepared in three different configurations, including ingot-shaped, film-shaped, and yarn-shaped. Based on the reviewed literatures, the superior output powers of all the three configurations were achieved by the inorganic, hybrid, and organic TE materials, respectively. It should be noted that the ingot- and the yarn- shaped legs were mostly composed of the inorganic and the organic TE materials, respectively. Whereas, all the three types of TE materials were almost equally used to prepare the film-shaped legs. Regarding power density, the ingot-shaped legs stood first followed by the film- and the yarn- shaped legs, respectively. Precisely, the output powers of the ingot- and the film- shaped legs were at μW/cm^2 level, dropping to nW/cm^2 for the yarn-shaped legs.

Keywords: Energy harvesting, wearable thermoelectric generators, power density, configuration of thermoelectric legs, thermoelectric materials.

Contents

1. Introduction 3
2. Theoretical principle of TEGs 5
3. Ingot-shaped thermocouples...10
   - 3.1. Inorganic TE materials...10
   - 3.2. Organic TE materials 27
   - 3.3. Hybrid TE materials...27
4. Film-shaped thermocouples..31
   - 4.1. Inorganic TE materials...31
   - 4.2. Organic TE materials 35
   - 4.3. Hybrid TE materials...41
5. Yarn-shaped thermocouples 50
   - 5.1. Inorganic TE materials...50
   - 5.2. Organic TE materials 51
   - 5.3. Hybrid TE materials...61
6. Challenges and future trends 65
7. Conclusions 66

Nomenclature

Symbols

α	Seebeck coefficient (μV/K)
σ	electrical conductivity (S/cm)
λ	thermal conductivity (W/mK)
$Z\overline{T}$	figure of merit
T_H	temperature of hot reservoirs
T_C	temperature of cold reservoirs
A	cross-sectional area (cm^2)

Acronyms

CNTs	carbon nanotubes
CNF	Cellulose nanofiber
CNTFs	carbon nanotube fibres
FPCB	flexible printed circuit board
MWCNT	multi-walled carbon nanotubes
PET	polyethylene terephthalate
PEI	polyethylenemine
PEDOT: PSS	poly(3,4-ethylenedioxythiophene) polystyrene sulfonate
PDMS	polydimethylsiloxane
PCM	phase change material
SWCNT	single-walled carbon nanotubes
TEG	thermoelectric generator
TE	thermoelectric module

1. Introduction

Progress in wearable technologies such as activity trackers and portable health monitors has emerged considerable interests in lightweight, endurable, and on-board power supplies [1]. Thus, harvesting the available energies in the daily environments has become a promising candidate. In general, there are two approaches to scavenging energies for wearable electronics, including active and passive [2]. The active approach is based on wireless power transmittance, sending a wireless power from one or more external power sources to wearable devices [3]. Thus, this approach can maintain normal device operation in long-term experiments [4]. However, its main drawback is limiting the wearers' movement to a specific distance from the external power source [5]. Regarding the passive approach, human body is used as the energy supplier. In general, the energy sources of human body include kinetic energy [6-8], thermal energy [9-10], chemical energy [6] [11], and respiration [12-13]. As Table 1 shows, there are specific energy harvesters to convert these energies into electrical energy.

Table 1. An overview of potential energy sources of the human body and their associated energy harvesters.

Energy Type	Energy Harvester Subcategories		Ref
Biochemical Energy	Biofuel cells	Microbial Fuel Cells	[14], [15], [16]
		Enzymatic Fuel Cells	[17], [18], [19]
Thermal Energy	Thermoelectric		[20], [21]
	Pyroelectric		[22], [23]
Kinetic Energy	Piezoelectric		[24], [25], [26], [27]
	Triboelectric		[24], [25], [28], [29]
	Electromagnetic	Inertial induction	[25], [30]
		Gear-and-generator	[31] , [32]
Exhaled Air Energy	Triboelectric		[33], [34]
	Piezoelectric		[35]
	Pyroelectric		[36]
	Thermoelectric		[37]

As a warm blooded species, human body continuously generates thermal energy in a range between 100W and 525W [38]. For example, as Fig. 1 shows, body temperature varies in a range of between 23°C and 37°C when room temperature fluctuates between 15°C and 47°C [39]. Capturing the dissipated heat from human body with TEGs (with ~1% conversion efficiency) generates ~1W to 5.25W electrical power. Although this amount of energy is sufficient to power a vast range of wearable sensors, it requires covering the whole body with TEGs, which is impractical [7]. In addition, achieving a wearable TEG with high conversion efficiency (~1%) depends on several critical factors, including the thermoelectric (TE) materials [40], the geometry of the TE legs [39, 41-42], the structure of heatsinks [43-45], the metabolic rate of wearers (e.g. resting, walking or running state) [46], the mounting position of the TEGs (e.g. wrist, chest, arm) [46-47], and ambient thermal conditions (e.g. dry bulb temperature, relative humidity, and air velocity) [48]. Therefore, precise considerations are required at the design stage of wearable TEGs, because any deficiency at this stage impacts the output power of the TEGs.

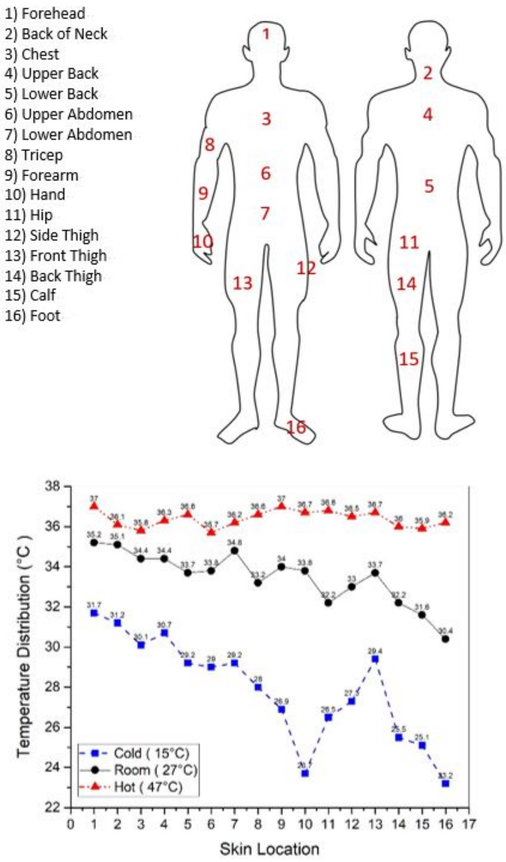

Color in online

Fig. 1. Variations in the temperature of body parts at different ambient temperatures, adapted from [39].

Hence, this study aims to thoroughly review the recent studies on wearable TEGs concerning the configuration and materials of their TE legs. Precisely, herein, wearable TEGs are categorized based on the configuration and materials of their TE legs to provide a reliable comparison between their output voltages/powers. This is significantly important because, several excellent reviews have been conducted recently on wearable TEGs with a specific focus on either the TE materials [49-54] or a specific configuration of TE legs [9, 38, 55-57]. Nevertheless, to the best of our knowledge, so far no study has considered the impacts of both factors (i.e. the configurations and materials of the TE legs) on the output voltage/power of wearable TEGs at the same time. However, since both factors have direct impacts on the output voltage/ power of wearable TEGs, it is not reliable to compare the performances of the TEGs with each other concerning only one factor.

Accordingly, the paper is organized as follows. First, the theoretical basis of TEGs is summarized in Section 2, including different configurations and materials of wearable TEGs. Section 3 reviews wearable TEGs comprising of ingot-shaped legs with regard to their TE materials. Likewise, Sections 4 and 5 respectively review the recent researches on film-shaped and yarn-shaped legs regarding their TE materials. Section 6 explains some challenges and future trends. Section 7 summarises the main outcomes of this review.

2. Theoretical principle of TEGs

Thermoelectric generators (TEGs) are solid-state semiconductor devices that convert waste heat directly into electrical energy. The TE theories are based on the Seebeck effect, which was discovered in 1821 by a German physicist called Thomas Johann Seebeck. Based on the Seebeck effect, an electrical power is generated when a temperature gradient exists between the two ends of a thermocouple. To illustrate, a thermocouple consists of two electrically different conductors or semiconductors that are directly in contact or electrically connected together, allowing the charge carriers flow between the materials. Thus, when a temperature difference occurs between the two ends of a thermocouple, the charge carriers diffuse away from the warmer side of the thermocouple and build up at the cooler end. This movement results in more charge carriers at the colder part than the warmer part, leading to the generation of an open circuit voltage called the Seebeck voltage (V). Following Equation 1, the Seebeck voltage is directly related to the temperature difference (ΔT) along the thermocouple by a proportional factor called the Seebeck coefficient (α).

$$\mathrm{V} = \alpha\Delta\mathrm{T} \qquad (1)$$

Accordingly, a wearable TEG consists of an array of *p*- and *n*-type semiconducting legs comprising surplus holes and electrons, respectively. Using metal electrodes/interconnects, the TE legs (i.e. the semiconductors) are connected electrically in series and thermally in parallel to form thermocouples. A conventional TEG is composed of a large number of thermocouples sandwiched between two electrically insulating and thermally conductive substrates. A temperature difference between the substrates leads to a temperature gradient along the legs. Thus, the free charges (i.e. electrons and holes) in the legs start moving from the hot side to the cold side, converting the thermal energy into the electrical energy. In general, higher output voltage/power can be achieved by increasing the temperature gradient in the thickness direction of the legs. Maintaining an adequate temperature difference along the legs, a heatsink is usually attached to the cold side of the TEGs to accelerate the heat dissipation [58]. Fig. 2 depicts the standard configuration of a conventional TEG.

Color in online

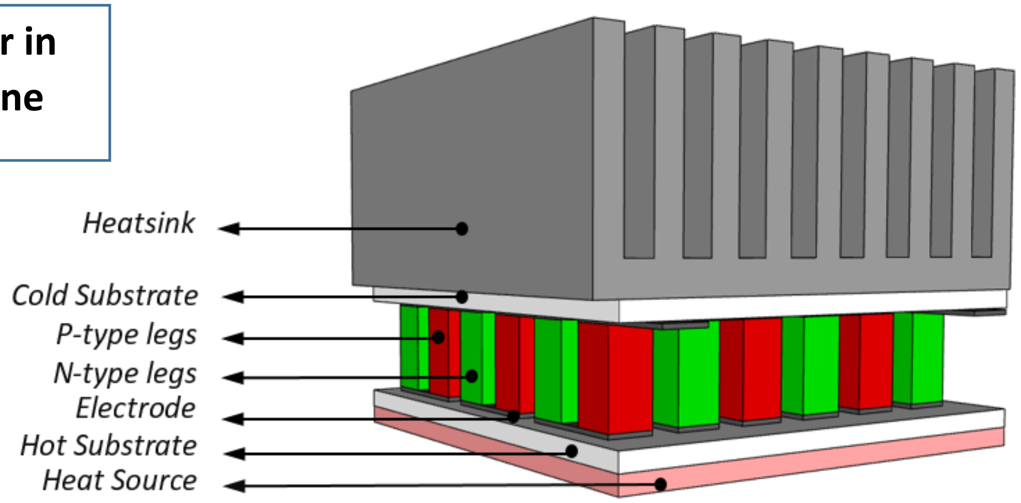

Fig. 2. A schematic diagram of a typical wearable TEG and its components.

In general, the energy conversion efficiency of a TEG depends on the TE properties of its constituent legs' materials and the temperature difference along the legs [51]. Accordingly, the maximum theoretical conversion efficiency (η_{max}) of a TEG can be expressed by [57]:

$$\eta_{max} = \left(\frac{T_H - T_C}{T_H}\right) \cdot \left(\frac{\sqrt{1+Z\overline{T}}-1}{\sqrt{1+Z\overline{T}}+\frac{T_C}{T_H}}\right) \tag{2}$$

where T_C and T_H are the cold- and hot-side temperatures, respectively, and $Z\overline{T}$ is the figure of merit of the TE materials. The term in the left parenthesis is called Carnot efficiency (η_C), which is an upper limit on using the waste heat for TE power generation [51]. According to Carnot efficiency (η_C), the conversion efficiecy (η_{max}) of TEGs is directly related to the temperature difference between the hot and cold junctions of the TE legs. To specify, increasing the temperature difference along the legs rises the conversion efficiency of the TEGs. To tune the Carnot efficiency (η_C), one of the most promising approach is manipulating the structural design of the TE legs respective to the optimal ratio of the cross-sectional area of the *p*-type (A_p) and *n*-type (A_n) legs. The optimal ratio could be measured by:

$$\left[\frac{A_n}{A_P}\right] = \sqrt{\frac{\sigma_P \lambda_P}{\sigma_n \lambda_n}} \tag{3}$$

where σ_P and σ_n are the electrical conductivity (S/cm) and λ_P and λ_n are the thermal conductivity (W/m K) of the *p*- and *n*-type materials, respectively. Regarding the cross-sectional area of the legs, their configurations can be classified into two main categories: transversal (cross-plane) and lateral (in-plane). This classification is related to the manner of arranging the legs on the substrates and subsequently to the direction of the temperature gradient within them [59]. Regarding the cross-plane design, the TE legs are perpendicular to the hot (i.e. the skin) and cold (i.e. the environment) sources, as Fig. 3a shows. Notably, the temperature difference between the human body and the environment results in a perpendicular heat flux direction to the skin. Therefore, the temperature difference in the direction of the legs' thickness encourages the free holes and electrons in the legs to move vertically and generate electricity. However, it is desirable for a wearable TEG to be lightweight and flexible to take on the arbitrary shape of the body's surfaces (e.g. wrist) [60]. Conversely, the cross-plane design suffers from rigidity and bulkiness due to the high thickness of the legs, causing cumbersome for the wearers. Thus, the most promising alternative to solve this issue is the in-plane design, consisting of two dimensional (2D) film-shaped thermocouples fabricated onto a supporting substrate and in parallel with the skin, see Fig. 3b [61]. Thus, splitting the substrate in half either from the length or width, the opposite halves serve as the hot and cold substrates. As a result, the film-shaped legs merely harvest the temperature gradient in the length/width direction and rarely capture the desirable temperature difference in the thickness direction. Accordingly, the in-plane design usually suffers from lower conversion efficiency than the cross-plane one [62-63]. To solve the rigidity and efficiency issues at the same time, researchers have proposed to combine these two designs together, resulting in the yarn-shaped thermocouples. As Fig. 3c depicts, 2D TE yarns are knitted together or sewn onto a three dimensional (3D) or 2D flexible substrate, allowing the flexible yarns to utilize the temperature difference in the thickness direction [64].

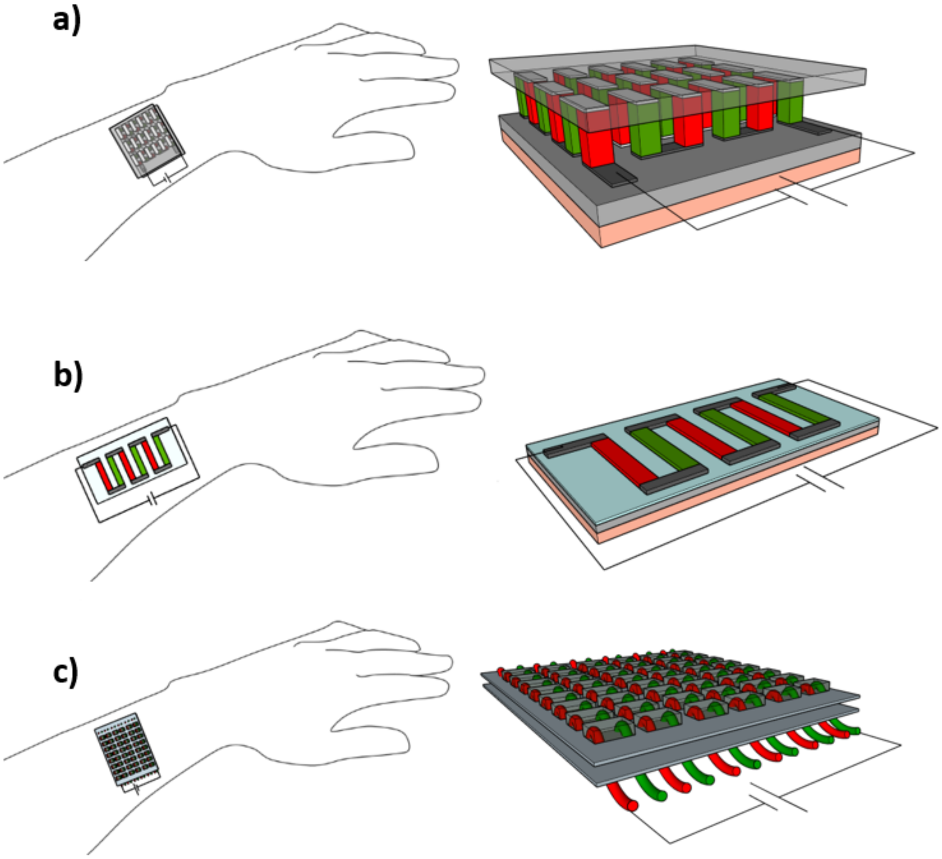

Color in online

Fig. 3. Schematics of different configurations of thermocouples in wearable TEGs: a) ingot-shaped; b) film-shaped; and c) yarn-shaped.

Apart from the configuration of the TE legs, it is also of critical importance to generate them with high $Z\overline{T}$ value materials. To specify, $Z\overline{T}$ value expresses the heat-to-power conversion efficiecy of materials and is measured by:

$$Z\overline{T} = \frac{(\alpha^2 \sigma \mathrm{T})}{\lambda} \tag{4}$$

where α is the Seebeck coefficient (μV/K), σ is the electrical conductivity (S/cm), T is the absolute temperature (K), and λ is the thermal conductivity (W/m K) of the materials. Notably, the numerator, $\alpha^2\sigma$, is called the power factor (PF). To obtain a high $Z\overline{T}$ value material, it is required to increase the Seebeck coefficient and the electrical conductivity but reduce the thermal conductivity. Designing such a material is challenging because these three TE properties are interdependent, thus it is impractical to individually tune one property without affecting the others [51]. To clarify, although increasing the carrier concentration improves the electrical conductivity of TE materials, it also undesirably decreases and increases their Seebeck coefficient and thermal conductivity, respectively [52]. In fact, the constituent raw materials of the TE materials have direct impact on their TE properties (i.e. Seebeck coefficient, electrical conductivity, and thermal conductivity). To illustrate, TE materials can be classified into three categories, including inorganic, organic, and hybrid (inorganic-organic). The inorganic type consists inorganic elements, such as bismuth telluride (Bi_2Te_3) and its alloys, Lead telluride (PbTe) and its alloys, silicon-germanium (SiGe) alloys, antimony telluride (Sb_2Te_3), and tin selenide (SnSe). This type benefits from high electrical conductivity but suffers from rigidity, scarcity, and toxicity [65]. In addition, based on the life cycle impact assessment of Soleimani et al. [66], it is proved that the inorganic type causes significantly greater environmental impacts than the other two types due to its extremely energy-intensive manufacturing processes. Accordingly, there is a growing interest to switch from the inorganic TE materials to the organic ones, such as carbon nanotubes, graphene, and conductive/non-conductive polymers. Although the organic type privileges low thermal conductivity, its electrical conductivity and Seebeck coefficient are by far lower than those of the inorganic one [52]. Accordingly, the inorganic and organic types are combined together to benefit from the high power factor of the former and the low thermal conductivity of the latter at the same time. The result is called the hybrid type, and it mostly consists of an inorganic material (e.g. metal-based chemicals) as an additive doped into an organic material as the matrix. For example, Lei et al. [67] developed a hybrid TE material by coating $MgAg_{0.97}Sb_{0.99}$ composites with multi-walled carbon nanotubes (CNTs) as the inorganic and organic parts, respectively. However, still the hybrid type suffers from two deficiencies, such as consisting toxic and rare inorganic elements in addition to lower conversion efficiency than the inorganic type [52].

Therefore, in accordance with Equation 2, the configuration of the TE legs and the $Z\overline{T}$ value of their constituent material directly impact on the conversion efficiency of the TEGs [68]**.** Accordingly, this study aims to comprehensively review the recent studies on wearable TEGs concerning the configuration and materials of their thermocouples. Ultimately, the output powers/voltages of the reviewed studies were compared with each other to find out the contribution of these two factors to the TE performance of the TEGs.

3. Ingot-shaped thermocouples

3.1. Inorganic TE materials

Using ingot-shaped thermocouples can be traced back to the generation of very conventional TEGs, when TE mixtures were synthesised via ball milling or melting/heating the TE powders [69]. To obtain the ingot-shaped legs, the as-prepared TE mixtures were consolidated into ingots via cold or hot pressing [70]. Next, the generated TE ingots were bonded together with electrical shunts, resulting in the ingot-shaped thermocouples. Regarding wearable TEGs, their ingot-shaped legs are mostly consisting of Bi_2Te_3-based alloys. In particular, their *p*-type legs mostly comprised of either Bi_2Te_3 or $Bi_{0.3}Sb_{1.7}Te_3$ composites, while either Bi_2Te_3 or $Bi_2Te_{2.7}Se_{0.3}$ composites are used in the generation of the *n*-type legs. The superiority of these inorganic TE materials is attributed to their dominant energy conversion efficiencies [52]. It should be noted that the ingot-shaped thermocouples could be integrated together using either a flexible or a rigid substrate. However, following recent progresses in wearable TEGs, using flexible substrates such as polymers, printed circuit board (FPCB), holders, and fabrics have drawn growing attentions compared with the conventional rigid (Aluminum Oxide-based) ones. For example, Kim et al. [71] generated a flexible wearable TEG via encapsulating 72 couples of TE legs in a flexible polymer, as Fig. 4 shows. To specify, the *p*-type ($Bi_{0.3}Sb_{1.7}Te_3$) and *n*-type ($Bi_2Sb_{0.3}Te_{2.7}$) ingot-shaped legs were connected together with copper strips as electrodes. To hold the legs in place, the gaps between them were filled with a very low thermal conductivity ($0.03\ W\ m^{-1}K^{-2}$) polymer. The authors specified different variables for tuning the output power of the fabricated TEG, such as varying the legs' height (i.e. 0.8 mm and 2.5 mm), the fill factor (i.e. 15.1%, 19.8%, and 27.2%), and the air velocity (i.e. 0 to 3m/s with 1m/s interval). The results showed that increasing the legs' height from 0.8 mm to 2.5 mm raised the power density by four times. Furthermore, the authors demonstrated that a higher fill factor (the ratio of the area covered by the TE legs to the surface area of the TE module) is more efficient at higher air velocities. The authors demonstrated that at 8.9°C temperature difference and zero air velocity, the maximum obtained output power was 2.5 $\mu W/cm^2$ that was achieved by 15.1% fill factor.

Color in online

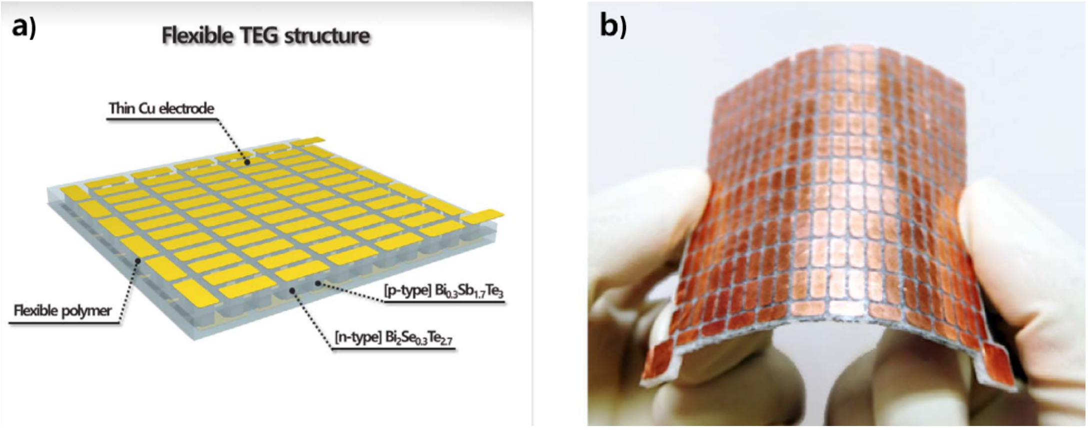

Fig. 4. a) Schematic of the flexible TEG; b) Photo of the actual fabricated TEG [71].

Likewise, Suarez et al. [72] used one of the most common flexible polymer called polydimethylsiloxane (PDMS) to serve as the flexible substrate, see Fig. 5. In particular, the thermocouples consisted of *p*-type ($Bi_{0.5}Sb_{1.5}Te_3$) and *n*-type ($Bi_2Se_{0.3}Te_{2.7}$) ingot-shaped legs were electrically connected together using EGaIn. When the TEG comprised of 32 pairs of legs was worn on the wrist (~37°C) at 24°C ambient temperature, the results showed that the maximum recorded output power was 1 $\mu W/cm^2$. However, the authors demonstrated that using a porous polymer-based substrate was superior to the solid one. To illustrate, the performance of the developed TEG was compared with that of a conventional rigid TEG surrounded with air. The results proved that fully coating the legs with the PDMS layer led to a lower output voltage and power than a conventional rigid TEG. This was mainly because the PDMS layer with 0.15W/mK thermal conductivity served as a thermal pass compared with the surrounding air layer (0.025 W/m.K) in the rigid TEGs. Therefore, the authors proposed using a porous PDMS substrate to decrease its thermal conductivity down to 0.08 W/mK, which resulted in 86% greater output voltage.

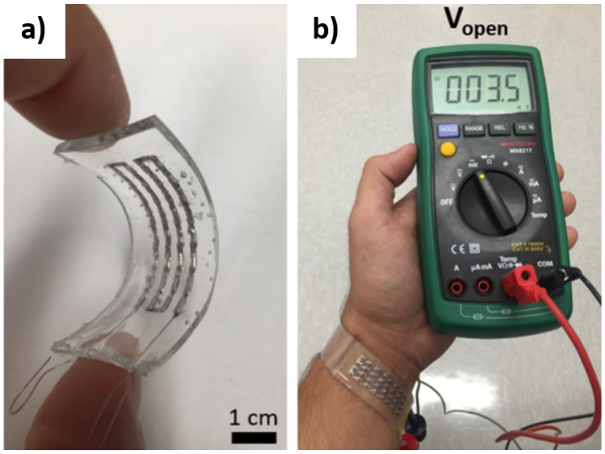

Color in online

Fig. 5. a) Photo of the fabricated TEG; b) The open circuit voltage of the fabricated TEG at room temperature [72].

Regarding the negative effect of the polymer substrate on the output power of the TEGs, Jung et al. [73] attempted to reduce the thermal conductivity of the PDMS substrate by producing it spongy. To clarify, the authors encapsulated the legs in a PDMS sponge (0.08 W/mK) possessing a lower thermal conductivity than a plain PDMS substrate. To prepare the sponge, the authors developed sugar template by pressing granule-sized sugar (~300 μm) in a stainless-steel mold for 60 seconds. Then the prepared sugar template was dipped into the plain PDMS mixture. After degassing the mixture, the PDMS-coated template was put in deionized water and stirred thoroughly at 100°C for 5hrs, leading to the generation of the PDMS sponge. Next, the as-prepared PDMS sponge was inserted into 47 Bi_2Te_3 – based thermocouples each with the dimensions of 1.2mm × 1.2mm × 2.6mm, as Fig. 6 illustrates. Finally, the thermocouples were connected together using copper-foils as electrodes. The results demonstrated that the fabricated TEG generated nearly 130 $\mu W/cm^2$ at 8°C temperature difference.

Color in online

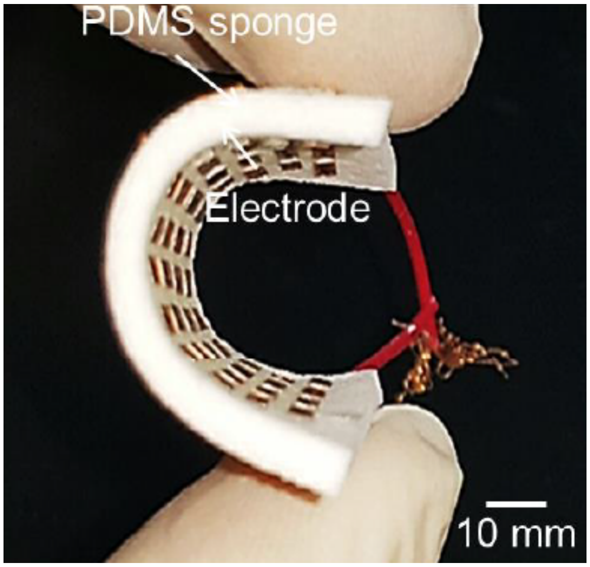

Fig. 6. Photo of the actual fabricated TEG [73].

To further diminish the negative effect of coating the legs with a polymer-based substrate, Hong et al. [74] coated only a small part of the legs with a commercial flexible polymer called Ecoflex. To specify, 24 thermocouples were prepared using $Bi_{0.5}Sb_{1.5}Te_3$ (*p*-type) and $Bi_2Te_{2.7}Se_{0.3}$ (*n*-type) composites, while they were electrically connected together by copper strips as electrodes. Then, Ecoflex was poured at the two ends of the thermocouples to form two separate 1mm thick substrates. It should be noted that only 0.5mm of each end was coated with the flexible substrate, leaving the rest height (i.e. 4mm) of the legs exposed to the ambient air, see Fig. 7. In addition, the authors attempted to improve the lateral thermal conductivity of the Ecoflex layer by adding aluminium nitride micro particles to it. The results revealed that at ΔT of 10°C, the fabricated TEG achieved the highest output powers of 4.5 $\mu W/cm^2$ and 10.7 $\mu W/cm^2$ under the sitting and walking conditions, respectively.

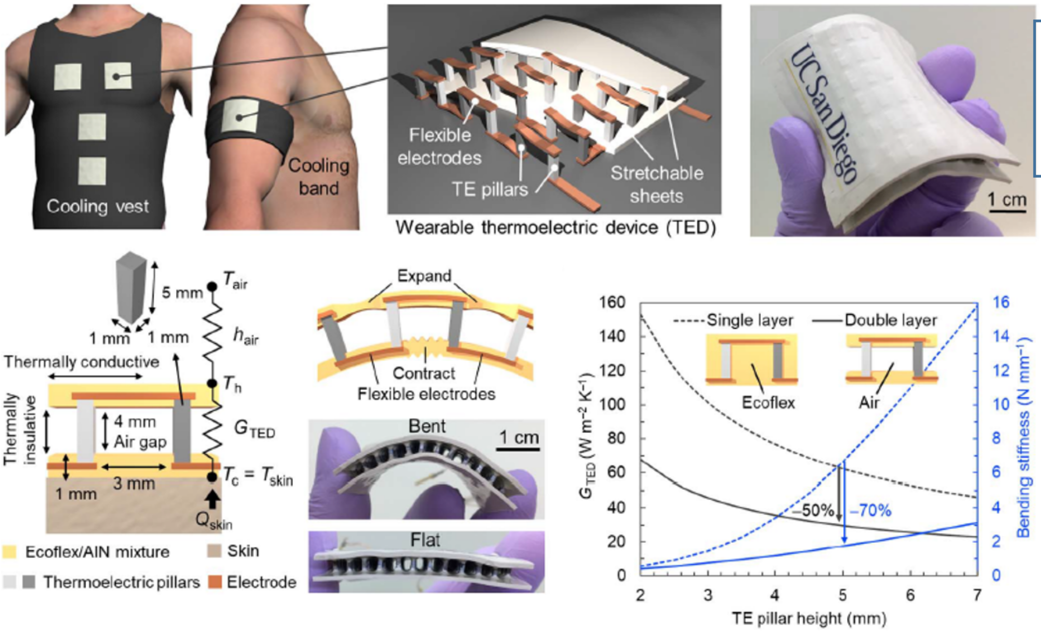

Color in online

Fig. 7. Internal and external configurations of the developed TEG [74].

Apart from applying a flexible substrate, Wang et al. [75] focused on improving the flexibility of the TEG via replacing the rigid electrodes with the flexible ones. Accordingly, the authors replaced the bottom copper strips with a flexible printed circuit board (FPCB). To specify, 52 pairs of *p*- ($Bi_{0.5}Sb_{1.5}Te_3$) and *n*- ($Bi_2Se_{0.5}Te_{2.5}$) type legs were soldered onto a FPCB from the bottom, as Fig. 8 shows. Notably, several holes were cut in the FPCB to further increase its bendability. Then, the legs were soldered from the top (i.e. the cold junctions) onto copper strips as the top electrodes. Holding the legs in place, the fabricated TEG was immersed in a PDMS mixture to fill the gaps between the legs. The results revealed that at 18°C temperature difference, the generated output power of the developed TEG was 3.9 µW/cm^2.

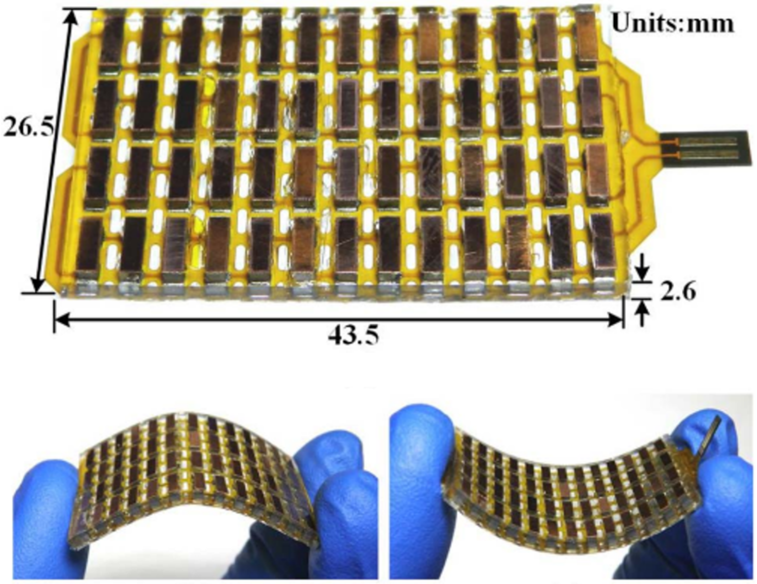

Color in online

Fig. 8. Combination of the PCB and the thermocouples [75].

Instead of encapsulating the thermocouples in a single PDMS block, Liu et al. [76] encapsulated each of them in an individual PDMS block to address the flexibility of the TEG. Accordingly, the authors soldered 18 pairs of ingot-shaped and Bi_2Te_3-based legs each with the dimensions of 2 mm × 2mm × 1.5mm onto a FPCB. Then, the legs were connected together from their cold junctions with silver pastes as electrodes. To prevent electric shock, a polyimide film possessing super thermal and electrical resistivity was placed on the silver pastes. Finally, a thin (i.e. 1mm) layer of PDMS was poured around each thermocouple to encapsulate them in separate PDMS blocks. The results demonstrated that the as-prepared TEG generated the maximum power density of 3 $\mu W/cm^2$ at ΔT of 12°C.

To eliminate the negative impact of coating the legs with a polymer substrate, Yuan and Zhu [77] omitted the PDMS encapsulation and left the legs exposed to the ambient air, see Fig. 9. To illustrate, 47 pairs of *p*-type ($Bi_{0.5}Sb_{1.5}Te_3$) and *n*-type ($Bi_2Te_{2.8}Se_{0.2}$) legs were soldered onto a FPCB from the bottom. Next, the legs were electrically connected together from the top by being soldered onto copper strips. Leaving the legs exposed to the ambient air, the results showed that the power density of the TEG at 14°C temperature gradient was 3.5 $\mu W/cm^2$. In addition, it was demonstrated that there was a direct relationship between the output voltage of the TEG and the legs' height. However, there was a converse relationship between its output voltage and fill factor. Precisely, when the fill factor was 4%, increasing the legs' height from 1 mm to 3mm raised the voltage by five times. Whereas, this increase was less than one half by 20% fill factor.

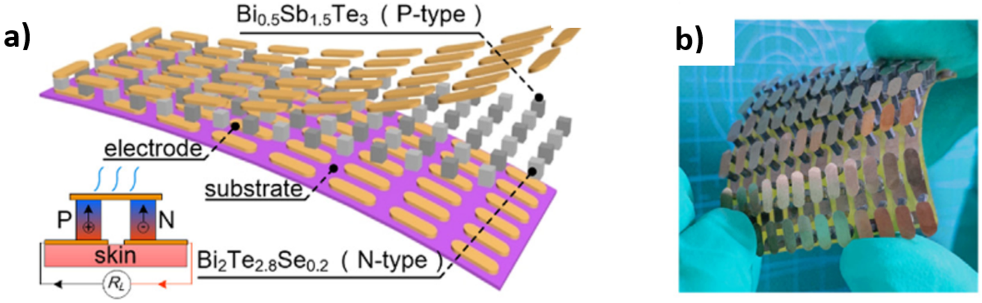

Color in online

Fig. 9. a) Schematic view of the TEG's component; b) Photo of the fabricated TEG [77].

Shi et al. [61] applied the same principles to fabricate a flexible and wearable TEG. However, the number of the thermocouples reduced to 24, and the utilized *p*-type and *n*-type TE materials were $Bi_{0.5}Sb_{1.5}Te_3$ and $Bi_2Se_{0.5}Te_{2.5}$ composites, respectively. The results indicated that the fabricated TEG achieved the highest output power of 4.75 $\mu W/cm^2$ at ΔT of 35°C. Furthermore, the authors demonstrated that by wearing the fabricated TEG on the human wrist, it generated 10.5mV that was adequate for powering an LED.

Instead of holding the legs in place by a polymer-based substrate, Eom et al. [78] developed a flexible holder in the shape of a flexible bracelet, see Fig. 10. The bracelet consisted of ten separate modular units, and each unit held four ingot-shaped TE legs arranged in an array of 2 × 2. It should be noted that the *p*- and *n*-type legs were respectively composed of $Bi_{0.5}Sb_{1.5}Te_3$ and $Bi_2Te_{2.7}Se_{0.3}$ composites. The legs were electrically connected together from the top and the bottom with copper foils. Integrating the ten units (each with the surface area of 14 mm × 12 mm) together, a shaft was passed through the punched holes in the legs and sides of the units. Finally, top of the legs was covered with a copper sheet as the heatsink. The results showed that at ΔT of 20°C, the highest obtained output powers under sitting, walking and running conditions were 2 $\mu W/cm^2$, 2 .9 $\mu W/cm^2$, and 4.7 $\mu W/cm^2$, respectively.

Color in online

Fig. 10. The designed flexible TE module consisting a flexible holder [78].

Instead of preparing the ingot-shaped legs by cold/hot pressing of the TE powders, Siddique et al. [79] prepared TE pastes and manually screen printed them into a pre-prepared fabric. To illustrate, the authors demonstrated that they have used this technique due to its simplicity, low cost, and low curing temperature (i.e. in the range of between 100-200°C). Accordingly, as Fig. 11 depicts, 24 holes were cut in a thick polyester fabric to manually spread the *p*- and *n*-type pastes into them. Notably, the employed TE materials were $(0.25Bi,0.75Sb)_2(0.95Te,0.05Se)_3$ for the *p*-type and $(0.98Bi,0.02Sb)_2(0.9Te,0.1Se)_3$ for the *n*-type legs. After curing the pastes, the ingot-shaped legs were connected together with a silver thread as the electrodes. The results showed that when the TEG was placed on the arm, the highest achieved output power was $1*10^{-5}$ μW/cm^2 at ΔT of 32.9°C.

Color in online

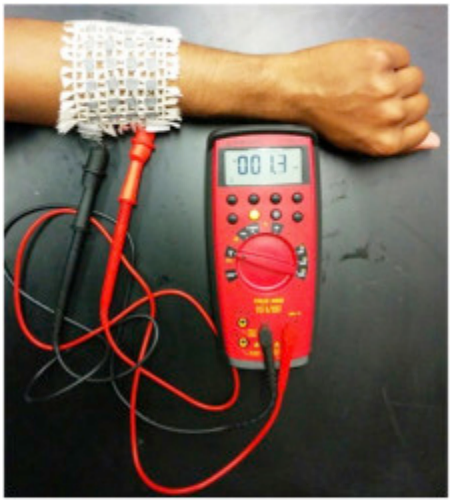

Fig. 11. The fabricated flexible TEG worn on the arm [79].

Likewise, Lu et al. [80] applied a manually dispenser printing technique to fill the 24 holes of a silk fabric with TE pastes. Accordingly, Bi_2Te_3 (*n*-type) and Sb_2Te_3 (*p*-type) pastes were prepared and deposited into the punched holes. Next, the legs were connected together with silver foils as interconnects, resulting in 12 thermocouples, see Fig. 12. The authors demonstrated that the fabricated TEG obtained the maximum output power of 4.7×10^{-4} $\mu W/cm^2$ at 35°C temperature gradient.

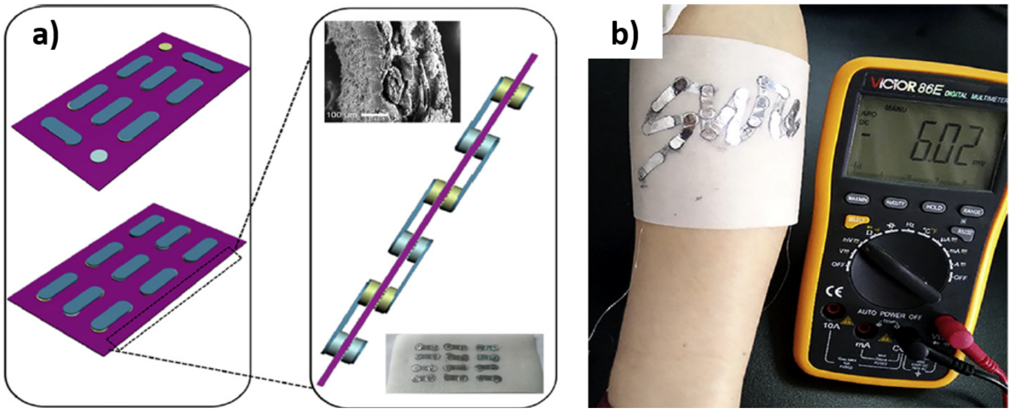

Color in online

Fig. 12. a) Schematic of the legs integration with the polyester fabric; b) Photo of the fabricated silk-based TEG [80].

3.1.1 Heatsink

As mentioned before, a TEG generates a high open circuit voltage when a large temperature gradient exists between its hot and cold junctions. This high temperature difference could be obtained when a large heat flux is applied on the hot junctions, but at the same time the cold junctions dissipate a large amount of heat to the ambient. Accordingly, an effective heatsink is required to accelerate absorbing the thermal energy from the hotter side and releasing it to the cooler ambient. Notably, applying a heatsink with a low heat removal efficiency possibly damages the TE legs at high temperatures [81]. Thus, in order to increase the rate of heat dissipation from heatsinks, it is necessary to increase either their thermal conductivity, heat transfer coefficient, or surface area [82]. Concerning wearable TEGs, the heatsinks are cooled either by phase change cooling (active cooling) or natural air cooling (passive cooling) techniques. Therefore, herein, it is intended to focus on the studies that designed heatsinks particularly to cool down wearable TEGs. It is noteworthy that this sub-section (i.e. 3.1) is selected for raising this topic because so far heatsinks have been only fabricated onto the wearable TEGs comprising inorganic ingot-shaped legs. Regarding the air cooled heatsinks, they are prepared in the form of either a fin-shaped anodized aluminium, a high thermal conductive polymer-based substrate, a copper sheet, a copper foam block, a copper plate-fins, or a cooling gel. For example, Nozariasbmarz et al. [83] fabricated an aluminium plate and a fin-shaped anodized aluminium heatsink respectively onto the cold substrate of a conventional rigid TEG. The TEG consisted of 6 pairs of Bi_2Te_3 -based TE legs that were electrically connected together with gold-coated copper strips as electrodes. The authors defined two fill factors for the investigation, including 36% and 12%. The tests were conducted on different parts of the body at 17°C ambient temperature. The results showed that the 12% fill factor was superior to the 36% one regarding the output power. Precisely, the former generated 34 $\mu W/cm^2$, 16 $\mu W/cm^2$, 14 $\mu W/cm^2$, and 12 $\mu W/cm^2$ power densities when placed on the arm, foot, forearm, and wrist, respectively. In addition, the 12% fill factor provided greater temperature gradient (i.e. ΔT = 2.5°C) along the legs than the 36% one (i.e. ΔT = 1.2°C).

However, the ongoing progress in flexible wearable TEGs has triggered extensive research on flexible heatsinks. For instance, instead of using rigid aluminium-based heatsinks, Shi et al. [84] developed flexible copper-based heatsinks comprising of either copper foam blocks or copper plate-fins, see Fig. 13. In fact, the authors developed these two heatsinks for the flexible cross-plane TEG that they had developed in their previous research [75]. While the overall dimensions of the TEG were 26.5 mm × 43.5 mm × 2.6 mm, the thickness of both heatsinks was approximately 4 mm. The heatsinks were separately adhered to the top surface of the pre-developed TEG using a 0.1 mm thick thermal conductive adhesive. The results showed that both heatsinks slightly improved the output power of the TEG at temperature differences higher than 15°C. However, the foam block heatsink was slightly superior to the plate-fins one, because it achieved the highest output power of 3.5 $\mu W/cm^2$ at ΔT of 20°C.

Color in online

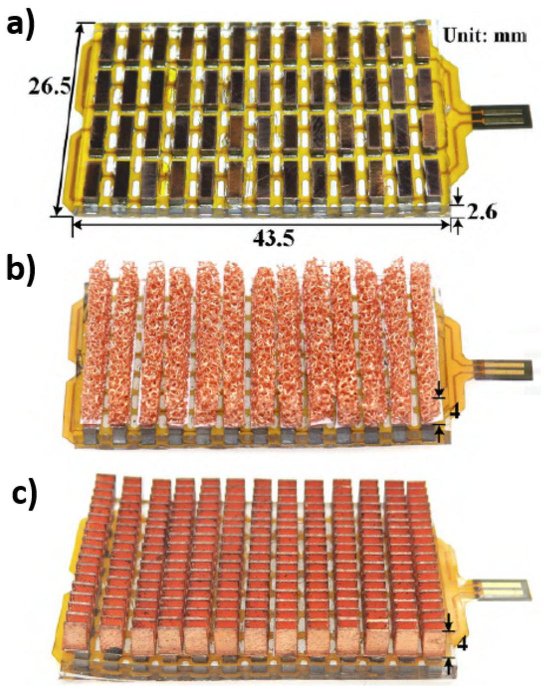

Fig. 13. Fabricated wearable TEGs: a) without heatsink; b) with copper-foam heatsink; and c) with plate-fins heatsink [84].

Instead of applying a thermal conductive adhesive to couple the copper-based heatsink with the flexible TEG, Park et al. [85] screwed the heatsink into the TEG. To clarify, 20 couples of ingot-shaped legs were soldered onto a FPCB served as the bottom electrode. Then, the thermocouples were inserted into the 40 holes of a bendable Bakelite holder arranged in an array of 4 × 10. It should be noted that the legs were composed of *p*-type $Bi_{0.5}Sb_{1.5}Te_3$ and *n*-type $Bi_2Te_{2.7}Se_{0.3}$ composites. Next. the legs were electrically connected together from their top sides with copper films. Finally, a fin-shaped copper heatsink was placed on the copper films and screwed into the Bakelite holder, as Fig. 14 depicts. The authors demonstrated that the developed TEG with approximately 79 mm × 17 mm base area obtained the highest output power of 6.97 $\mu W/cm^2$ at ΔT of 12.5°C.

Color in online

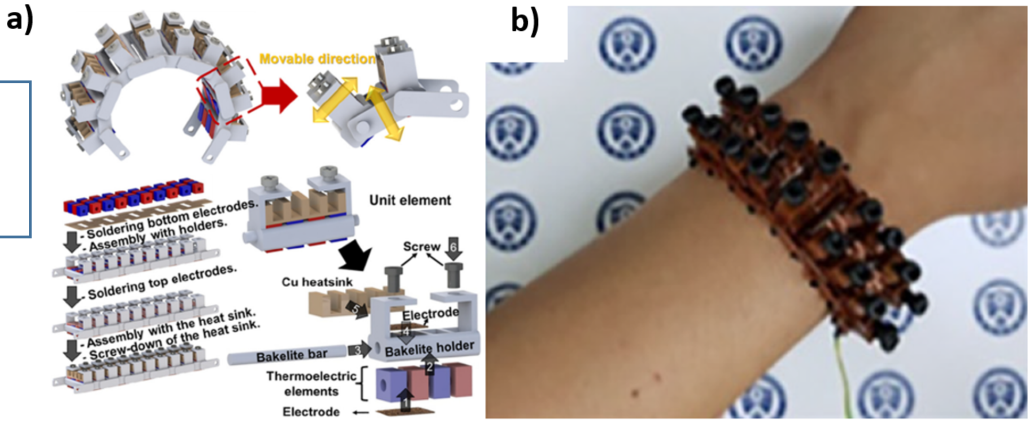

Fig. 14. a) Schematic of the entire device and its fabrication processes; b) The fabricated device worn on the wrist [85].

To increase the flexibility of the copper-based heatsinks, Hyland et al. [47] replaced the 3D copper heatsinks with two copper sheets, see Fig. 15. In particular, the authors sandwiched 25 Bi_2Te_3-based thermocouples between two rigid Aluminium Oxide ceramic substrates. Then, two separate copper sheets were attached to the cold and hot substrates of the TEG as the heatsinks. The results proved that the TEG generated higher output power compared with that of without a heatsink. Furthermore, concerning the output power, there was a direct relationship between the heatsinks' size and the air velocity. The paper concluded that at roughly 18°C temperature gradient, the developed TEG generated the output powers of 6µW/cm^2, 5.5µW/cm^2, 5µW/cm^2, and 1.5 µW/cm^2 when placed on the wrist, upper arm, chest, and T-shirt, respectively.

Color in online

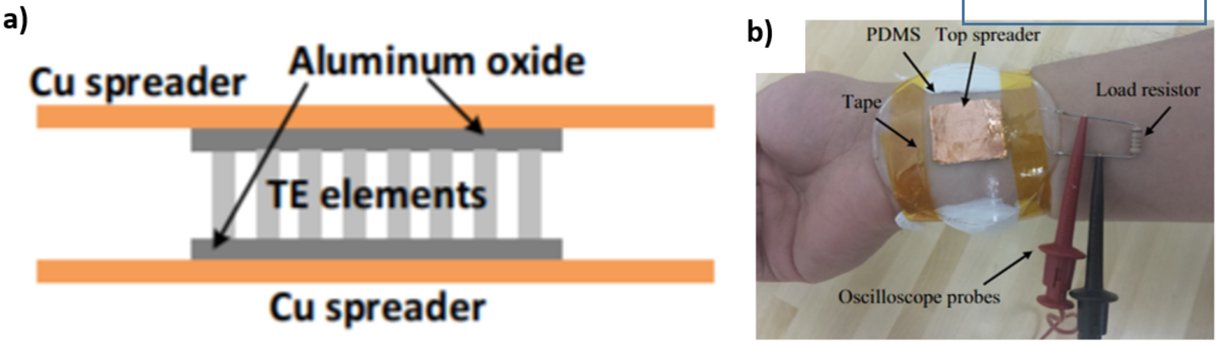

Fig. 15. a) Schematic of the developed TEG; b) The experimental setup of the TEG on the arm [47].

Likewise, Settaluri et al. [86] used two separate copper sheets to perform both as the heatsinks and the integrating units. The TEG consisted of 256 Bi_2Te_3-based thermocouples that were electrically connected together with copper strips and sandwiched between two ceramic substrates. Both substrates were covered with separate copper plates (each with the dimensions of 292 mm × 964 mm) as the heatsinks. Then, the gap between the two copper plates was filled with a flexible thermal insulator. The authors determined three individual grooving patterns for the upper copper plate, namely; flat, stripe, and checkerboard. The results showed that at 10°C temperature gradient, the highest achieved output powers by the checkerboard, strip, and flat patterns were 28.5 $\mu W/cm^2$, 21.6 $\mu W/cm^2$, and 17.6 $\mu W/cm^2$, respectively.

As mentioned before, one of the most promising approach to flexibly hold the legs in place is applying polymer-based substrates. Jeong et al. [87] used the same approach to develop a flexible polymer-based heatsink. Precisely, the authors utilized a polymer-based substrate that simultaneously served as a flexible heatsink and the coating layer of the electrodes. To specify, 8 pairs of Bi_2Te_3-based TE legs were electrically connected together using Gallium-based liquid alloy. Then, the gaps between the ingot-shaped legs were filled with the polymer-based plain Ecoflex substrate. However, the electrodes were coated with EcoFlex: Gallium substrates, which possessed a higher thermal conductivity than the plain Ecoflex substrate. As a result, due to the higher thermal conductivity of the outmost EcoFlex: Gallium layers than the middle plain Ecoflex layer, the outmost layers performed as flexible heatsinks. The results showed that the maximum output power of the fabricated TEG was 40.6 $\mu W/cm^2$ at ΔT of 20°C. Whereas, coating both the legs and the electrodes with the plain EcoFlex substrate resulted in the remarkably lower output power of 19.8 $\mu W/cm^2$.

Likewise, Sargolzaeiaval et al. [88] encapsulated the electrodes in a flexible high thermal conductivity mixture to serve both as a coating substrate and a flexible heatsink. To specify, the ingot-shaped *p*- and *n*-type TE legs were composed of $Bi_{0.5}Sb_{1.5}Te_3$ and $Bi_2Se_{0.3}Te_{2.7}$ composites, respectively. After arranging the 32 thermocouples in an array of 4×16, they were connected together with EGaIn as liquid metal electrodes. Then, the spaces between them were filled by PDMS, leaving the electrodes exposed to the ambient air. To examine the impact of the coating substrate of the electrodes on the TE performance of the TEG, two individual substrates were determined to coat the EGaIn electrodes, including plain PDMS and PDMS: EGaIn mixture. Concerning the output power of the TEG, the results showed the superiority of the latter to the former. This was mainly because the latter possessed higher thermal conductivity than the former. The authors also fabricated a thin copper sheet onto the top PDMS: EGaIn layer to intensify the heat dissipation from the cold junctions, see Fig. 16. The results illustrated that 5 μW/cm^2 was the highest output power achieved by the TEG at ΔT of 11°C.

Color in online

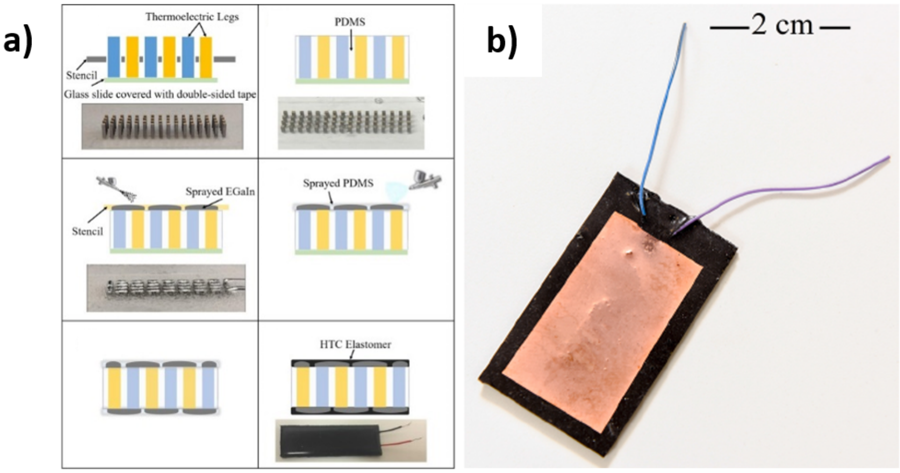

Fig. 16. a) Fabrication processes of the TEG; b) Photo of the fabricated TEG with copper sheet as the heatsink [88].

Increasing the thermal conductivity of the PDMS substrate, Lee et al. [89] replaced EGaIn with silver-nickel (Ag–Ni) particles. To specify, as soft heat conductors, Ag–Ni particles were initially added to the PDMS mixture followed by pouring the mixture into a pre-prepared mould. Then, silver-nanowires (Ag-NW) were mask printed as soft electrodes onto the mixture. After that, the Ag–Ni particles in the mixture were magnetically aligned in the direction of the legs to facilitate the heat transfer from the skin to the legs, as Fig. 17 illustrates. Next, using a fully automated epoxy printing technique, 440 ingot-shaped and Bi_2Te_3-based legs were integrated onto the Ag-NW electrodes followed by filling the gaps between them with plain PDMS. Then, silver-nanowires (Ag-NW) were mask printed onto the plain PDMS substrate as the top electrodes followed by pouring a layer of Ag–Ni: PDMS mixture onto it. Next, the Ag–Ni particles in the upper substrate were magnetically aligned in the direction of the legs to facilitate the heat transfer from the legs to the ambient. Thus, both the top and the bottom Ag–Ni: PDMS layers performed as flexible heatsinks. The results revealed that when the prepared flexible TEG with an area of 39 × 43 mm^2 was mounted on the hand, it generated the highest power density of 6.96 μW/cm^2 at 10°C temperature gradient.

Color in online

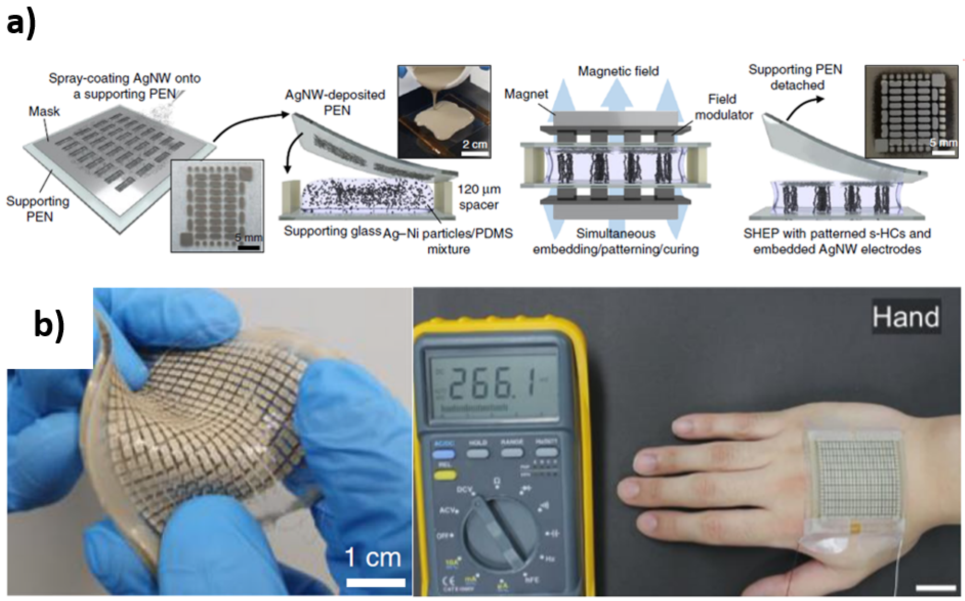

Fig. 17. a) Schematic illustration; and b) the photos of the fabricated TEG [89].

However, rather than conductive cooling, Park et al. [90] applied evaporative cooling to cool down their fabricated wearable TEG. Notably, the authors used a water-absorbing polymer (i.e. hydrogel) as the heatsink to cool down the TEG based on liquid evaporation. Regarding hydrogels, they are considered as porous materials in which a fluid (e.g. water) is entrapped into a polymeric matrix [91]. In fact, hydrogels can absorb 10 to 1000 times its own weight in water [92]. In particular, the authors used *p*-type ($Bi_{0.5}Sb_{1.5}Te_3$) and *n*-type ($Bi_2Te_{2.7}Se_{0.3}$) ingot-shaped TE legs to fabricate a mat-shaped flexible TEG. The TEG consisted of 15 thermocouples that were placed inside Bakelite holders and electrically connected together using FPCBs, see Fig. 18. The holders were connected together by passing flexible wires through the punched holes in the opposite sides of the holders. Then, a layer of hydrogel was spread on the cold side of the TEG (i.e. over the upper FPCB) as the heatsink. Since the performance of hydrogel is based on liquid evaporation, the evaporation of the trapped water over time allowed the absorbed heat to be continuously released to the ambient air. Finally, the mat-shaped flexible TEG with 55 mm × 45 mm base area was embedded in an armband to be mounted on the lower arm. The results showed that the highest output power of the TEG at 9.3°C temperature difference was 5.60 $\mu W/cm^2$.

Color in online

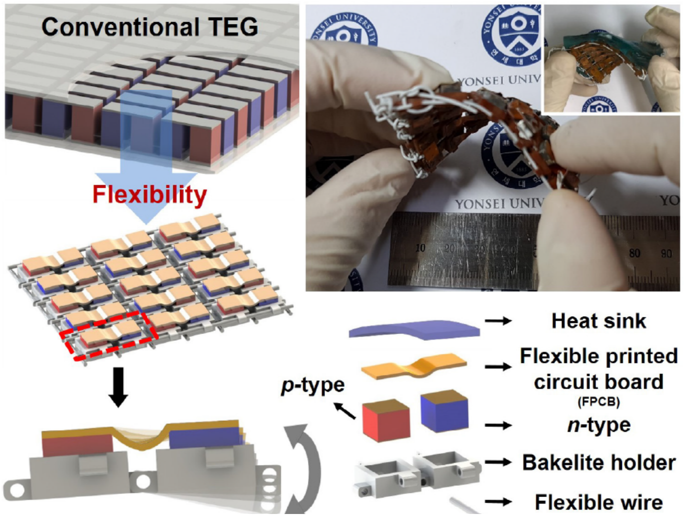

Fig. 18. The consisting elements of the fabricated TEG and the photo of the developed prototype [90].

Likewise, Lee et al. [93] used hydrogel as the heatsink of their developed flexible wearable TEG. Precisely, 15 pairs of ingot-shaped *p*- ($Bi_{0.5}Sb_{1.5}Te_3$) and *n*- ($Bi_2Te_{2.7}Se_{0.3}$) type legs were soldered onto a FPCB as the bottom electrode. From the top, the legs were electrically connected together with EGaIn. To hold the bulk legs in place, a flexible resin holder was placed around them followed by filling the gaps between them with PDMS. While the PDMS substrate was coated the EGaIn electrodes, a flexible hydrogel-based heatsink was fabricated onto it, see Fig. 19. When the TEG was placed on the upper arm, the results demonstrated that it generated 8.30 µW/cm^2 at 8°C temperature difference.

Color in online

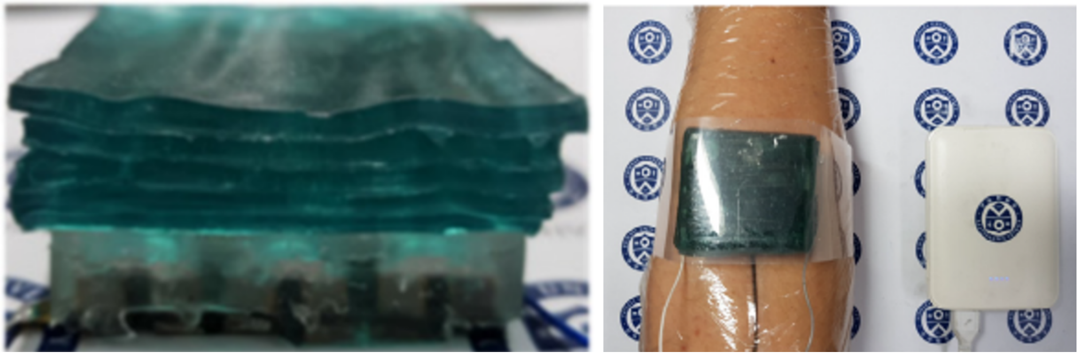

Fig. 19. Fabricated hydrogel-based heatsink onto the TEG [93].

Rather than spreading hydrogel on the cold side of the TEG, Kim et al. [94] embedded it within a fabric to be coupled with the TEG. To illustrate, 170 ingot-shaped thermocouples were prepared from *p*-type $Bi_{0.5}Sb_{1.5}Te_3$ and *n*-type $Bi_2Te_{2.7}Se_{0.3}$ composites. While the thermocouples were connected together with copper electrodes, the gaps between them were filled with a polymer-based material as the flexible integrating substrate. Regarding the heatsink, the authors encapsulated a hydrogel material (e.g. a superabsorbent polymer) inside a fabric followed by integrating it with the TEG from its cold side. The results demonstrated that at 12°C temperature difference, the TEG generated over 38 $\mu W/cm^2$ and 13 $\mu W/cm^2$ after 10 min and over 22 hrs, respectively.

Instead of evaporative cooling, Lee et al. [95] used exothermic and endothermic reactions to maintain a constant temperature on the cold side of the TEG over a period of time. Accordingly, the authors used a phase change material (PCM) called n-octadecane (C18H38) as the heatsink to absorb latent heat from the cold side of the TEG and release it to the ambient air. N-octadecane was selected as the PCM due to its low melting point (28°C), resulting in a large amount of heat absorption at the low temperature difference between the skin and ambient air. To fabricate the heatsink, 25 copper foam blocks each with the dimensions of 10 mm × 10 mm × 5 mm were filled with the PCM. This was because, the foam blocks could spread the heat uniformly within the PCM. Then, the filled foam blocks were arrayed in an array of 5×5, and the spaces between them were filled with a polyurethane elastomer. Next, the top and the bottom sides of the filled foam blocks were covered with a metal foil to intensify the vertical heat flow, see Fig. 20. Finally, the generated heatsink was attached to the top substrate of a cross-plane TEG comprising 50 ingot-shaped thermocouples. To specify, the legs were Bi_2Te_3 -based and the gaps between them were filled with a polymer-based filler. The results showed that combining the as-prepared heatsink with the 65 mm × 65 mm base area TEG resulted in an output power of 20 $\mu W/cm^2$ at ΔT of 3°C.

Color in online

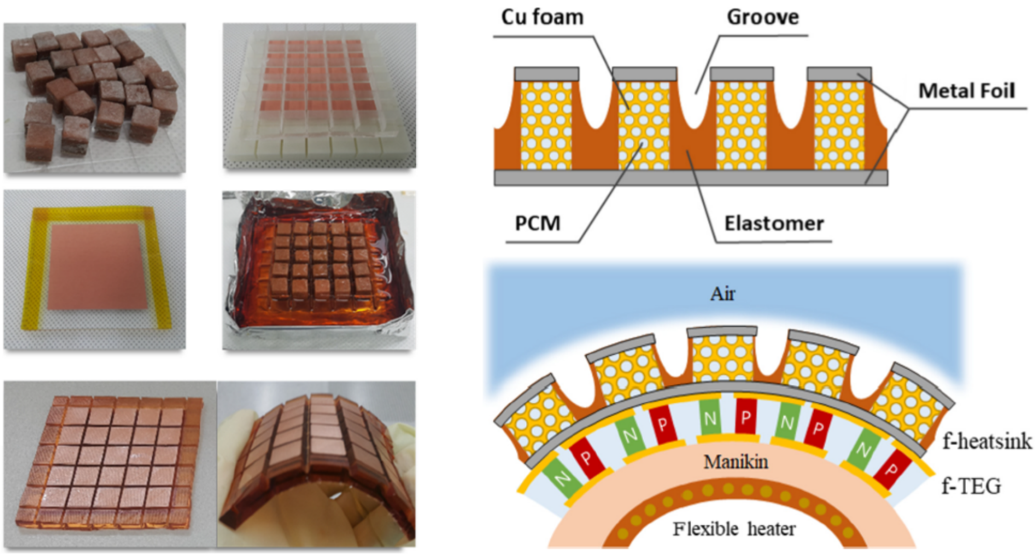

Fig. 20. Fabrication processes of the flexible heatsink consisting of copper foam blocks and PCM [95].

3.2. Organic TE materials

Although organic TE materials benefit from an intrinsic low thermal conductivity, it is not prevalent to use them for the preparation of the ingot-shaped TE legs. This is mainly because their low thermal conductivity could be replaced by the high power factor of the inorganic type. In addition, it will be explained in section 4.2 that organic TE materials (e.g. polymers) possess a great mechanical flexibility, thus it is too tough to overcome this feature to turn them into ingot-shaped TE legs. Therefore, so far, no study has used a pristine organic TE material to prepare an ingot-shaped TE leg.

3.3. Hybrid TE materials

As reviewed in section 3.1, the inorganic ingot-shaped TE legs should be embedded in a flexible substrate to address the flexibility requirement of wearable TEGs. However, when the TEG bends, a bending force is applied on the flexible substrate due to the rigidity of the inorganic TE materials. Precisely, the bending force is concentrated on the junctions of the rigid legs and the flexible substrate, reducing the flexibility of the device. Allowing the bending force to distribute uniformly throughout the TEG, Jung et al. [60] attempted to increase the flexibility of the ingot-shaped legs themselves by applying hybrid TE materials. To specify, the authors replaced the inorganic ingot-shaped legs with the hybrid ones to benefit both from the high conversion efficiency and the flexibility of the inorganic and organic types, respectively. To prepare the hybrid TE pastes, the authors separately added Bi (*p*-type) and Te (*n*-type) powders to CNTs followed by mixing them with PDMS. Then, the as-prepared *p*- and *n*-type pastes were poured into 100 holes of an aluminium stencil followed by being cured for 3 hrs to become stiff. Then, the stiffed legs were electrically connected together in series with aluminium strips, resulting in 50 thermocouples. Finally, the gaps between the legs were filled with PDMS as the flexible substrate, see Fig. 21. The results showed that the highest output power generated by the developed TEG was 80 μW/cm^2 at ΔT of 293°C.

Color in online

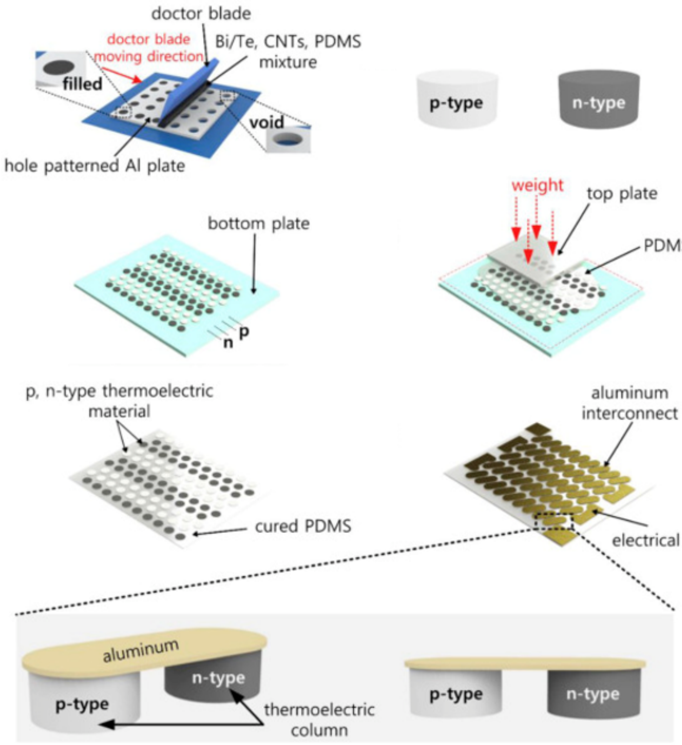

Fig. 21. Schematic of the fabrication processes of the proposed TEG [60].

Instead of preparing a hybrid TE material, Park et al. [96] connected 36 pairs of organic *p*-type and inorganic *n*-type legs together. In particular, the *p*-type legs were film-shaped and consisted of doped poly(3,4-ethylenedioxythiophene) (PEDOT) in tosylate. After preparing the *p*-type polymer film, it was cut into smaller area films (18×2 mm^2) to be individually rolled up in an elliptical shape. The *n*-type legs were composed of Bi_2Te_3 ingots with the dimensions of 2 mm× 2mm× 0.2mm. In accordance with the dimensions of the *n*-type legs, the polymer films were rolled up with a 4:1 ratio in the horizontal diameter (8 mm) against the vertical diameter (2 mm). The authors selected a polyimide film as a flexible substrate and coated it with a gold sheet in a specific pattern. To electrically connect the 36 prepared thermocouples together, they were soldered onto a gold sheet from the bottom and wired with a polytetrafluoroethylene coated wire from the top. The results showed that when the TEG was worn on the wrist, it generated an output voltage of 10.6 mV. Table 2 illustrates the summary of the reviewed literatures on wearable TEGs consisting ingot-shaped legs.

Table 2. Summary of the recently developed wearable TEGs comprising ingot-shaped thermocouples.

***P*-type**	***N*-type**	**Couple Number**	**Electrode**	**Packaging**	**Heatsink**	**ΔT (°C)**	**Output voltage or power**	**Ref**
Inorganic								
Bi_2Te_3	Bi_2Te_3	25	Copper	Rigid ceramic substrates	Copper sheet	18	6 μW/cm^2	[47]
$Bi_{0.5}Sb_{1.5}Te_3$	$Bi_2Se_{0.5}Te_{2.5}$	24	Copper	FPCB	n/a	35	4.75 μW/cm^2	[61]
$Bi_{0.3}Sb_{1.7}Te_3$	$Bi_2Sb_{0.3}Te_{2.7}$	72	Copper	Flexible polymer	n/a	8.9	2.5 μW/cm^2	[71]
$Bi_{0.5}Sb_{1.5}Te_3$	$Bi_2Se_{0.3}Te_{2.7}$	32	EGaIn	PDMS	n/a	13	1 μW/cm^2	[72]
Bi_2Te_3	Bi_2Te_3	47	Copper	PDMS sponge	n/a	8	130 μW/cm^2	[73]
$Bi_{0.5}Sb_{1.5}Te_3$	$Bi_2Te_{2.7}Se_{0.3}$	24	Copper	Flexible polymer	n/a	10	4.5 μW/cm^2	[74]
$Bi_{0.5}Sb_{1.5}Te_3$	$Bi_2Se_{0.5}Te_{2.5}$	52	Copper	FPCB + PDMS	n/a	18	3.9 μW/cm^2	[75]
Bi_2Te_3	Bi_2Te_3	18	Silver paste and Copper	FPCB + PDMS	n/a	12	3 μW/cm^2	[76]
$Bi_{0.5}Sb_{1.5}Te_3$	$Bi_2Te_{2.8}Se_{0.2}$	47	Copper	FPCB	n/a	14	3.5 μW/cm^2	[77]
$Bi_{0.5}Sb_{1.5}Te_3$	$Bi_2Te_{2.7}Se_{0.3}$	20	Copper	Flexible holder (Bakelite)	n/a	20	2 μW/cm^2	[78]
$(0.25Bi,0.75Sb)_2(0.95Te,0.05Se)_3$	$(0.98Bi,0.02Sb)_2(0.9Te,0.1Se)_3$	12	Silver thread	Polyester fabric	n/a	32.9	$1*10^{-5}$ μW/cm^2	[79]
Sb_2Te_3	Bi_2Te_3	12	Silver foils	Silk fabric	n/a	35	4.7×10^{-4} μW/cm^2	[80]
Bi_2Te_3	Bi_2Te_3	6	Gold-coated copper	Rigid ceramic substrates	Fin-type anodized aluminium	2.5	34 μW/cm^2	[83]
$Bi_{0.5}Sb_{1.5}Te_3$	$Bi_2Se_{0.5}Te_{2.5}$	52	Copper	FPCB + PDMS	Copper foam	3.5	20 μW/cm^2	[84]
$Bi_{0.5}Sb_{1.5}Te_3$	$Bi_2Te_{2.7}Se_{0.3}$	20	Copper	Flexible holder (Bakelite)	Fin-type copper	12.5	6.97 μW/cm^2	[85]
Bi_2Te_3	Bi_2Te_3	256	Copper	Rigid ceramic substrates and Thermal Insulator	Copper sheet	10	28.5 μW/cm^2	[86]
Bi_2Te_3	Bi_2Te_3	8	Gallium-based liquid alloy	Flexible polymer	EcoFlex: Gallium Layer	20	40.6 μW/cm^2	[87]
$Bi_{0.5}Sb_{1.5}Te_3$	$Bi_2Se_{0.3}Te_{2.7}$	32	EGaIn	PDMS	PDMS: EGaIn Layer and Copper Sheet	11	5 μW/cm^2	[88]
Bi_2Te_3	Bi_2Te_3	220	Silver-nanowires	PDMS	Ag–Ni :PDMS Layer	10	6.96 μW/cm^2	[89]

$Bi_{0.5}Sb_{1.5}Te_3$	$Bi_2Te_{2.7}Se_{0.3}$	15	Soldered to FPCB	Flexible holder (Bakelite)	Solid-state cool gel	9.3	5.6 μW/cm^2	[90]
$Bi_{0.5}Sb_{1.5}Te_3$	$Bi_2Te_{2.7}Se_{0.3}$	15	Soldered to FPCB from bottom and connected with EGaIn from top	PDMS and resin holder	Hydrogel	8	8.30 μW/cm^2	[93]
$Bi_{0.5}Sb_{1.5}Te_3$	$Bi_2Te_{2.7}Se_{0.3}$	170	Copper	Flexible polymer	Liquid evaporative polymer	12	13 μW/cm^2	[94]
Bi_2Te_3	Bi_2Te_3	50	Copper	Flexible polymer	Phase change material	3	20 μW/cm^2	[95]
Hybrid								
Bi: CNTs: PDMS	Te :CNTs: PDMS	50	Aluminium	PDMS	n/a	293	80 μW/ cm^2	[60]
PEDOT doped in tosylate	Bi_2Te_3	36	Gold and Flexible wire	Polyimide film	n/a	36	10.6 mV	[96]

4. Film-shaped thermocouples

4.1. Inorganic TE materials

As mentioned before, flexible wearable TEGs have many advantages over the rigid ones due to their flexibility, allowing them to conform to the arbitrary surfaces of the body. Accordingly, as reviewed in Section 3, a flexible wearable TEG can be fabricated by embedding ingot-shaped thermocouples in a flexible polymer-based substrate such as PDMS. To further increase the flexibility of wearable TEGs and reduce the bending force, the ingot-shaped thermocouples can be replaced by the film-shaped ones. Accordingly, various printing techniques can be applied to deposit TE materials onto flexible substrates (e.g. plastic films or fabrics). These printing techniques are namely, dispenser printing, inkjet printing, screen printing, roll to roll printing, and aerosol jet printing [97]. All these printing techniques aim to synthesize high-performance TE inks and obtain printed TE films with high density and electrical conductivity [98].

Regarding the screen printing technique, TE inks are pushed through the openings of a stencil or a patterned mesh onto a flexible substrate. Precisely, a fill blade or squeegee is used to force the viscous ink through the mesh, onto the substrate. The advantages of screen printing, as compared to the other printing methods, are its compatibility with a broader range of available substrates and inks as well as allowing greater ink thickness [99]. Notably, film-shaped TEGs are fabricated either unipolar or bipolar, depending on the applied TE material.

Accordingly, Varghese et al. [98] developed a unipolar film-shaped TEG by applying the screen printing technique. Precisely, the authors employed microwave stimulated wet chemical method to prepare *n*-type $Bi_2Te_{2.8}Se_{0.2}$ nanocrystals. Then, the prepared *n*-type ink was screen printed onto a flexible polyimide substrate, generating 5 film-based TE legs each with the dimensions of 10 mm × 2 mm × 0.01 mm, see Fig. 22. To remove any solvent and binders, the printed TE films were dried on a hot plate at 200°C. Next, the films were consolidated by cold compaction followed by being sintered in the vacuum at 430°C for 45 min. To electrically connect the TE films together, the authors soldered them to thin copper foils as electrodes. The results revealed that at a temperature difference of 20°C, 500 $\mu W/cm^2$ was the greatest achieved output power of the TEG.

Color in online

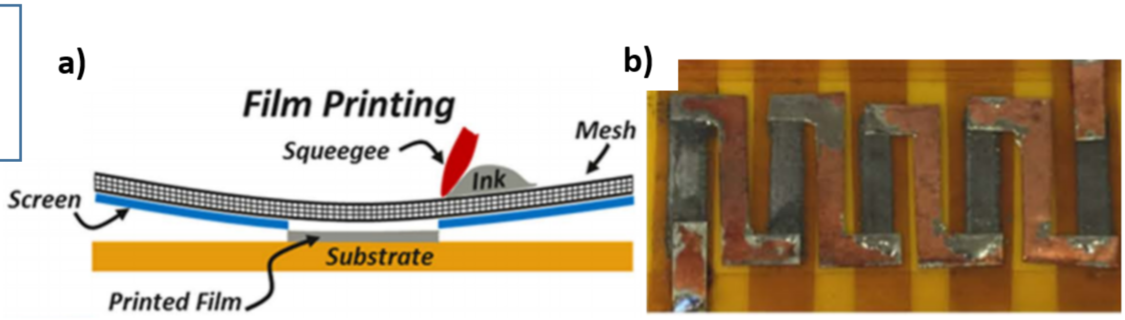

Fig. 22. a) Schematic of the screen printing process; and b) photo of the fabricated TEG [98].

Guo et al. [100] replaced the *n*-type TE material with a *p*-type one called molybdenum disulphide (MoS_2) to fabricate it onto a fibre-based underlying substrate. To illustrate, the authors added $HAuCl_4 \cdot 4H_2O$ to MoS_2 to improve its TE performance, resulting in an Au decorated 2D MoS_2 nano-sheets. Next, the Au-MoS_2 solution was deposited onto a 2D support unit via vacuum filtration to form the TE films. The authors then cut five strips (5 mm × 45 mm) out of the *p*-type Au-MoS_2 film and crossed them into the five pierced holes (6 mm × 1 mm) in a fabric. Then, a copper adhesive tape was used to attach the two ends of the Au-MoS_2 strips to the sides of the fabric. Finally, the *p*-type strips were electrically connected together with a commercial metal yarn. The results proved that the fabricated TEG comprising five TE legs achieved the maximum output voltage of 2.5mV at ΔT of 5°C.

Instead of a unipolar film-shaped TEG, Cao et al. [101] developed a bipolar one by alternately screen printing $Bi_{1.8}Te_{3.2}$ (*n*-type) and Sb_2Te_3 (*p*-type) pastes onto a polyimide substrate. To specify, the TE pastes were alternately poured over the stencil and forced into its openings by a blade. To smooth the outmost surface of the pastes and evenly squeeze them into the openings, a pressure squeegee passed across the stencil. After lifting off the stencil, the experiment was finished by drying the pasted substrate at 80°C for 2 min followed by curing it in an N_2 atmosphere at 253°C for 3 hrs. Finally, the cured pastes were connected together with SbTe electrodes to generate 8 film-shaped thermocouples. The results illustrated that at 20°C temperature gradient, 0.016 $\mu W/cm^2$ was the maximum achieved output power of the TEG.

Concerning the inkjet printing technique, it is a derivative of the dispenser printing technique where ink drops are transferred onto a substrate by a nozzle. Adjusting expansion/contraction of the piezoelectric actuator, a single ink droplet can be ejected from the nozzle forming the desired pattern on the substrate [102]. Thus, Chen et al. [103] applied the inkjet printing technique to transfer Bi_2Te_3 (*n*-type) and $Bi_{0.5}Sb_{1.5}Te_3$ (*p*-type) nanowire inks onto a polyimide substrate. To improve the TE properties of the 5 film-shaped thermocouples, they were annealed in a tube furnace using forming gas. Notably, EGaIn liquid metal was used as electrodes to connect the films together. Finally, the developed TEG was coated by a silicon elastomer to be protected from the ambient conditions. The results showed that at 7°C temperature difference, the printed TEG delivered the maximum output power of 14.1 nW.

Thermal evaporation is another technique to deposit TE thin films onto flexible substrates. In this technique, the TE material is evaporated in a vacuum, where allows the vapour particles to travel to the target substrate and condense back to the solid state in the form of a thin film [104]. Therefore, Karthikeyan et al. [105] applied this technique to deposit *p*-type Tin telluride(SnTe) and *n*-type Lead Telluride (PbTe) thin films onto a flexible polyimide substrate. Next, the 64 prepared legs were connected together with aluminium films as electrodes, see Fig. 23. The results showed that the fabricated TEG delivered 8.5 mW/cm^2 at a temperature difference of 120°C.

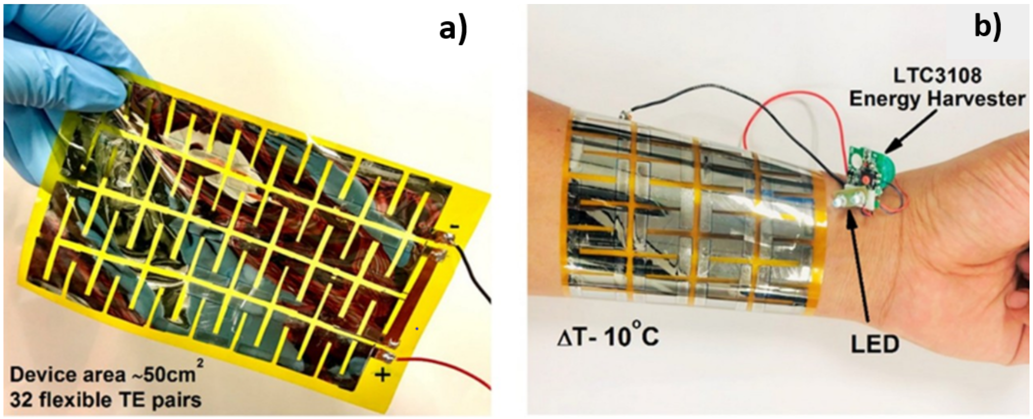

Color in online

Fig. 23. a) Photo of the fabricated flexible SnTe–PbTe based TEG; b) Photo of the TEG placed on the arm as the power source of an LED [105].

Likewise, Ren et al. [106] used thermal evaporation to fabricate 14 TE chips onto a polyimide film. Precisely, each TE chip was generated by alternately thermal evaporating 4 pairs of $Bi_{0.5}Sb_{1.5}Te_3$ (*p*-type) and $Bi_2Te_{2.8}Se_{0.3}$ (*n*-type) thin films onto the polyimide film. Then, the TE legs of each chip were connected together with Au-Ge electrodes. To integrate the 14 TE chips together, 14 slots were laser cut in the polyimine substrate. Next, the opposite ends of the alternate slots were connected together by screen-printing liquid metal as electrodes. After that, the chips were slightly inserted into the slots and stiffly bonded with the polyimide film by dropping a small amount of the polyimine solution at the junctions. The results proved that at 93°C temperature gradient, the fabricated TEG with 56 thermocouples generated the highest output power of 18.625 $\mu W/cm^2$.

So far, all of the reviewed wearable TEGs only served as power sources of a sensor network. However, none of them served as a sensor themselves along with being a power source. To fill this gap, Wen et al. [107] replaced the single-chain thermocouples of film-shaped TEGs with complementary double-chain thermocouples to provide a space for fabricating a dielectric material as a temperature & humidity sensor. To specify, the authors screen printed *n*-type $Bi_2Te_{2.7}Se_{0.3}$ and *p*-type Sb_2Te_3 pastes onto a polyimide film. In particular, the *n*- and *p*-type TE pastes were alternately screen printed onto the underlying substrate in two separate complementary chains, see Fig. 24. While each individual TE chain possessed 5 thermocouples, the gap between the two chains was filled by silk fibroin solution. Notably, silk fibroin served as the dielectric material, changing (i.e. increasing/decreasing) at different air temperatures and humidity. The results demonstrated that the developed wearable TEG with one complementary double-chain thermocouple achieved the highest output power of 0.095 $\mu W/cm^2$ at ΔT

of 20°C. Regarding the silk fibroin, absorbing and desorbing water molecules intensified and lessened its molecular motion, leading to an increase and a decrease in its dielectric constant, respectively. Likewise, increasing and decreasing the air temperature raised and reduced the dielectric constant of the silk fibroin, resulting in an increase and a decrease in the capacitance of the double-chain TEG, respectively.

Color in online

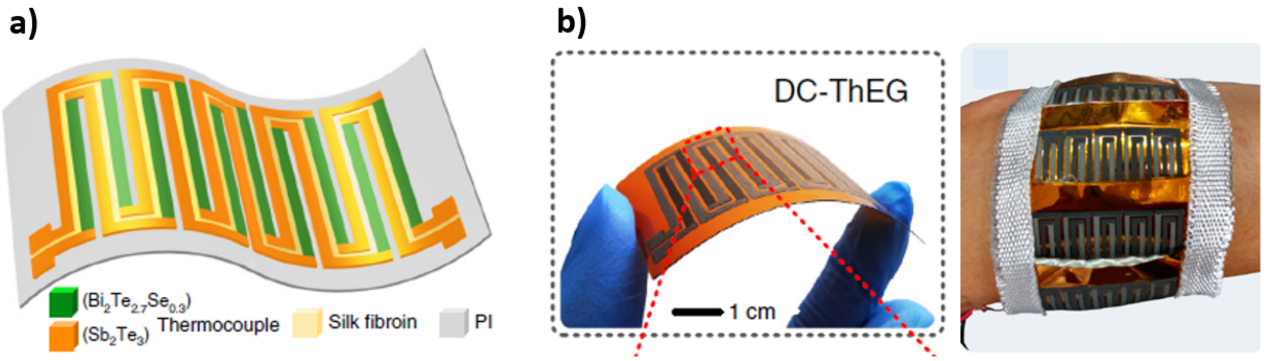

Fig. 24. a) Schematic illustration; and b) the photos of the fabricated TEG [107].

4.2. *Organic TE materials*

Although inorganic TE materials possess high energy conversion efficiency, they are intrinsically rigid and unsuitable for enduring a wide range of dynamic motions. This is mainly attributed to their limited elasticity and tensile strength as well as great hardness [108]. As a result, they cause a considerable bending force at their junctions with flexible substrates, resulting in lower flexibility of TE modules or cracks around the junctions. To overcome these issues, many researchers attempted to further improve the flexibility of the film-shaped legs via preparing them with flexible TE materials (i.e. organic TE materials). To specify, organic TE materials (e.g. conducting and non-conducting polymers) benefit from unique merits such as inexpensive and convenient manufacturing process, lightweight, mechanical flexibility, and intrinsically low thermal conductivity [109].

Accordingly, Elmoughni et al. [110] used polymer-based TE materials to fabricate 16 film-shaped thermocouples onto a polyester knitted fabric. For the *p*-type films, dry pellets (8 wt%) of poly(3,4-

ethylenedioxythiophene) polystyrene sulfonate (PEDOT: PSS) were added to 5 vol% DMSO followed by mixing the dispersion for 15 min in a micro vibration mill. For the *n*-type films, Poly[Na(NiETT)] ink was synthesized, while its viscosity was optimized by micro ball milling of the ETT in PVDF/DMSO solution at a weight ratio of 4:1 (ETT:PVDF). To fabricate the TEG, initially 32 holes were burnt out of a polyester fabric to deposit the *p*- and *n*-type inks into them. Then, the *p*- and *n*-type inks were alternately deposited into the holes using the screen printing technique. This step was repeated on the other side of the fabric to ensure the penetration of the ink into the holes. Finally, the TE legs were electrically connected together by hot pressing silicone-based silver ink at the ends of the legs. The results revealed that the developed prototype yielded 3mV at ΔT of 3°C.

As a derivative of the screen printing technique, Zhang et al. [111] used roll-to-roll printing to print PEDOT: PSS (*p*-type) and nitrogen-doped graphene (*n*-type) inks onto a flexible plastic substrate, see Fig. 25. Concerning roll to roll printing, a rotary screen is used to transfer the ink continuously to the substrate with tuneable rotation pressure and speed. Then, the TE legs were electrically connected together using PEDOT: PSS aqueous solutions. After that, the substrate was treated alternately by UV irradiation and oxygen plasma treatment for 2 hrs in total. The authors reported that the 18 printed thermocouples obtained the maximum output power of ~0.024μW/cm^2 at ΔT of 10°C.

Color in online

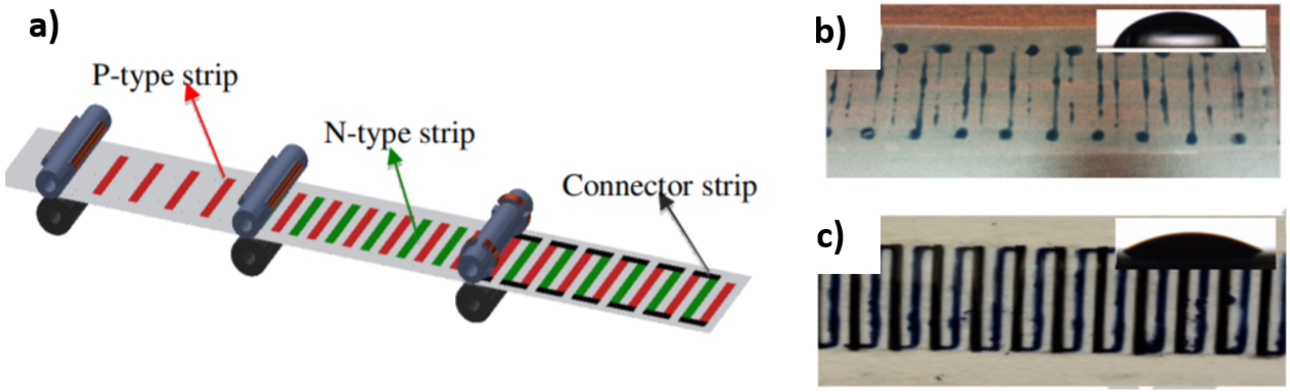

Fig. 25. a) Illustration of roll to roll printing of the flexible TE devices; b) UV treated plastic substrate; c) Plasma-treated plastic substrate [111].

Zhang et al. [112] combined roll to roll and inkjet printing techniques together to develop a film-shaped TEG. To specify, the authors used single-walled carbon nanotubes (SWCNT) /PEDOT:PSS composites and SWCNTs/ triphenylphosphine for the *p*- and *n*-type legs, respectively. Using roll to roll printing, PEDOT: PSS ink was deposited onto a polyimide substrate to serve as electrodes. Notably, the PEDOT: PSS films (possessed 20 mm length each) were printed with 20 mm intervals. Then, following the length and intervals of the electrodes, a PDMS film was prepared and pierced with holes with 20 mm intervals. Next, the pierced PDMS film was placed on the PEDOT: PSS printed substrate, while its holes were aligned with the two ends of the electrodes. After that, using inkjet printing, the holes were alternately filled with the *p*- and *n*-type TE materials followed by drying them on a hotplate. Finally, the holes were covered by another PEDOT: PSS printed polyimide substrate as the upper electrode, see Fig. 26. The results revealed that the fabricated TEG comprised of 10 thermocouples obtained the maximum power density of 0.05 μW/cm^2 at a temperature gradient of 20°C.

Color in online

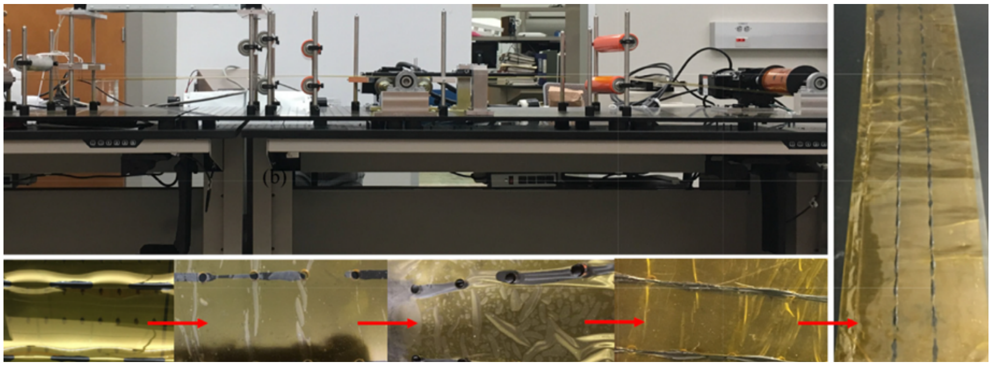

Fig. 26. Demonstration of the applied roll to roll and inject printing techniques to fabricate the film-shaped TEG [112].

Obtaining an air-stable and high performance *n*-type TE material is recognized as an important and challenging topic in the TE field [113]. This is mainly because, *n*-type organic materials are mostly prepared by chemical doping, resulting in their highly volatility upon air exposure. Due to the correlation between the air stability of the *n*-type TE materials and their power factor, their air stability is evaluated by the change in their power factor over time [114]. Accordingly, to generate a TEG possessing an air-stable and a high power factor *n*-type material, Zhou et al. [115] proposed developing a film-based TEG via alternately converting a pristine *p*-type film to an *n*-type one. Accordingly, the authors developed a *p*-type carbon nanotube (CNT) film with the dimensions of 16 mm × 10 mm ×

0.15 mm onto a glass substrate. Then the film was mask shaded in a strip pattern using polyethylene terephthalate (PET) double-sided adhesive tapes, see Fig. 27. Then, the *n*-type 1wt.% polyethylenemine (PEI) solution was dropped onto the unshaded parts of the *p*-type film. After treating the doped film for 5 min at 50°C, the adhesive tapes were removed and the prepared TEG was repeatedly folded. The results showed that three pairs of this continuous TE films obtained the maximum power density of 0.06 μW/cm^2 at ΔT of 19°C. Furthermore, the variations of electrical conductivity and Seebeck coefficient were less than 5% during 3 months.

Color in online

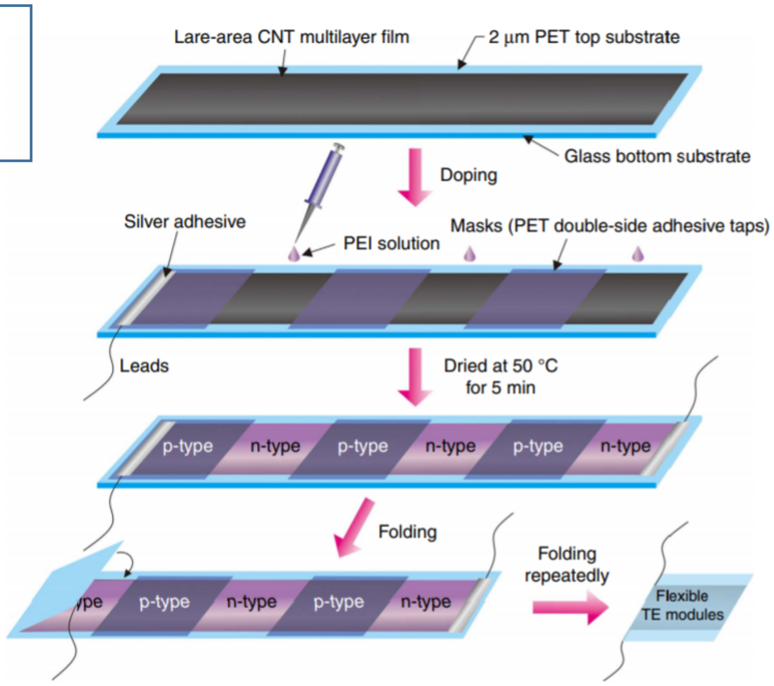

Fig. 27. The processes of fabricating the foldable TE module [115].

Instead of a bipolar film-shaped TEG, Wang et al. [116] developed a unipolar one by drop casting *p*-type 65wt% SWNTs/polyaniline (PANI) solution onto a glass substrate. To illustrate, initially the substrate was mask shaded in a strip pattern followed by dropping the composite solution and drying it at 408°C. Finally, the four *p*-type legs each with the dimensions of 22 mm × 10 mm × 0.15 mm were connected together using silver paste and gold wires as electrodes. The results showed that the developed TEG generated the maximum output power of ~0.012 μW/cm^2 at ΔT of 30°C.

Stepien et al. [117] replaced the drop casting technique with dispenser printing to fabricate *p*-type film-shaped legs onto a glass substrate. Regarding the dispenser printing, a nozzle dispensed continuous filament of *p*-type PEDOT: PSS ink onto the substrate without any mask shading. Then, the 61 printed TE legs were connected together with silver paste as electrodes. The results showed that at a temperature gradient of 90°C, the maximum recorded output power of the TEG was 0.025 μW/cm^2. Likewise, Liu et al. [118] electrochemically inkjet printed *n*-type poly[Kx(Ni-ethylenetetrathiolate)] film onto a PET substrate. Then the 108 TE films were connected electrically together using gold interconnections. The results demonstrated that the highest output power was 577.8 μW/cm^2 at 12°C temperature gradient.

Some studies developed cross-plane TEGs via fabricating the organic film-shaped legs onto a 3D supporting structure. Thus, these studies benefited both from the flexibility aspect of the organic TE materials and the greater temperature difference between the skin and the ambient air. For example, Park et al .[119] developed a bracelet TEG via automate printing of TE inks onto a flexible polyurethane cable. In particular, the authors doped separately CNT ink with poly (acrylic acid) (PAA) and poly(ethylenimine) (PEI) to prepare the *p*- and *n*-type inks, respectively. Then, the PAA doped CNT ink was printed in a strip pattern onto one half of the polyurethane cable (having 3mm diameter) served as the flexible supporting structure, see Fig. 28. After drying the printed *p*-type ink at 85°C vacuum for 1hr, the *n*-type ink was printed onto the other half of the cable with the same pattern and dried overnight under the same condition. It should be noted that the legs were printed with 1mm width and with 2mm intervals. Finally, the cured *p*- and *n*-type inks were electrically connected together via dispenser printing of silver pastes as electrodes. The results showed that the generated springy-shaped TEG comprising 60 thermocouples obtained the maximum output power of 0.2 μW and 1.95 μW at ΔT of 10°C and 30°C, respectively.

Color in online

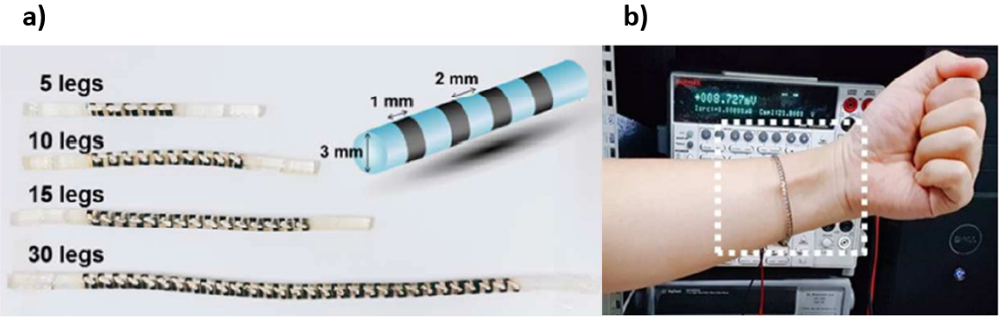

Fig. 28. a) Photo of the fabricated TEG with 5, 10, 15 and 30 *p-n* pairs; b) Demonstration of the TE bracelet wrapped around the wrist [119].

To develop a cross-plane TEG based on film-shaped legs, Zeng et al. [120] coated seven 3D PDMS-based grids with an organic TE material and connected them together with conducting fabrics as electrodes, see Fig. 29. To specify, the authors directly 3D printed each PDMS grid onto a Cu/Ni coated conducting fabric served as the integrating band and the bottom electrode, respectively. Then, the PDMS-based grid (10 mm × 10 mm × 2 mm) was coated with a very thin copper film via radio frequency sputtering followed by being immersed into graphene oxide dispersion as a *p*-type TE material. To evenly coat the grid with the TE material, the immersed substrate was subsequently coated by reduced graphene oxide (rGO) nano-sheets. After that, the top side of the developed TEG was covered with another conducting fabric as the upper electrode. The results showed that the fabricated TEG generated the output voltage of 57.33 mV/g at a temperature difference of 50°C. In addition, integrating 7 units of the developed grid-based TEG together generated the maximum power density of 4.19 μW/g at a temperature difference of 15°C.

Color in online

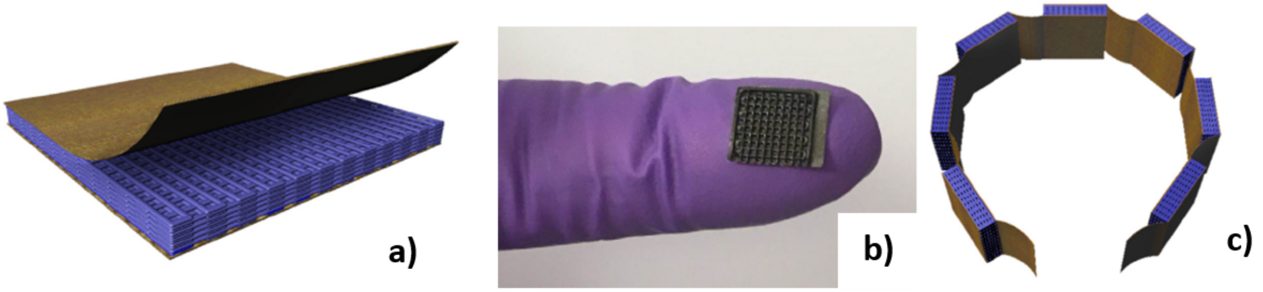

Fig. 29. a) Schematic of the 3D printed PDMS grid; b) Photo of the fabricated grid-based TEG; c) Schematic design of integrating 7 units of the developed grid-based TEGs together [120].

Likewise, Liu et al. [121] developed a cross-plane TEG based on film-shaped legs, but the authors utilized the electrokinetic effect rather than the Seebeck effect to harvest the thermal energy and convert it into electrical energy. To specify, the authors developed a hollow cuboid bracelet as a wearable TEG enclosed with an aluminium sheet from the top and bottom. The other four sides of the cuboid bracelet were covered with a transparent sideboard (from the lengths) and a thermal insulator (from the widths). In the hollow, the hot substrate (i.e. the bottom aluminium sheet) was covered with an insulation layer to tune the heat transfer from the skin into the bracelet. As part of the TE generation process, the bracelet was partially filled with deionized water from the widths.

To generate electricity, a porous carbon film consisted of a carbon film and interconnected carbon nanoparticles was mounted on the insulation layer of the hot substrate, while its two ends were immersed into the deionized water. Due to the temperature difference between the hot and cold substrates, a vapour pressure gradient occurred inside the bracelet, resulting in the evaporation of the absorbed water in the carbon film. After facing the cold substrate, the escaped vapour condensed and flowed back to the water reservoir to repeat the cycle. Therefore, this closed cycle constantly generated electricity based on water flow through the porous carbon film. The results revealed that at 13°C temperature gradient, the TE bracelet generated the highest output voltage of 1V. It should be noted that to guarantee a constant temperature difference, an aluminium heatsink in the form of plate fins were attached to the cold substrate (i.e. top aluminium sheet) and the spaces between them were filled with phase change materials.

4.3. Hybrid TE materials

Inorganic TE materials benefit greatly from excellent Seebeck coefficients but suffer from high thermal conductivities and brittleness. Regarding organic TE materials, they take advantage from low thermal conductivities and proper film-forming performance, they but suffer from extremely low power factors and stability issues [122]. Thus, it is expected to make up the shortages of these two types of TE materials by combining them together. To put it another way, hybrid TE materials comprised of inorganic nanostructures in a matrix of conducting polymer take advantage from both the inherently low thermal conductivity of the polymer and the high power factor of the inorganic filler [123]. The promising methods for preparing hybrid TE materials include physical mixing, in situ polymerization, in situ synthesis, ex-situ synthesis, and layer-by-layer self-assembling [124-126]. As mentioned before, power factor is a critical parameter for assessing the performance of a TEG. Thus, so far, extensive research has been conducted on fabricating hybrid TE materials possessing high power factor. For example, Bae et al. [127] applied H_2SO_4 chemical treatment to improve the power factor of Te-PEDOT: PSS as the hybrid TE material of a unipolar film-shaped TEG. To illustrate, initially, the *p*-type hybrid TE material was spin-coated onto a flexible PET (30mm × 10mm) substrate to fabricate 32 film-shaped TE legs, see Fig. 30. Next, the power factor of the Te-PEDOT: PSS films were improved by being immersed in H_2SO_4 solution. Then, the conductive silver paste was printed onto the glass substrate to electrically connect the legs together. The results showed that the TEG generated the highest output power of 0.7 nW/cm^2 at ΔT of 10°C.

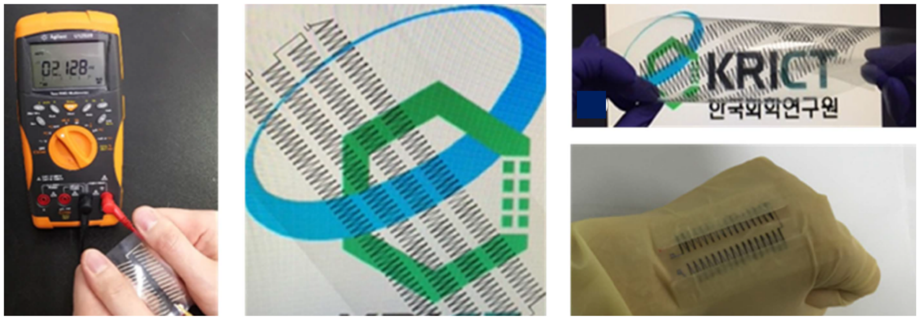

Color in online

Fig. 30. Photos of the flexible and twistable TE generator comprising 240 legs arranged in four rows [127].

Likewise, Bae et al. [128] employed H_2SO_4 chemical treatment to improve the TE properties of the Te–Bi_2Te_3/PEDOT:PSS composites. Using a stencil comprised of 6 rectangular openings, the generated *p*-type TE ink was spray-printed onto a glass substrate. Next, the printed legs were electrically connected together using silver paste. The results showed that at ΔT of 10°C, the fabricated TEG generated the maximum output voltage of 1.54 mV.

However, in another study, Bae et al. [129] replaced the H_2SO_4 chemical treatment with adding a small amount of nanocarbon material to the hybrid composite. The two selected nanocarbon materials were graphene nanoparticles (GNPs) and small bundled single-walled carbon nanotubes (SSWNTs).

Thus, these two additives were individually added to the *p*-type hybrid Te-PEDOT: PSS composite. Then, the two obtained hybrid composites were separately spray-printed onto a glass substrate to fabricate 14 TE legs. Next, the legs were electrically connected together using silver paste as electrodes. The results revealed that at ΔT of 20°C, the TEGs comprised of 8 wt% GNPs -Te-PEDOT: PSS and 3wt% SSWNTs-Te-PEDOT: PSS composites obtained the maximum output powers of 1.7 nW/cm^2 and 31.5 nW/cm^2, respectively.

Regarding hybrid TE materials, since an inorganic TE filler usually shows higher TE properties than the polymer matrix, superior TE properties could be achieved by increasing the inorganic TE component. Accordingly, in situ synthesis is one of the most effective technique to adequately disperse the inorganic nanoparticles in the polymer matrix. Precisely, in this technique, the inorganic nanoparticles are grown inside the polymer matrix using corresponding precursors [130]. Lu et al. [126] applied this technique to grow polycrystal Cu_xSe_y (PC-Cu_xSe_y) nanowires inside the PEDOT: PSS matrix. Then, the prepared flexible PEDOT:PSS/Cu2Se nanocomposite films on nylon membranes was cut into 25 legs (25 mm × 5 mm). Next, the *p*-type legs were pasted onto a polyimide substrate with ~5 mm intervals and electrically connected together with silver paste, see Fig. 31. The results showed that the developed prototype generated the maximum voltage of 4.5 mV at a temperature difference of 6.5°C.

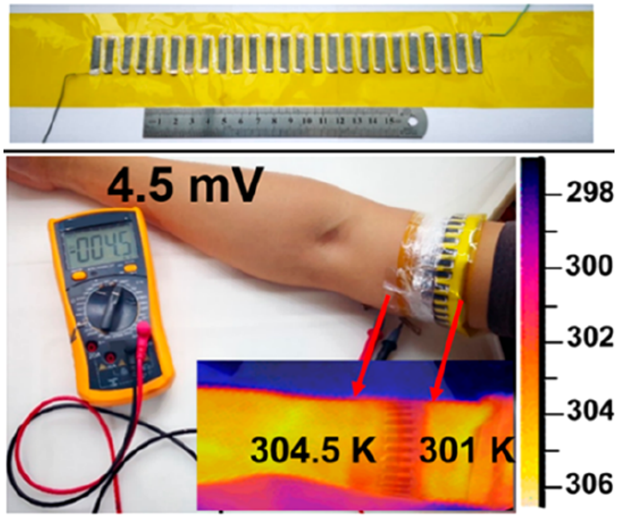

Color in online

Fig. 31. Photos of the developed TEG and the 4.5 mV voltage created at 3.5°C temperature difference [126].

Among all the conducting polymers and inorganic TE materials at room temperature, PEDOT:PSS and BiTe based alloys show the highest TE properties, respectively. However, mixing them together (i.e.

BiTe based alloy/ PEDOT:PSS nanocomposites) results in a lower TE properties than each one. This is owing to the easy oxidation of BiTe based alloy nanostructures and its difficult dispersion in the PEDOT:PSS matrix [131]. Addressing these two issues, Du et al. [131] initially exfoliated the BiTe based alloy particles into nanosheets. Next, the BiTe based nanosheets/ PEDOT:PSS nanocomposites was prepared on nylon membranes by vacuum assisted filtration followed by hot pressing. Then, the prepared *p*-type TE film was cut into five strips (25 mm × 5 mm) followed by being adhered onto a polyimide substrate with ~ 5 mm intervals. Next, the *p*-type TE strips were connected together using silver paint as electrodes. The authors demonstrated that the developed TEG generated 16.9 nW at 47.2°C temperature gradient.

To homogeneously disperse the inorganic TE nanostructures in the polymer matrix, Lu et al. [132] combined in situ synthetization with vacuum assisted filtration. Precisely, the authors prepared *n*-type PEDOT/Ag_2Se/CuAgSe composite film by initially growing Ag2Se/CuAgSe nanowires in PEDOT: PSS. Next, the PEDOT/Ag_2Se/CuAgSe composite was prepared on porous nylon membranes by vacuum assisted filtering followed by hot pressing. After that, the *n*-type film was cut into 11 legs (25 mm × 5 mm) and pasted onto a polyimide substrate with ~5 mm intervals. Then, the two ends of each leg were masked with a layer of gold evaporation as electrodes, see Fig. 32. Next, the electrodes were connected together by painting silver adhesive from one end of each strip to the opposite end of the next closest strip. The authors demonstrated that the maximum power density of the fabricated TEG was about 840 µW/cm^2 at a temperature difference of 36°C.

Color in online

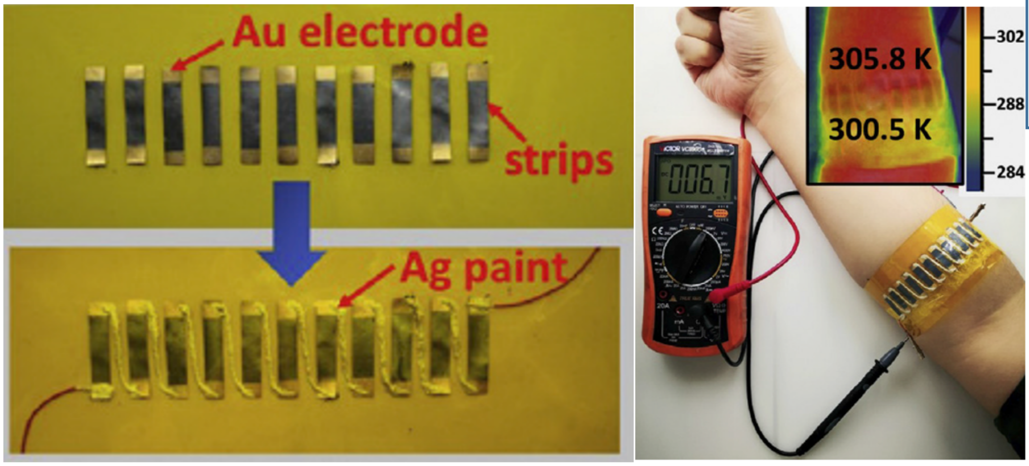

Fig. 32. Photos of the fabricated TEG and its open-circuit voltage after being placed on the arm [132].

However, due to the aging potential and poor biocompatibility of polymers, Zhao et al. [133] proposed replacing the polymer matrix with cellulose nanofibers (CNFs). Regarding cellulose, it is a great substitute for synthetic polymers owing to be abundant, renewable, and natural polymer [134]. Accordingly, Zhao et al. [133] added a small quantity of cellulose nanofibers into *p*-type $Bi_{0.5}Sb_{1.5}Te_3$ and *n*-type $Bi_2Se_{0.3}Te_{2.7}$ powders, resulting in a stable and uniformly dispersed suspension. Then, a vacuum filtration method was applied to prepare the self-supporting *p*-type (CNFs/ $Bi_{0.5}Sb_{1.5}Te_3$) and *n*-type (CNFs/ $Bi_2Se_{0.3}Te_{2.7}$) films. After that, 12 circles (each with the diameter of 5mm) were cut out of the two films in total followed by arranging them in two groups of six on both sides of the arm, see Fig. 33. Then, the TE films were connected together by a silver wire as an electrode. Notably, a silver paste was deposited at the junctions of the wire and TE films to reduce their contact resistance. Ultimately, a carbon conductive tape firmly attached the wire to the films. The results showed that when the TEG was tested at ΔT of 35°C, it generated the highest output voltage of 6.3mV.

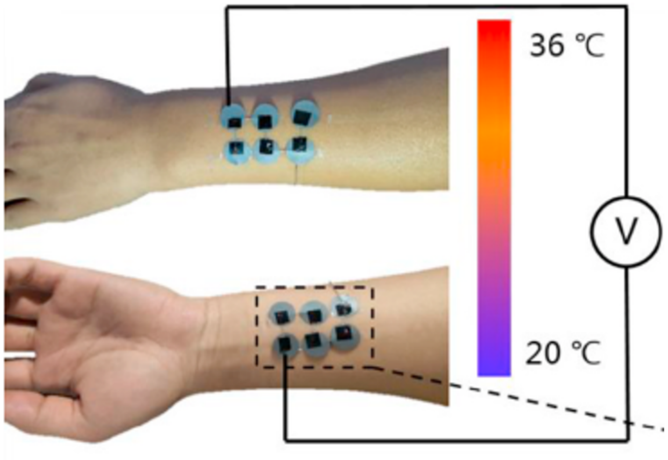

Color in online

Fig. 33. Photo of the fabricated TEG and its mounting position on the arm [133].

Another approach to improve the electrical conductivity and flexibility of hybrid films is using conductive skeletons. To clarify, conductive skeleton performs as a bridge to connect large nanoplates together. Accordingly, Wu et al. [135] used the reduced graphene oxide (RGO) and SWCNTs networks as the conductive skeletons of Bi_2Te_3 and Sb_2Te_3 nanoplates, respectively. Then, the as-assembled flexible *n*-type (RGO/Bi_2Te_3) and *p*-type (SWCNTs/Sb_2Te_3) films were cut into ten uniform strips (30 mm × 3 mm). Next, the TE strips were alternately fabricated onto a one-sided adhesive polyimide tape as the underlying substrate followed by being electrically connected together with a highly conductive silver paste. To isolate the skin from the potential toxicity of the carbon nanomaterials, the air exposed side of the TEG was covered with a soft polyamide film. The results proved that the fabricated TEG comprising 10 thermocouples obtained ~0.7 μW/cm^2 at a temperature gradient of 70°C.

Instead of fabricating the film-shaped hybrid legs onto a flat underlying surface, some researches attempted to fabricate them onto a 3D substrate to take advantage from a greater temperature difference along/across the legs. For example, Xu et al. [136] developed a helical TE bracelet via brush printing TE pastes onto a helical polymer substrate. Precisely, the authors obtained a viscous polymer solution by dissolving Polyurethane (PU) in N,*N*dimethylformamide. Then, a screw was fully coated with the as-prepared polymer solution and dried naturally to develop a helical polymer substrate. To prepare the TE pastes, Bi_2Te_3 (*p*-type) and Bi_2Se_3 (*n*-type) powders were separately mixed with a homemade polyvinylidene fluoride (PVDF) binder. Next, the pastes were split-brushed onto the helical polymer substrate such that they filled the pitches of the screw. After drying the TE films at 80°C for 15 min, they were electrically connected together via a conductive silver paste. When the silver paste was cured in an 80°C oven for about 10 min, the fabricated TEG was peeled off the screw. The results showed that wearing the helical TEG on the arm generated the highest output voltage of 8.9mV at an ambient temperature of ~16°C.

Rather than printing the film-shaped legs onto a 3D substrate, Choi et al. [137] embedded a hybrid film sheet within a 3D substrate. To illustrate, a highly aligned CNT sheet (200 mm × 15 mm) was doped alternately with $FeCl_3$ (*p*-type) and Polyethylenimine (*n*-type) solutions. Notably, the *p*- and *n*-type solutions were doped with 2 mm intervals and the un-doped areas performed as electrodes to connect the legs electrically together. Finally, the doped CNT sheet comprising 9 continuous thermocouples was embedded in a pre-prepared PDMS block, see Fig. 34. Accordingly, the p- and n- parts of the CNT sheet were embedded in the PDMS substrate, leaving the un-doped regions (i.e. electrodes) exposed to the ambient air. The results revealed that when the fabricated prototype was worn on the wrist, it achieved 3.4mV at ΔT of ~7°C.

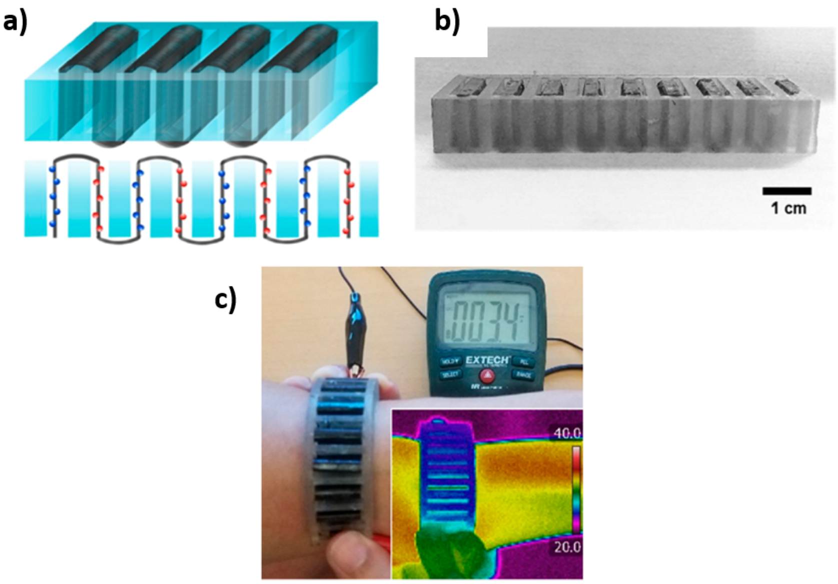

Color in online

Fig. 34. a) Schematic structure of the developed prototype; b) Photo of the prototype; c) Demonstration of the prototype fabricated on the arm [137].

Instead of preparing hybrid films, some researches combined the electrically opposite inorganic and organic legs together. For example, Na et al. [138] electrodeposited *p*-type PEDOT and *n*-type Bi_2Te_3 films onto a fluorine-doped tin oxide (FTO) glass substrate and a stainless steel substrate (SSS), respectively. Then the electrodeposited films were detached from the FTO and SSS substrates using an adhesive tape. Finally, the 10 adhered TE films (each with the dimensions of 5 mm × 15 mm) to the adhesive tape were connected together with a layer of gold evaporation as electrodes. The results proved that at ΔT of 12°C, the highest power density generated by the fabricated TEG was 3.45 nW/cm^2.

Likewise, Du et al. [139] integrated *p*-type organic legs with *n*-type inorganic ones, but the main difference was that only the *p*-type legs were film-shaped and the *n*-type ones comprised of wire. To specify, the authors fabricated an air-permeable and wearable TEG via combining PEDOT: PSS coated films (*p*-type) with Constantan wires (*n*-type). Accordingly, the *p*-type legs were produced by coating a commercial cotton fabric with PEDOT: PSS followed by cutting it into five strips (each strip was 35 mm long and 5 mm wide). Using silver paint as a *p*-type adhesive, the *p*-type strips were adhered with 6 mm intervals to another cotton fabric. Finally, the strips were connected together with a Constantan wires served both as the electrodes and the *n*-type legs. The results demonstrated that the generated

TEG obtained 10.63 nW/cm^2 at ΔT of 74.3°C. Table 3 illustrates the summary of the reviewed literatures on wearable TEGs consisting film-shaped legs.

Table 3. Summary of the recently developed wearable TEGs comprising film-shaped thermocouples.

***P*-type**	***N*-type**	**Couple Number**	**Electrode**	**Substrate**	**ΔT (°C)**	**Output voltage or power**	**Ref**
Inorganic							
n/a	$Bi_2Te_{2.8}Se_{0.2}$	5	Copper foils	Polyimide substrate	20	500 $\mu W/cm^2$	[98]
Au-MoS_2 film	n/a	5	Metal yarn	Fabric	5	2.5mV	[100]
Sb_2Te_3	$Bi_{1.8}Te_{3.2}$	8	SbTe	Polyimide substrate	20	0.016 $\mu W/cm^2$	[101]
$Bi_{0.5}Sb_{1.5}Te_3$	Bi_2Te_3	5	EGaIn	Polyimide substrate	7	14.1 nW	[103]
SnTe	PbTe	32	Aluminium films	Polyimide substrate	120	8.5 mW/cm^2	[105]
$Bi_{0.5}Sb_{1.5}Te_3$	$Bi_2Te_{2.8}Se_{0.3}$	56	Au-Ge	Polyimide substrate	93	18.62 $\mu W/cm^2$	[106]
Sb_2Te_3	$Bi_2Te_{2.7}Se_{0.3}$	10	n/a	Polyimide substrate	20	0.095 $\mu W/cm^2$	[107]
Organic							
PEDOT: PSS: DMSO	Poly[Na(NiETT)]	16	Silicone-based silver ink	Polyester knitted fabric	3	3mV	[110]
PEDOT: PSS	Nitrogen-doped graphene	18	PEDOT: PSS	Plastic substrate	10	0.024 $\mu W/cm^2$	[111]
SWCNT/PEDOT:PSS	SWCNTs/ triphenylphosphine	10	PEDOT: PSS	Polyimide substrate+ PDMS film	20	0.05 $\mu W/cm^2$	[112]
CNT film	polyethylene terephthalate (PET)	3	n/a	Glass substrate	19	0.06 $\mu W/cm^2$	[115]
SWNTs/ PANI	n/a	4	Silver paste	Glass substrate	30	0.012 $\mu W/cm^2$	[116]
PEDOT: PSS	n/a	61	Silver paste	Glass substrate	90	0.025 $\mu W/cm^2$	[117]
n/a	poly[Kx(Ni-ethylenetetrathiolate)]	108	Gold	PET substrate	12	577.8 $\mu W/cm^2$	[118]
poly (acrylic acid) doped CNT	poly(ethylenimine) doped CNT	60	Silver paste	Flexible cable	30	1.95 µW	[119]
Graphene oxide	n/a	7	Cu/Ni coated conducting fabric	PDMS grid	15	4.19 µW/g	[120]
Hybrid							
PEDOT: PSS coated PC-Cu_xSe_y film	n/a	25	Silver paste	Polyimide substrate	6.5	4.5 mV	[126]
Te-PEDOT:PSS	n/a	32	Silver paste	PET substrate	10	7e-4 $\mu W/cm^2$	[127]
Te–Bi_2Te_3/PEDOT:PSS	n/a	6	Silver paste	Glass substrate	10	1.54 mV	[128]
SSWNTs-Te-PEDOT: PSS	n/a	14	Silver paste	Glass substrate	20	0.031 $\mu W/cm^2$	[129]
BiTe /PEDOT:PSS	n/a	5	Silver paint	Polyimide substrate	47.2	16.9 nW	[131]

n/a	PEDOT/Ag_2Se/CuAgSe	11	Gold	Polyimide substrate	36	840 μW/cm^2	[132]
CNF/$Bi_{0.5}Sb_{1.5}Te_3$	CNF/$Bi_2Se_{0.3}Te_{2.7}$	6	Silver wire	n/a	35	6.3mV	[133]
SWCNTs/Sb_2Te_3 film	RGO/Bi_2Te_3 film	10	Silver paste	Polyimide substrate	70	0.7 μW/cm^2	[135]
Bi_2Te_3/PVDF	Bi_2Se_3/PVDF	-	Silver paste	Helical polymer substrate	16	8.9mV	[136]
$FeCl_3$ doped CNT	Polyethylenimine doped CNT	9	CNT	PDMS	7	3.4mV	[137]
PEDOT	Bi_2Te_3	5	Gold	Adhesive film substrate	12	0.003 μW/cm^2	[138]
PEDOT: PSS coated cotton fabric	Constantan wires	5	Constantan wires	TE-strips attached to a cotton fabric using silver paint	74.3	10.63 nW/cm^2	[139]

5. Yarn-shaped thermocouples

5.1. *Inorganic TE materials*

As reviewed in section 4, film-shaped TE legs generate considerably lower output power than the ingot-shaped ones. This is mainly because the former harvests the thermal energy in the in-plane (i.e. length/width) direction, while the latter utilizes the perpendicular temperature gradient formed between the human body and the environment. However, the main privilege of the film-shaped legs over the ingot-shaped ones is their 2D architecture, making them compatible with the curved surfaces of the body. Accordingly, yarn-shaped legs have been developed to take advantage from both the temperature gradient in the thickness direction and flexibility. Regarding the perpendicular temperature difference, a 3D flexible substrate is required to hold thin TE yarns/threads/fibres in 3D space (i.e. upright in the practical direction of the heat flow). For example, Lee et al. [140] attempted to provide an appropriate thickness for a TE yarn by specifying three different weaving patterns for it, including zigzag weave, garter-stitch weave, and plain weave. Based on these three specified weaving patterns, the authors developed three different TE yarns, including *p*- type yarn, *n*-type yarn, and the yarn containing alternate *p*- and *n*-type segments (i.e. integral *p*-*n* yarn). To specify, the individual *p*- and *n*-type yarns were developed by separately coating electrospun polymer nanofiber cores with *n*- (Bi_2Te_3) and *p*- (Sb_2Te_3) type semiconductor sheaths, using radio-frequency-magnetron sputtering technique. Then the coated cores were twisted into separate *n*- and *p*-type yarns. For the integral *p-n* yarn, the authors alternately sputtered strips of Sb_2Te_3 and Bi_2Te_3 on both sides of the electrospun polymer nanofiber cores. Furthermore, narrow gold strips were sputtered at the intervals of the *p*- and *n*-type segments to electrically connect them together. After preparing the TE yarns, the separate *p*- and *n*-type yarns were used for fabricating the zigzag and garter-stitch weaves, whereas the integral *p-n* yarn was used for developing the plain weave. The results demonstrated that at ΔT of 20°C, the approximate output power of the zigzag, garter-stitch, and plain weaving patterns were 0.02 W/m^2, 0.01 W/m^2, and 0.08 W/m^2, respectively.

Apart from providing an appropriate thickness, another approach to improve the efficiency of yarn-based TEGs is applying highly efficient TE martials. To illustrate, Zhang et al. [141] prepared TE fibres with single-crystal SnSe rods owing to their superior mechanical stability, low optical loss, and excellent electrical conductivity. Precisely, *p*-type multicore SnSe fibres were prepared by cladding several single-crystal SnSe rods with borosilicate glass and borosilicate glass rods. Then, 6 multicore SnSe fibres were weaved into a shirt followed by holding them in place by depositing silver films at their two ends. Finally, the TE fibres were serially connected together with copper wires as electrodes. The results illustrated that the TE shirt delivered 30 mV at ΔT of 10 °C.

5.2. *Organic TE materials*

Although inorganic TE materials can be used for fabricating TE yarns, their intrinsic rigidity limits the flexibility of the yarns. Therefore, it is prevalent to apply organic or hybrid TE materials in the fabrication of TE yarns. Furthermore, as mentioned before, using a 2D flat substrate (in-plane design) restricts the output voltage/power of wearable TEGs, because it poorly fit to the perpendicular temperature gradient formed between the human body and the environment. Thus, it is desirable to consider a solution to change the 2D flat substrate into a 3D architecture. Accordingly, using either a 3D spacer fabric or a thick textile is a promising candidate for holding the TE yarns upright in the direction of the perpendicular temperature gradient. Accordingly, Wu & Hu [142] utilized a 3D spacer fabric as the underlying substrate to embroider the TE yarns into it. Regarding the spacer fabric, it consisted of two separate outer fabric layers joined together but kept apart by spacer yarns. To specify, the authors introduced a fibre-shaped TEG by coating commercial polyester yarns with *p*- and *n*-type organic composites. In particular, NWPU/PEDOT: PSS/multi-walled carbon nanotube (MWCNT) and NWPU/nitrogen doped MWCNT were used as the *p*- and *n*-type TE composites, respectively. Then, the prepared TE yarns were alternately embroidered into the lock-nit surface of the 3D spacer fabric. Next, the legs were connected together from the top and the bottom with silver paint as electrode. The results exhibited that the resultant TE fabric comprising 10 thermocouples produced the maximum output power of 0.21 nW/cm^2 at ΔT of 66°C.

Instead of a 3D spacer fabric, Lund et al. [143] used a 3D textile to stitch the p- (PEDOT:PSS coated silk thread) and *n*-type (silver-plated polyamide thread) threads through it. To prepare the *p*-type thread, 100 m of a silk sewing thread was passed through a dye bath that was filled with aqueous PEDOT: PSS dispersion and ethylene glycol. Then the coated thread was dried and treated with dimethyl sulfoxide for 1 hr and 20 min. Finally, the coated thread was dried again at 100°C with a heat gun. Next, the TE legs were formed by stitching the TE threads through 9 layers of a felted wool fabric followed by being electrically connected together with silver paste, as Fig. 35. To cure the paste, the TE textile was placed in a100°C oven for 10 min. The results showed that the developed TE textile comprising 8 thermocouples obtained the maximum output power of 0.04 μW/cm^2 at ΔT of 65°C.

Color in online

Fig. 35. Photos of the embroidered thread-based thermopile [143].

Qu et al. [144] replaced the separate *p*- and *n*-type threads with an integral *p*-*n* thread to sew it onto a 3D fabric-based substrate. To illustrate, the authors developed the *p*-type thread by immersing a cotton thread in the poly(3-hexylthiophene) (P3HT) solution as the *p*-type material. Then, the P3HT coated thread was wrapped around a supporting cell block. To obtain the *n*-type thread, on half of the P3HT coated thread wrapped around the block was brushed with an Ag paste as an *n*-type material. After that, the serial P3HT /Ag coated cotton thread was released from the supporting cell and sewn onto a flexible 3D fabric, see Fig. 36. The results demonstrated that the maximum output power of the device with 13 thermocouples was 1.15 µW at a temperature gradient of 50°C.

Color in online

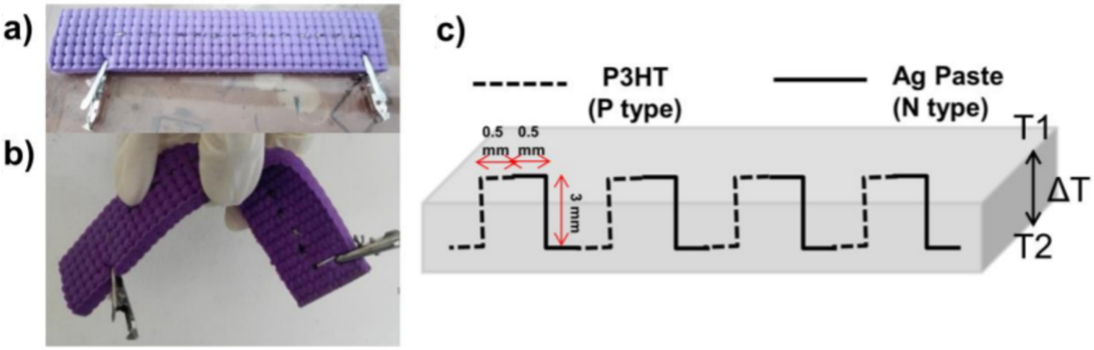

Fig. 36. a) Photo of the fabricated TEG; b) Flexibility of the fabric; c) Schematic of the TEG's structure [144].

Ito et al. [145] not only applied the same technique to fabricate an integral *p*-*n* type thread, but also used electrodes to electrically connect the *p*- and *n*-type segments together. To illustrate, a SWCNT thread was initially injected into a methanol bath and left there for 24 hrs to be converted into a *p*-type thread. Then, the wet thread was pulled out and dried, resulting in a CNT/PEG composite thread. To generate the *n*-type segments, the as prepared *p*-type CNT/PEG composite thread was winded around a long and narrow plastic plate. Then, an *n*-type doping agent called 1-butyl-3-methylimidazolium hexafluorophosphate ([BMIM]PF6) was doped onto one side of the plastic plate, converting the *p*-type thread into the *n*-type. Next, the *p*- and *n*-type segments were electrically connected together by painting conductive silver paste at their junctions. Finally, the stripe patterned thread was sewn onto a thick felt fabric having 3 mm thick and 400mm^2 base area. The authors revealed that at 22°C ambient temperature, the TEG obtained the maximum output power of 0.125 nW/cm^2 when heated by the human body (~37°C).

Zheng et al. [64] applied a weft-knitted spacer fabric as the 3D substrate to directly knit the integral *p-n* type yarn into it. To prepare the *p-n* segmented yarn, a pristine CNT yarn was rolled onto a thin PET-based cylindrical structure. Using a silver paste, two parallel lines were drawn onto the rolled CNT yarn to divide it into three equal segments. Subsequently, the two end segments were immersed into aqueous PEDOT: PSS and PEI/ethanol solutions to form the *p*- and *n*-type legs, respectively, leaving the middle segment pristine. Finally, 966 pairs of the alternately PEDOT: PSS- CNT- PEI immersed yarn was woven into the spacer fabric. The results showed that the developed TE textile generated the maximum output power of 0.14 μW/cm^2 when it was directly put on the arm (ΔT of ~7°C).

To provide the required thickness for the yarn-shaped legs, Lin et al. [146] replaced the 3D fabric-based substrate with a PDMS block. To illustrate, initially *p*-type graphene fibre was developed by sealing a homogeneously mixed graphene oxide and ascorbic acid solution in a polytetrafluoroethylene tube. Then, the obtained *p*-type graphene fibre was taken out of the tube followed by being chemically treated with $N_2H_4 \cdot H_2O$. Next, to obtain an integral *p-n* segmented fibre, the as-prepared *p*-type graphene fibre was rolled onto a plastic rod followed by immersing one half of the rod into the electron donating polyethyleneimine ethoxylated solution, see Fig. 37. Finally, the integral *p-n* graphene fibre comprising 20 thermocouples was woven into a PDMS block to obtain a flexible fibre-based TE device. The results recorded that the highest delivered output power was ~1.3 pW at ΔT of 10 ± 0.5°C.

Color in online

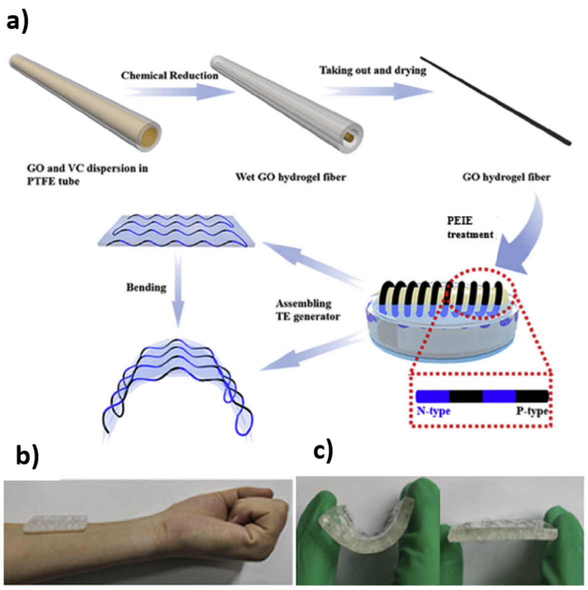

Fig. 37. a) Schematic of the fabrication processes of the integral *p-n* fibre; b) Photo of the fabricated TEG; c) Bendability of the developed TEG [146].

However, the main disadvantages of using a 3D flexible substrate for a yarn-based TEG is that they may cause parasitic loss of temperature difference or deteriorate the flexibility. Thus, rather than using an external object as the 3D substrate, Sun et al. [147] hold the TE yarns in the vertical direction by specifying two different knitting patterns. To illustrate, the authors developed integral *p-n* carbon nanotube fibres (CNTFs) by alternately coating it with active *p-* and *n*-type materials. Accordingly, each carbon nanotube fibre was initially generated by twisting four CNT films together. Then, each CNTF was divided into three alternate segments, including *p*-hybridized, electrode (i.e. the un-doped CNTF), and *n*-doped segments. To fabricate the p-hybridized segments, CNTFs were dipped into a commercial poly(3,4-ethylenedioxythiophene): poly(styrenesulfonate) (PEDOT: PSS) solution. To electrospray the *n*-type oleamine solution onto the CNTFs, both the p-hybridized and the electrode segments were mask shaded with a polypropylene mask. After that, the coated CNTFs were wrapped with acrylic fibres to avoid any short circuit, see Fig. 38. Finally, the authors interlocked 15 thermocouples together in two different patterns, including warp knitting and weft knitting. The results showed that at ΔT of 44°C, the highest output power was achieved by the warp knitting with 7 μW/cm^2.

Color in online

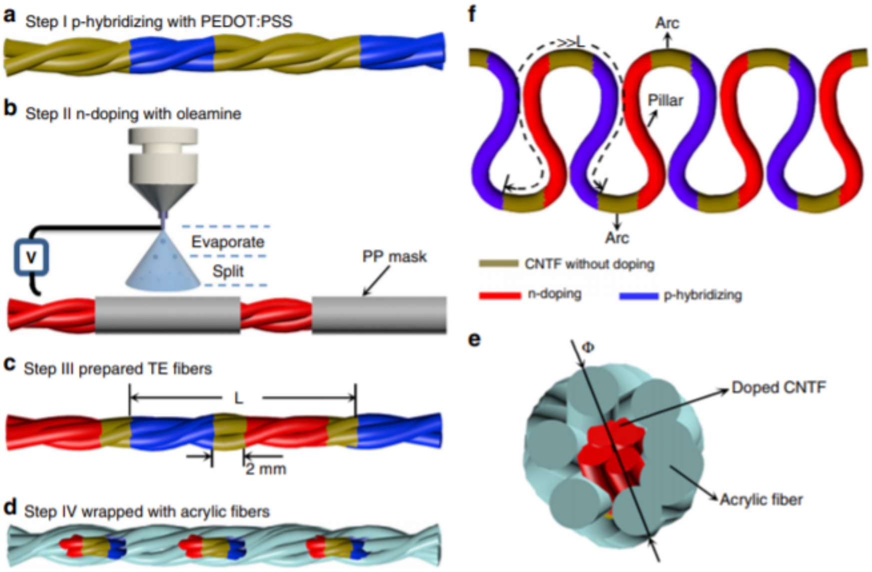

Fig. 38. Schematic of the fabrication procedure of the TE fibre [147].

Allison et al. [148] developed the 3D flexible substrate via folding a 2D flat substrate in half along its x-axis. It is noteworthy that the authors combined *p*-type film-shaped and *n*-type yarn-shaped legs together to develop their fabric-based TEG. To specify, initially p-doped poly(3,4-ethylenedioxythiophene) (PEDOT-Cl) was persistently vapour printed onto a commercial cotton fabric. Then, two rectangles each with the dimensions of 45 mm × 5 mm were cut out of a polyimide stencil to mask shade the vapour printed cotton fabric. Next, *p*-type PEDOT-Cl was screen printed onto the fabric through the two openings of the stencil. After that, the *n*-type carbon fibres were sewn onto the PEDOT-Cl coated fabric such that the two opposite ends of the PEDOT-Cl legs were bonded together. Using cotton thread, squares of silver coated nylon were sewn onto the junctions of the *p*-type PEDOT-Cl films and *n*-type carbon fibres to connect them electrically together. To increase the temperature gradient in the length direction, the cotton substrate was folded in half along the x-axis and then sewn onto a knitted band such that one half was exposed to the ambient air and the other half was buried under the knitted band. The authors demonstrated that the highest output power generated by the as-developed fabric-based TEG was 0.4 nW/cm^2 at ΔT of 30°C.

As mentioned before, apart from holding the TE yarns in the vertical direction, another approach for developing a highly efficient fabric-based TEG is applying highly efficient TE materials. In general, *n*-type organic materials (e.g. conducting polymers and CNTs) show poorer stability (i.e. air and electrical stabilities) and relatively lower TE performance than the *p*-type ones, which greatly hinders the development of the organic-based TE devices [149]. For example, carbon nanotube (CNT) represent a unique 1D carbon allotrope that its structural, electrical, and thermal properties lead to an efficient thermoelectric energy conversion [150]. In spite of the competitive performance of *p*-type CNTs in carbon-based TE materials, the work on *n*-type CNTs is very lacking due to their less stability than *p*-type CNTs. In particular, *n*-type CNTs can be obtained by the introduction of electron donating dopants. However, not only they are susceptible to be de-doped by oxygen in ambient conditions, such that their Seebeck coefficient becomes positive over time, but also they suffer from poor air stability [151-152].

To provide a stable *n*-type CNTs yarn, Lan et al. [153] proposed a chemical treatment to convert a *p*-type CNT yarn into an *n*-type. Accordingly, the authors used common cotton and CNT fibres to develop *p*- and *n*-type fibres, respectively. To prepare the *p*-type fibres, the cotton fibres were treated with absolute ethanol, deionized water, and DMSO followed by being soaked five times in PEDOT: PSS for 24 hrs. To obtain the *n*-type fibres, the *p*-type CNT fibres were treated with PEI, resulting in a high electrical conductivity and Seebeck coefficient with excellent environmental stability. As Fig. 39 shows, 8 pairs of the as-prepared *p*- and *n*-type fibres each with 15 mm length were electrically connected together using silver paste. The results revealed that the developed TEG generated 10 μW at ΔT of 10°C.

Color in online

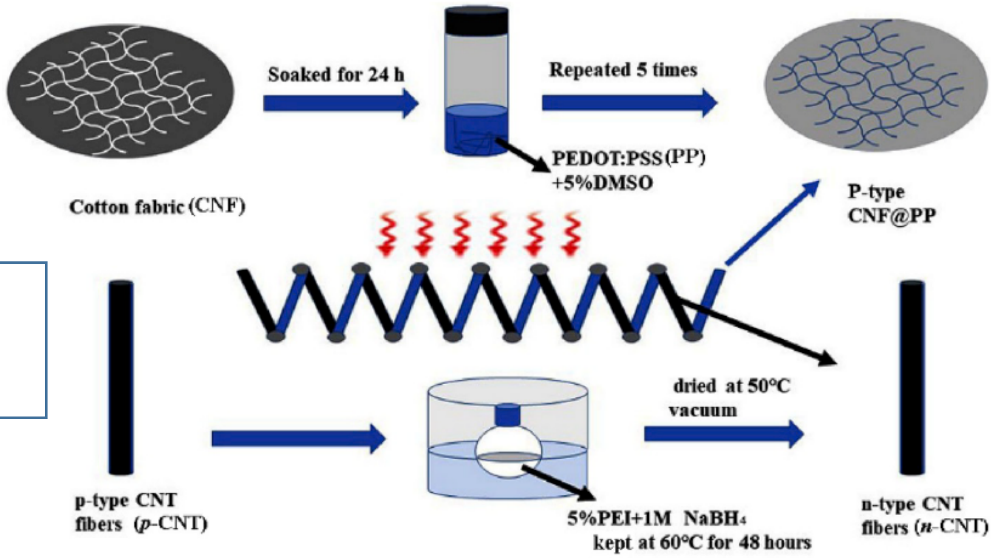

Fig. 39. Schematic of the fabrication processes of the CNF@PP (*p*-type) and the PEI treated CNT (*n*-type) fibres [153].

Ryan et al. [154] demonstrated air-stable organic *n*-type yarns by coating commercial poly(ethylene terephthalate) (PET) sewing threads with the nanocomposits of multiwalled carbon nanotubes (MWNTs) and poly(N-vinylpyrrolidone)(PVP). The authors selected MWNT:PVP nanocomposites owing to its readily air stable *n*-type behaviour. In particular, the authors developed a TE textile via generating *n*- and *p*-type yarns separately and sewing them onto a wool fabric. To produce the *n*-type yarns, commercial PET sewing threads were sequentially coated with poly(N-vinylpyrrolidone), MWNTs, and polystyrene-b-polyisoprene-b-polystyrene block copolymer served as the adhesion layer, the conducting layer, and the protection layer, respectively. To prepare the *p*-type yarns, commercial silk yarns were dyed by being submerged in pol y (3, 4 - ethylenedioxythiophene): poly(styrenesulfonate) (PEDOT: PSS) solution. Then, as Fig. 40 depicts, 38 pairs of the TE yarns (with 40 mm length) were alternately sewn onto a fabric followed by being electrically connected together with a conductive carbon-based paste. The results depicted that when the TE textile was heated and cooled from the opposite lengths, it obtained the maximum output power of 7.1 nW at a temperature gradient of 80°C.

Color in online

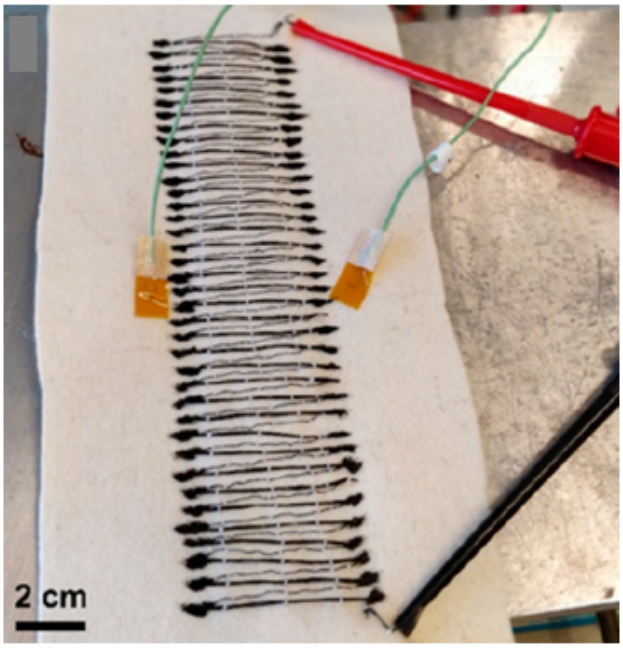

Fig. 40. All organic in-plane embroidered textile TE device with 38 *n-p* elements [154].

Hardianto et al. [155] replaced CNT with carbon fibre owing to its fantastic strength and lightweight. Accordingly, the authors stitched an *n*-type pristine carbon fibre tow onto a 120 mm × 120 mm polyester fabric in a way that the carbon fibre floated on both sides of the polyester fabric. Notably, the length of each float was around 10 mm. As a prerequisite, roughly half of every floats on both sides of the fabric was mask shaded by acrylic dispersion to electroplate the other half with nickel particles as the *p*-type material, see Fig. 41. The results illustrated that the prototype with 105 carbon-nickel thermojunctions generated the highest output power of 0.041 nW/cm^2 at ΔT of 2°C.

Color in online

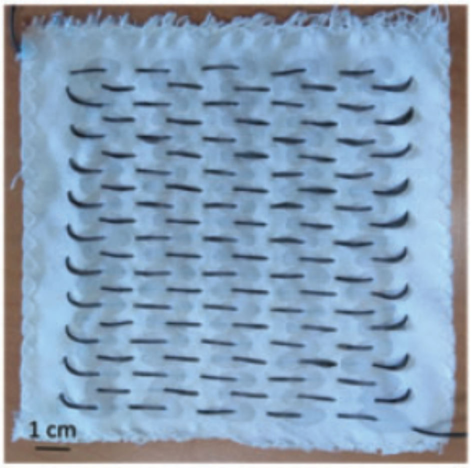

Fig. 41. The fabricated textile-based TEG [155].

Conducting polymers are another organic TE materials that have gained extensive attention for fabricating textile-based TEGs. For example, the electrically conductive polymer PEDOT:PSS has gained particular attention due to its highly conductive properties, solution processability, and remarkable easy doping [156]. In fact, the chain packing order of conducting polymers have strong impact on their TE properties [157]. For example, the power factor of a one-dimensional PEDOT:PSS fibre is 15 times greater than that of a two-dimensional PEDOT:PSS film processed at the same condition. Thus, Wen et al. [158] attempted to produce one-dimensional PEDOT:PSS fibres through a continuous wet-spinning process followed by a one-step treatment with sulfuric acid (H_2SO_4). Regarding wet spinning, polymer powder is dissolved in a suitable solvent followed by the extrusion of the polymer solution through spinning into a solvent-non solvent mixture (coagulant). After preparing one dimensional PEDOT: PSS fibres, they were sewn in diagonal pattern onto a flexible Kapton tape, resulting in 5 *p*-type legs, as Fig. 42 depicts. Then, *n*-type nickel wires (with 30 mm length) were sewn from one end of each *p*-type leg to the opposite end of the closet leg, resulting in 5 thermocouples. The results showed that when one end of the fibrous TEG was touched by fingertip and the other end was exposed to the air, it delivered an open-circuit voltage of 0.72 mV at ΔT of 3.6°C.

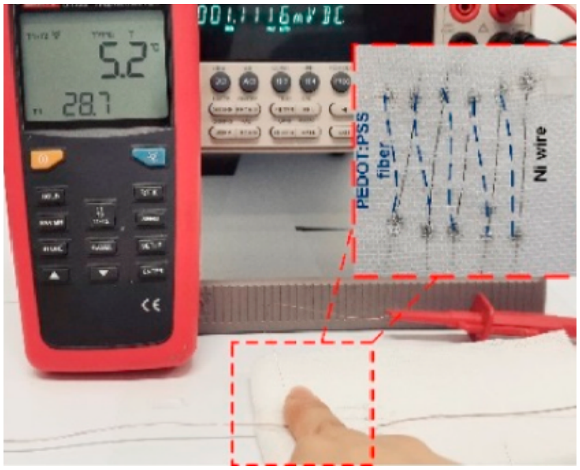

Color in online

Fig. 42. The in-plane TE power generation with fingertip, while the fibrous TEG was sewn onto a piece of cloth [158].

Likewise, Kim et al. [159] combined the wet-spinning and post-treatment methods together to prepare single-walled CNT/PEDOT:PSS composite fibres. To clarify, aqueous CNTs / PEDOT: PSS paste was directly spun into methanol as the coagulation solvent. Notably, the CNTs and PEDOT: PSS content of the paste acted as the *n*- and *p*-type materials, respectively. Thus, the spun paste was extruded into the solvent and turned into the CNT/PEDOT: PSS composite fibres. Next, the fibres were removed from the methanol bath and dried on a hotplate at 180°C for 10 min. Then, either the *p*- or *n*-type power factor of the composite fibres was improved by being immersed in hydrazine solutions or PEI infiltration, respectively. Finally, the authors fabricated a TEG by sewing 12 pairs of *p*- and *n*-type fibres (with 15 mm length) onto a PDMS substrate, see Fig. 43. While the legs were sewn in a zigzag pattern, they were electrically connected together with a silver paste. The results revealed that the TEG generated the maximum output power of 0.015 μW/cm^2 at 10°C temperature difference.

Color in online

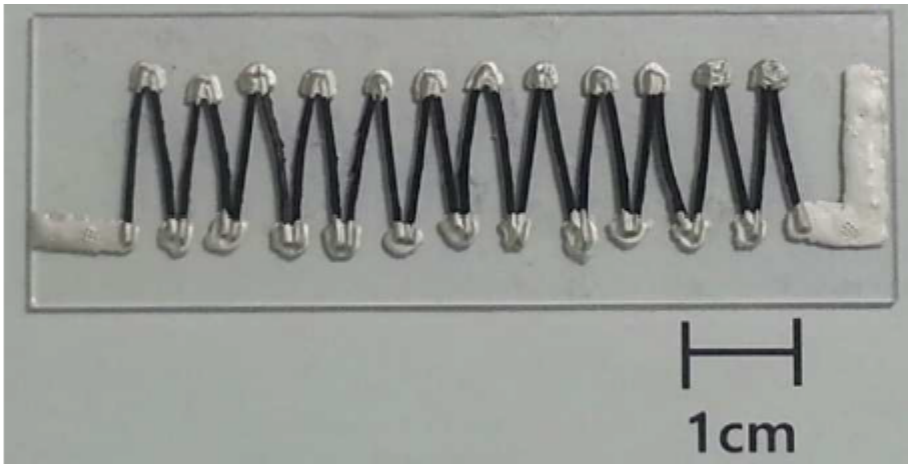

Fig. 43. Photo of the organic fibre-based TE generator sewn onto a PDMS substrate [159].

5.3. Hybrid TE materials

Hybrid TE materials benefit from both the low thermal conductivity and flexibility of TE polymers and the high power factor of inorganic TE materials [160]. Moreover, the combination of organic and inorganic materials arises interfacial transport properties in the resultant hybrid TE material, resulting in the enhancement of the $Z\overline{T}$ value [161]. Thus, Xu et al. [162] combined PEDOT: PSS and tellurium (Te) nanowires together to take advantage from both the high flexibility and low thermal conductivity of the former and the high Seebeck coefficient of the latter. Precisely, the authors generated *p*-type

PEDOT: PSS/ Te fibres by a wet-spinning process to develop a TE textile. Accordingly, tellurium (Te) nanowires were dispersed into deionized water followed by adding PEG and PEDOT: PSS pellets to it, respectively. Then, the dispersions were extruded in the coagulation bath (i.e. Isopropanol solution). The resultant fibre was collected from the bath and placed in a sealed device containing 1 mL of ethylene glycol and dried at 120°C for 1 hr. Next, the surface of the *p*-type PEDOT: PSS/ Te fibre was periodically brushed at equal intervals (i.e. 6.5 mm) with conductive silver paste as electrodes, see Fig.44. Finally, the as-prepared TE fibre was sewn onto a polymer textile and worn on the arm. The authors revealed that the highest output power of the developed TEG at ΔT of 41°C was 197.9 nW.

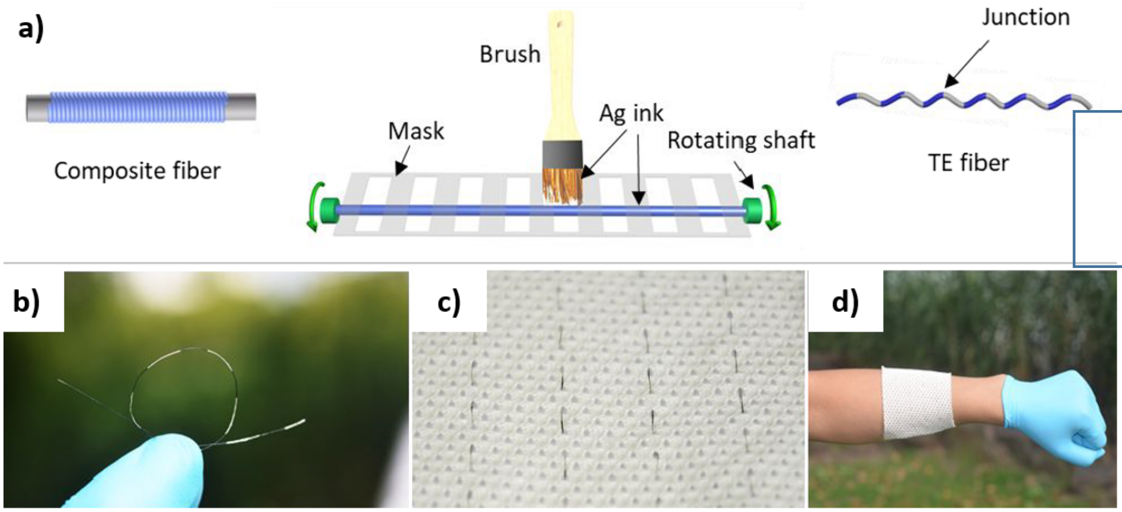

Color in online

Fig. 44. a) Schematic illustration of the fabrication processes of the TE fibres; b-d) Photos of TE fibre, TE fabric, and the application demo [162].

Choi et al. [163] considered a 3D flexible structure to not only hold the TE yarn in the 3D space, but also use it as the supporting unit to produce the TE yarn. To specify, initially a carbon nanotube yarn was wounded around a PDMS block. Then, one side of the block was p-doped by being immersed into $FeCl_3$ ethanol solution for 30 min followed by being well dried in the ambient condition, as Fig. 45 illustrates. For the n- doping, the opposite side of the PDMS block was doped with polyethyleneimine ethanol solution for 30 min. Therefore, the two opposite un-doped sides of the PDMS block served as electrodes. The results demonstrated that at ΔT of 65°C, the output power of the TEG increased from 1.4 μW to 4 μW when the number of thermocouples raised from 60 to 240. Table 4 illustrates the summary of the reviewed literatures on wearable TEGs consisting yarn-shaped legs.

Color in online

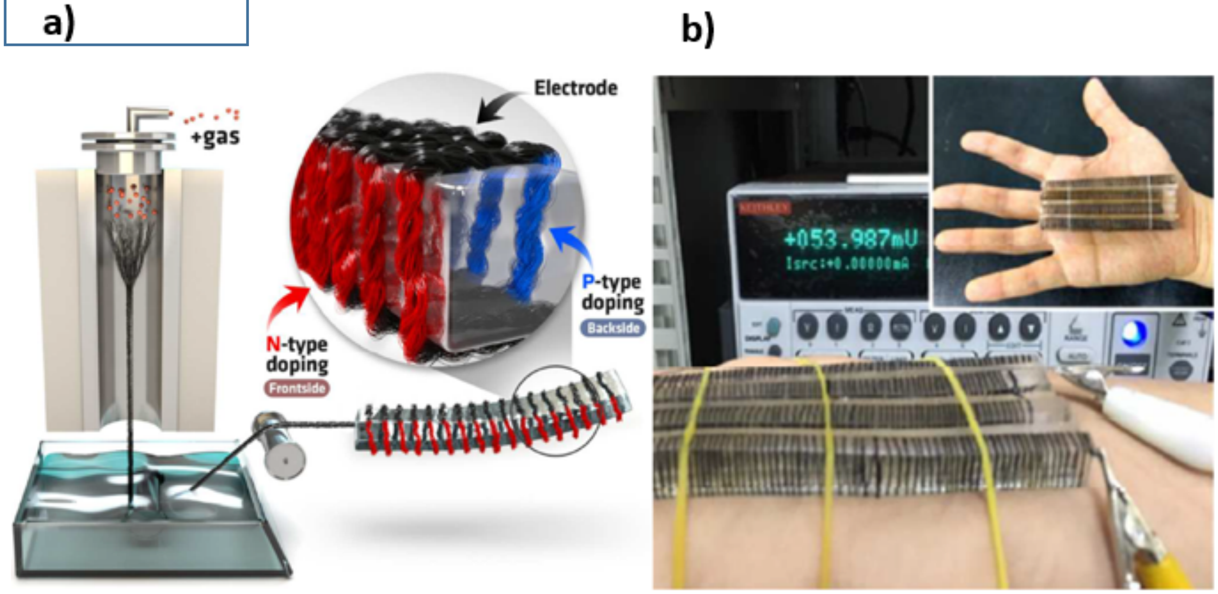

Fig. 45. a) Schematic illustration of the doping process; b) Photo of the fabricated TEG [163].

Table 4. Summary of the recently developed wearable TEGs comprising yarn-shaped thermocouples.

***P*-type**	***N*-type**	**Number**	**Electrode**	**Substrate**	**ΔT (°C)**	**Output**	**Ref**
Inorganic							
Sb_2Te_3	Bi_2Te_3	30	Gold	Knitting into a textile	20	8 μW /cm^2	[140]
SnSe	n/a	6	Copper wire	Weaving into a fabric	10	30mV	[141]
Organic							
PEDOT: PSS coated CNT yarn	PEI/ethanol coated CNT yarn	966	Pristine CNT yarn	Weaving into a fabric	7	0.14 μW/ cm^2	[64]
NWPU/PEDOT: PSS/ MWCNT coated polyester yarn	NWPU/ MWCNT coated polyester yarn	10	Silver paint	Embroidered into the lock-nit surface of a spacer fabric	66	0.21 nW/cm^2	[142]
PEDOT:PSS coated silk thread	Silver-plated polyamide embroidery thread	8	Silver paste	Stitching through 9 layers of felted wool fabric	65	0.04 μW/ cm^2	[143]
P3HT coated cotton thread	Ag pasted P3HT/ cotton thread	13	n/a	Sewing into a fabric	50	1.15 μW	[144]
CNT/PEG	1-butyl-3-methylimidazolium hexafluorophosphate doped CNT/PEG	-	Silver paste	Sewing into a felt fabric	15	0.125 nW/cm^2	[145]
Graphene fibres	PEIE coated graphene fibres	20	n/a	Weaving into PDMS substrate	10	1.3 pW	[146]
PEDOT:PSS doped carbon nanotube fibres	Oleamine solution sprayed carbon nanotube fibres	15	Carbon nanotube fibres	Wrapping with acrylic fibres	44	7 μW /cm^2	[147]
PEDOT-Cl printed cotton fabric	Carbon fibres	2	Silver-coated nylon	Printing and sewing onto a commercial cotton fabric	30	0.4 nW/ cm^2	[148]
PEDOT:PSS coated cotton fabric	Polyethylenemine treated carbon nanotube	8	Silver paste	Connecting with silver paste	10	10 μW	[153]
PEDOT: PSS dyed silk yarns	PVP- MWNTs- SIS coated PET yarns	38	Conducting carbon-based paste	Sewing into a fabric	80	7.1 nW	[154]
Nickle coated carbon fibre	Carbon fibres	105	n/a	Stitching onto polyester fabric	2	0.041 nW/cm^2	[155]
PEDOT: PSS fibres	nickel wires	5	n/a	Sewing into a fabric	3.6	0.72 mV	[158]
Hydrazine immersed	PEI infiltrated CNT/PEDOT: PSS composite fibre	12	Silver paste	Sewing into PDMS substrate	10	0.015 μW /cm^2	[159]

CNT/PEDOT: PSS composite fibre							
Hybrid							
PEDOT: PSS/ tellurium nanowires	n/a	-	Silver paste	Sewing into a polymer matrix	41	197.9 nW	[162]
FeCl$_3$ ethanol doped carbon nanotube yarn	Polyethyleneimine ethanol doped carbon nanotube yarn	240	Un-doped carbon nanotube yarn	Wounding around a PDMS block	65	4 µW	[163]

6. Challenges and future trends

As a relatively new research field, the development of wearable TEGs is confronted with several challenges that can be classified into passive and active categories. Regarding the passive challenges, the output voltage/power of wearable TEGs depend on several environmental factors that are variable and out of the control of the designers, such as air temperature, air velocity, air humidity, and skin temperature. Notably, human body sustains its basic functions by maintaining a stable internal temperature. Thus, the brain regulates the body temperature by shivering, sweating, vasodilation, and vasoconstriction to function within a narrow range (3°C to 4°C) from 36.8°C [164]. Based on Fig. 1, the temperature differences between different body parts and the ambient environment are no more than 20°C. As a result, the expected energy from wearable TEGs is in the range of between µW/cm^2 and nW/cm^2. Therefore, the challenges for practical application of wearable TEGs at such a low temperature difference are related to the active categories, meaning the design of the TEGs. In fact, the key challenge is addressing the following active challenges/requirements simultaneously.

First and foremost, the most fundamental requirement according to Equations 2 and 4 is developing air-stable and high performance TE materials at room temperatures. Second, the structure of wearable TEGs must efficiently capture the perpendicular temperature gradient between the skin and the ambient to provide high power density. Third, wearable TEGs are required to be highly flexible to enable sufficient thermal contact with curved surfaces of the body and avoid cumbersome for the wearers. To fulfil the flexibility requirement, the promising approach is applying organic TE materials to fabricate 2D film- or yarn-shaped TE legs. However, this solution is in conflict with the first and second requirements, namely; applying high performance TE materials and capturing the cross-plane temperature gradient. This is mainly because inorganic TE materials are more efficient than the organic ones, but due to their rigidity they are not suitable for producing 2D film- or yarn-shaped TE legs. In addition, the 2D TE legs mostly harvest the low in-plane temperature gradient instead of the greater cross-plane one. Although it is possible to fabricate the 2D legs onto a 3D substrate, but this may cause the challenges of parasitic loss of temperature difference or offsetting the flexibility of the 2D legs.

Therefore, fulfilling these three incompatible requirements at the same time is the current challenge of researchers in this field. In addition, since wearable TEGs are subject to the low temperature differences and the consequent low properties of TE materials, they cannot always fulfil the power requirement of the electronic devices. To overcome this issue, hybrid energy harvesting technology is becoming an emerging consensus. This approach benefits from both scavenging energy from multiple sources and converting energy into electricity by multiple types of transduction mechanisms [165]. Accordingly, wearable TEGs can be coupled with either triboelectric generators [166], piezoelectric generators [167], or a light-to-thermal conversion layer [168] to fulfil the power requirement at different levels.

Addressing the requirements of flexibility and cross-plane design at the same time, the future trend would be toward fabricating the 2D legs onto a hollow and flexible 3D supporting structure, such as Y-type [169], corrugated [170], foldable origami [171], and spring-shaped [172] structures. It should be added that so far the flexible heatsinks developed for wearable TEGs are mostly composed of heavyweight materials (e.g. copper sheets, hydrogel layers, etc.). Thus, there is a tremendous opportunity to replace the 3D heavyweight heatsinks with either hollow and flexible 3D heatsinks or 2D heatsinks having higher thermal conductivities. Moving toward 2D heatsinks, it is possible to apply them for the film- and yarn-shaped legs as well. Last but not least, wearable TEGs are considered as a renewable alternative for fossil-fuel based power generations. Although a few studies carried out life cycle impact assessment of TE materials [66] and TEGs [173-174] from a specific perspective, but this part is heavily neglected in the existing research on wearable TEGs. Therefore, as part of the sustainability criteria for future technologies, the environmental performance of wearable TEGs requires careful attention.

7. Conclusions

This review provides an overview of different materials and configurations of the TE legs in wearable TEGs to pave the way for comparing the output voltages/powers of the resultant TEGs with each other. Accordingly, it demonstrates both the procedure of fabricating different configurations with different TE materials and the resultant output voltages/powers of the wearable TEGs. Among different types of TE materials, the inorganic ones specifically Bi_2Te_3 and its alloys are the most popular candidate to generate the ingot-shaped thermocouples. It has been attempted to improve the flexibility of the ingot-shaped legs by embedding them in a polymer-based flexible substrate. However, fully coating the legs with the polymer-based substrate negatively affects the output power of the wearable TEGs. To overcome this issue, high thermal conductivity additives can be added to the flexible substrates around the junctions. In addition, several heatsinks have been developed to further increase the output power of the ingot-shaped legs. However, since these heatsinks are bulky, they add to the weight of the wearable TEGs and inevitably cause cumbersome for the wearers. To solve these problems, the researchers switched their focus from the ingot-shaped legs to the film-shaped one. Notably, the contribution of all the three types of TE materials to the preparation of film-shaped legs is the same. Comparing the output power of the inorganic ingot-shaped thermocouples with that of the inorganic film-shaped ones, obviously the former is superior to the latter. To specify, to generate a specific amount of output power, the inorganic film-shaped legs require higher temperature gradient and number of thermocouples than the inorganic ingot-shaped ones. To solve this issue, some researchers attempted to replace the 2D underlying substrate of the film-shaped legs (mostly a polyimide-based substrate) with a 3D one such as a PDMS cable or block. Based on these attempts, yarn-shaped TE legs have been developed, which could be easily sewn onto fabrics and be worn. Based on the reviewed papers, the organic TE materials are the most dominant TE materials utilized for developing the yarn-shaped legs. Comparing the organic film-shaped thermocouples with the yarn-shaped ones, the former provides greater output power due to its larger contact area with the heat source (the skin). Therefore, further improvement of the wearable TEG requires addressing the flexibility and weight of the heatsinks, developing more efficient organic and hybrid TE materials, and increasing the contact area between the yarn-shaped legs and the skin.

References

[1] Z. Fan, Y. Zhang, L. Pan, J. Ouyang, Q. Zhang, Recent developments in flexible thermoelectrics: From materials to devices, Renew. Sustain. Energy Rev. 137 (2020) 110448, https://doi.org/10.1016/j.rser.2020.110448.

[2] Y.G. Park, S. Lee, and J.U. Park, Recent progress in wireless sensors for wearable electronics, Sens. 19 (20) (2019) 4353, https://doi.org/10.3390/s19204353.

[3] W.H. Cheong, B. Oh, S.H. Kim, J. Jang, S. Ji, S. Lee, J. Cheon, S. Yoo, S.Y. Lee, J.U. Park, Platform

for wireless pressure sensing with built-in battery and instant visualization, Nano Energy 62 (2019) 230-238, https://doi.org/10.1016/j.nanoen.2019.05.047.

[4] C.M. Nguyen, P.K. Kota, M.Q. Nguyen, S. Dubey, S. Rao, J. Mays, J.C. Chiao, Wireless power transfer for autonomous wearable neurotransmitter sensors, Sens. 15 (9) (2015) 24553-24572, https://doi.org/10.3390/s150924553.

[5] S.R. Khan, S.K. Pavuluri, G. Cummins, M.P.Y. Desmulliez, Wireless power transfer techniques for implantable medical devices: A review, Sens. 20 (12) (2020) 3487, https://doi.org/10.3390/s20123487.

[6] K. Li, Q. He, J. Wang, Z. Zhou, X. Li, Wearable energy harvesters generating electricity from low-frequency human limb movement, Microsyst. Nanoeng. 4 (2018) 24, https://doi.org/10.1038/s41378-018-0024-3.

[7] N. Sezer, M. Koç, A comprehensive review on the state-of-the-art of piezoelectric energy harvesting, Nano Energy 80 (2021) 105567, https://doi.org/10.1016/j.nanoen.2020.105567.

[8] P. Maharjan, T. Bhatta, M. Salauddin Rasel, M. Salauddin, M. Toyabur Rahman, and J. Y. Park, High-performance cycloid inspired wearable electromagnetic energy harvester for scavenging human motion energy, Appl. Energy 256 (2019) 113987, https://doi.org/10.1016/j.apenergy.2019.113987.

[9] A. Nozariasbmarz, H. Collins, K. Dsouza, M.H. Polash, M. Hosseini, M. Hyland, J. Liu, A. Malhotra, F.M. Ortiz, F. Mohaddes, V.P. Ramesh, Y. Sargolzaeiaval, N. Snouwaert, M.C. Özturk, D. Vashaee, Review of wearable thermoelectric energy harvesting: From body temperature to electronic systems, Appl. Energy 258 (2020) 114069, https://doi.org/10.1016/j.apenergy.2019.114069.

[10] A. Sultana, M.M. Alam, T.R. Middya, D. Mandal, A pyroelectric generator as a self-powered temperature sensor for sustainable thermal energy harvesting from waste heat and human body heat, Appl. Energy 221 (2018) 299-307, https://doi.org/10.1016/j.apenergy.2018.04.003.

[11] A. Zebda, Challenges for successful implantation of biofuel cells, Bioelectrochem. 124 (2018) 57-72, https://doi.org/10.1016/J.BIOELECHEM.2018.05.011.

[12] S. Wang, H. Tai, B. Liu, Z. Duan, Z. Yuan, H. Pan, Y. Su, G. Xie, X. Du, Y. Jiang, A facile respiration-driven triboelectric nanogenerator for multifunctional respiratory monitoring, Nano Energy 58 (2019) 312–321, https://doi.org/10.1016/j.nanoen.2019.01.042.

[13] J. Li, Y. Long, F. Yang, X. Wang, Respiration-driven triboelectric nanogenerators for biomedical applications, EcoMat 2 (3) (2020) e12045, https://doi.org/10.1002/eom2.12045.

[14] E. Katz, P. Bollella, Fuel cells and biofuel cells: From past to perspectives, Isr. J. Chem. 61 (2021) 68-84, https://doi.org/10.1002/ijch.202000039.

[15] A. Zebdaa, J.P. Alcaraz, P. Vadgama, S. Shleev, S.D. Minteer, F. Boucher, P. Cinquin, D.K. Martina, Challenges for successful implantation of biofuel cells, Bioelectrochem. 124 (2018) 57–72, https://doi.org/10.1016/j.bioelechem.2018.05.011.

[16] S. Cosnier, A. Le Goff, M. Holzinger, Towards glucose biofuel cells implanted in human body for powering artificial organs: Review, Electrochem. Commun. 38 (2014) 19-23, https://doi.org/10.1016/j.elecom.2013.09.021.

[17] C. Gonzalez-Solino M. Di Lorenzo, Enzymatic fuel cells: Towards self-powered implantable and wearable diagnostics, Biosens. 8 (1) (2018) 11, https://doi.org/10.3390/bios8010011.

[18] L. Barelli, G. Bidini, E. Calzoni, A. Cesaretti, A. Di Michele, C. Emiliani, L. Gammaitoni, E. Sisani, Enzymatic fuel cell technology for energy production from bio-sources, AIP Conf. Proc. 2191 (1) (2019)

20014, https://doi.org/10.1063/1.5138747.

[19] X. Huang, L. Zhang, Z. Zhang, S. Guo, H. Shang, Y. Li, J. Liu, Wearable biofuel cells based on the classification of enzyme for high power outputs and lifetimes, Biosens. Bioelectron. 124-125 (2019) 40–52, https://doi.org/10.1016/j.bios.2018.09.086.

[20] V.P. Ramesh, Y. Sargolzaeiaval, T, Neumann, V. Misra, D. Vashaee, M.D. Dickey, M.C. Ozturk, Flexible thermoelectric generator with liquid metal interconnects and low thermal conductivity silicone filler, npj Flex. Electron. 5 (2021) 1, https://doi.org/10.1038/s41528-021-00101-3.

[21] S. Khan, J. Kim, K. Roh, G. Park, W. Kim, High power density of radiative-cooled compact thermoelectric generator based on body heat harvesting, Nano Energy 87 (2021) 106180, https://doi.org/10.1016/j.nanoen.2021.106180.

[22] A. Thakre, A. Kumar, H.C. Song, D.Y. Jeong, J. Ryu, Pyroelectric energy conversion and its applications-flexible energy harvesters and sensors, Sens. 19 (9) (2019) 2170, https://doi.org/10.3390/s19092170.

[23] A. Sultana, M.M. Alam, T.R. Middya, D. Mandal, A pyroelectric generator as a self-powered temperature sensor for sustainable thermal energy harvesting from waste heat and human body heat, Appl. Energy 221 (2018) 299–307, https://doi.org/10.1016/j.apenergy.2018.04.003.

[24] Z. Li, Z. Saadatnia, Z. Yang, H. Naguib, A hybrid piezoelectric-triboelectric generator for low-frequency and broad-bandwidth energy harvesting, Energy Convers. Manag. 174 (2018) 188-197, https://doi.org/10.1016/j.enconman.2018.08.018.

[25] M. Zhou, M.S.H. Al-Furjan, J. Zou, W. Liu, A review on heat and mechanical energy harvesting from human - Principles, prototypes and perspectives, Renewable and Sustainable Energy Rev. 82 (2018) 3582–3609, https://doi.org/10.1016/j.rser.2017.10.102.

[26] D. L. Wen, P, Huang. H.Y. Qian, Y.Y. Ba, Z.Y. Ren, C. Tu, T.X. Gong, W. Huang, X.S. Zhang, Hybrid nanogenerator-based self-powered double-authentication microsystem for smart identification, Nano Energy 86 (2021) 106100, https://doi.org/10.1016/j.nanoen.2021.106100.

[27] D.L. Wen, D.H. Sun, P. Huang, W. Huang, M. Su, Ya Wang, M.D. Han, B. Kim, J. Brugger, H.X. Zhang, X.S. Zhang, Recent progress in silk fibroin-based flexible electronics, Microsyst. Nanoeng. 7 (2021) 35, https://doi.org/10.1038/s41378-021-00261-2.

[28] D.L. Wen, X. Liu, H.T. Deng, D.H. Sun, H.Y. Qian, J. Brugger, X.S. Zhang, Printed silk-fibroin-based triboelectric nanogenerators for multi-functional wearable sensing, Nano Energy 66 (2019) 104123, https://doi.org/10.1016/j.nanoen.2019.104123.

[29] Z. Zhang, J. Zhang, H Zhang. H. Wang, Z. Hu, W. Xuan, S. Dong, J. Luo, A portable triboelectric nanogenerator for real-time respiration monitoring, Nanoscale Res. Lett. 14 (2019) 354, https://doi.org/10.1186/s11671-019-3187-4.

[30] Y.M. Choi, M.G. Lee, Y. Jeon, Wearable biomechanical energy harvesting technologies, Energies 10 (10) (2017) 1-17, https://doi.org/10.3390/en10101483.

[31] J. Fan, C.H. Xiong, Z.K. Huang, C.B. Wang, W.B. Chen, A lightweight biomechanical energy harvester with high power density and low metabolic cost, Energy Convers. Manag. 195 (2019) 641-649, https://doi.org/10.1016/j.enconman.2019.05.025.

[32] H. Shi, Z. Liu, X. Mei, Overview of human walking induced energy harvesting technologies and its possibility for walking robotics, Energies 13 (1) (2020) 86, https://doi.org/10.3390/en13010086.

[33] J. Li, Y. Long, F. Yang, X. Wang, Respiration-driven triboelectric nanogenerators for biomedical

applications, EcoMat 2 (3) (2020) e12045, https://doi.org/10.1002/eom2.12045.

[34] M. Wang, J. Zhang, Y. Tang, J. Li, B. Zhang, E. Liang, Y. Mao, X. Wang, Air-flow-driven Ttriboelectric nanogenerators for self-powered real-time respiratory monitoring, ACS Nano 12 (6) (2018) 6156-6162, https://doi.org/10.1021/acsnano.8b02562.

[35] M.R. Mhetre H.K. Abhyankar, Human exhaled air energy harvesting with specific reference to PVDF film, Eng. Sci. Technol. Int. J. 20 (1) (2017) 332-339, https://doi.org/10.1016/j.jestch.2016.06.012.

[36] H. Xue, Q. Yang, D. Wang, W, Luo. W, Wang. M. Lin, D. Liang, Q. Luo, A wearable pyroelectric nanogenerator and self-powered breathing sensor, Nano Energy 38 (2017) 147-154, https://doi.org/10.1016/j.nanoen.2017.05.056.

[37] Y. Lu, X. Li, K. Cai, M. Gao, W. Zhao, J. He, P. Wei, Enhanced-performance PEDOT:PSS/Cu_2Se-based composite films for wearable thermoelectric power generators, ACS Appl. Mater. Interfaces 13 (1) (2021) 631-638, https://doi.org/10.1021/acsami.0c18577.

[38] A.R.M. Siddique, S. Mahmud, B.V. Heyst, A review of the state of the science on wearable thermoelectric power generators (TEGs) and their existing challenges, Renewable Sustainable Energy Rev. 73 (2017) 730-744, https://doi.org/10.1016/j.rser.2017.01.177.

[39] F. Suarez, A. Nozariasbmarz, D. Vashaee, M. C. Öztürk, Designing thermoelectric generators for self-powered wearable electronics, Energy Environ. Sci. 9 (6) (2016) 2099-2113, https://doi.org/10.1039/C6EE00456C.

[40] K. Pietrzyk, J. Soares, B. Ohara, H. Lee, Power generation modeling for a wearable thermoelectric energy harvester with practical limitations, Appl. Energy 183 (2016) 218-228, https://doi.org/10.1016/j.apenergy.2016.08.186.

[41] A. Fabián-Mijangos, G. Min, J. Alvarez-Quintana, Enhanced performance thermoelectric module having asymmetrical legs, Energy Convers. Manage. 148 (2017) 1372-1381, https://doi.org/10.1016/j.enconman.2017.06.087.

[42] A. Montecucco, J. Siviter, A.R. Knox, Constant heat characterisation and geometrical optimisation of thermoelectric generators, Appl. Energy 149 (2015) 248-258, https://doi.org/10.1016/j.apenergy.2015.03.120.

[43] R.A. Kishore, A. Nozariasbmarz, B. Poudel, M. Sanghadasa, S. Priya, Ultra-high performance wearable thermoelectric coolers with less materials, Nat. Commun. 10 (2019) 1765, https://doi.org/10.1038/s41467-019-09707-8.

[44] Y.G. Lee, Y.G. Lee, J. Kim, M.S. Kang, S.H. Baek, S.K. Kim, S.M. Lee, J. Lee, D.B. Hyuan, B.K. Ju, S.E. Moon, J.S. Kim, B. Kwon, Design and experimental investigation of thermoelectric generators for wearable applications, Adv. Mater. Technol. 2 (7) (2017) 1600292, https://doi.org/10.1002/admt.201600292.

[45] Z. Soleimani, S. Zoras, Y. Cui, B. Ceranic, S. Shahzad, Design of heat sinks for wearable thermoelectric generators to power personal heating garments: A numerical study, IOP Conf. Ser.: Earth Environ. Sci. 410 (2020), 012096, https://doi.org/10.1088/1755-1315/410/1/012096.

[46] A. Myers, R. Hodges, and J.S. Jur, Human and environmental analysis of wearable thermal energy harvesting, Energy Convers. Manage. 143 (2017) 218-226, https://doi.org/10.1088/1755-1315/410/1/012096.

[47] M. Hyland, H. Hunter, J. Liu, E. Veety, D. Vashaee, Wearable thermoelectric generators for human body heat harvesting, Appl. Energy 182 (2016) 518-524, https://doi.org/10.1016/j.apenergy.2016.08.150.

[48] S. Qing, A. Rezania, L.A. Rosendahl, A.A. Enkeshafi, X. Gou, Characteristics and parametric analysis of a novel flexible ink-based thermoelectric generator for human body sensor, Energy Convers. Manage. 156 (2018) 655-665, https://doi.org/10.1016/j.enconman.2017.11.065.

[49] Y. Zhang S.J. Park, Flexible organic thermoelectric materials and devices for wearable green energy harvesting, Polym. 11 (5) (2019) 909, https://doi.org/10.3390/polym11050909.

[50] Y. Wang, L. Yang, X.L. Shi, X. Shi, L. Chen, M.S. Dargusch, J. Zou, Z.G. Chen, Flexible thermoelectric materials and generators: challenges and innovations, Adv. Mater. 31 (29) (2019) 1807916, https://doi.org/10.1002/adma.201807916.

[51] Y. Du, J. Xu, B. Paul, P. Eklund, Flexible thermoelectric materials and devices, Appl. Mater. Today 12 (2018) 366-388, https://doi.org/10.1016/j.apmt.2018.07.004.

[52] Z. Soleimani, S. Zoras, B. Ceranic, S. Shahzad, and Y. Cui, A review on recent developments of thermoelectric materials for room-temperature applications, Sustainable Energy Technol. Assess. 37 (2020) 100604, https://doi.org/10.1016/j.seta.2019.100604.

[53] I. Petsagkourakis, K. Tybrandt, X. Crispin, I. Ohkubo, N. Satoh, T. Mori, Thermoelectric materials and applications for energy harvesting power generation, Sci. Technol. Adv. Mater. 19 (1) (2018) 836-862, https://doi.org/10.1080/14686996.2018.1530938.

[54] C. Li, F. Jiang, C. Liu, P. Liu, J. Xu, Present and future thermoelectric materials toward wearable energy harvesting, Appl. Mater. Today 15 (2019) 543-557, https://doi.org/10.1016/j.apmt.2019.04.007.

[55] L. Wang K. Zhang, Textile-based thermoelectric generators and their applications, Energy Environ. Mater. 3 (1) (2020) 67-79 https://doi.org/10.1002/eem2.12045.

[56] L. Zhang, S. Lin, T. Hua, B. Huang, S. Liu, X. Tao, Fiber-based thermoelectric generators: materials, device structures, fabrication, characterization, and applications, Adv. Energy Mater. 8 (5) (2018) 1700524, https://doi.org/10.1002/aenm.201700524.

[57] R. He, G. Schierning, K. Nielsch, Thermoelectric devices: a review of devices, architectures, and contact optimization, Adv. Mater. Technol. 3 (4) (2018) 1700256, https://doi.org/10.1002/admt.201700256.

[58] H.B. Gao, G.H. Huang, H.J. Li, Z.G. Qu, Y.J. Zhang, Development of stove-powered thermoelectric generators: a review, Appl. Therm. Eng. 96 (2016) 297-310, https://doi.org/10.1016/j.applthermaleng.2015.11.032.

[59] L. Francioso, C. De Pascali, V. Sglavo, A. Grazioli, M. Masieri, P. Siciliano, Modelling, fabrication and experimental testing of an heat sink free wearable thermoelectric generator, Energy Convers. Manage. 145 (2017) 204-213, https://doi.org/10.1016/j.enconman.2017.04.096.

[60] K.K. Jung, Y. Jung, C.J. Choi, J.M. Lee, J.S. Ko, Flexible thermoelectric generator with polydimethyl siloxane in thermoelectric material and substrate, Curr. Appl Phys. 16 (10) (2016) 1442-1448, https://doi.org/10.1016/j.cap.2016.08.010.

[61] Y. Shi, Y. Wang, D. Mei, B. Feng, Z. Chen, Design and fabrication of wearable thermoelectric generator device for heat harvesting, IEEE Rob. Autom. Lett. 3 (1) (2018) 373-378, Jan. 2018, https://doi.org/10.1109/LRA.2017.2734241.

[62] Q.H. Zhang, X.Y. Huang, S.Q. Bai, X. Shi, C. Uher, L.D. Chen, Thermoelectric devices for power generation: recent progress and future challenges, Adv. Eng. Mater. 18 (2) (2016) 194-213, https://doi.org/10.1002/adem.201500333.

[63] K.A. Borup, J. de Boor, H. Wang, F. Drymiotis, F. Gascoin, X. Shi, L. Chen, M.I. Fedorov, E. Müller,

B.B. Iversen, G.J. Snyder, Measuring thermoelectric transport properties of materials, Energy Environ. Sci. 8 (2) (2015), 423-435, https://doi.org/10.1039/C4EE01320D.

[64] Y. Zheng, Q. Zhang, W. Jin, Y. Jing, X. Chen, X. Han, Q. Bao, Y. Liu, X. Wang, S. Wang, Y. Qiu, C. Di, K. Zhang, Carbon nanotube yarn based thermoelectric textiles for harvesting thermal energy and powering electronics, J. Mater. Chem. A 8 (6) (2020) 2984-2994, https://doi.org/10.1039/C9TA12494B.

[65] S.A. Miller, P. Gorai, U. Aydemir, T.O. Mason, V. Stevanović, E.C. Toberer, G.J. Snyder, SnO as a potential oxide thermoelectric candidate, J. Mater. Chem. C 5 (34) (2017) 8854-8861, https://doi.org/10.1039/C7TC01623A.

[66] Z. Soleimani, S. Zoras, B. Ceranic, S. Shahzad, and Y. Cui, The cradle to gate life-cycle assessment of thermoelectric materials: A comparison of inorganic, organic and hybrid types, Sustainable Energy Technol. Assess. 44 (2021) 101073, https://doi.org/10.1016/j.seta.2021.101073.

[67] J. Lei, D. Zhang, W. Guan, Z. Ma, Z. Cheng, C. Wang, Y. Wang, Enhancement of thermoelectric figure of merit by the insertion of multi-walled carbon nanotubes in α-MgAgSb, Appl. Phys. Lett. 113 (2018) 083901, https://doi.org/10.1063/1.5042265.

[68] P. Camacho-Medina, M.A. Olivares-Robles, A. Vargas-Almeida, F. Solorio-Ordaz, Maximum power of thermally and electrically coupled thermoelectric generators, Entropy, 16 (5) (2014) 2890-2903, https://doi.org/10.3390/e16052890.

[69] M. Orrill S. LeBlanc, Printed thermoelectric materials and devices: Fabrication techniques, advantages, and challenges, J. Appl. Polym. Sci. 134 (3) (2017), https://doi.org/10.1002/app.44256.

[70] Y. Liu, Y. Du, Q. Meng, J. Xu, S.Z. Shen, Effects of preparation methods on the thermoelectric performance of SWCNT/Bi2Te3 bulk composites, Mater. 13 (11) (2020) 2636, https://doi.org/10.3390/ma13112636.

[71] C.S. Kim, C.S. Kim, G.S. Lee, H. Choi, Y.J. Kim, H.M. Yang, S.H. Lim, S.G. Lee, B.J. Cho, Structural design of a flexible thermoelectric power generator for wearable applications, Appl. Energy 214 (2018) 131-138, https://doi.org/10.1016/j.apenergy.2018.01.074.

[72] F. Suarez, D.P. Parekh, C. Ladd, D. Vashaee, M.D. Dickey, M.C. Öztürk, Flexible thermoelectric generator using bulk legs and liquid metal interconnects for wearable electronics, Appl. Energy 202 (2017) 736-745, https://doi.org/10.1016/j.apenergy.2017.05.181.

[73] S.J. Jung, J. Shina, S.S. Lim, B. Kwon, S.H. Baek, S.K. Kim, H.H. Park, J.S. Kim, Porous organic filler for high efficiency of flexible thermoelectric generator, Nano Energy 81 (2021) 105604, https://doi.org/10.1016/j.nanoen.2020.105604.

[74] S. Hong, Y. Gu, J.K. Seo, J. Wang, P. Lin, Y.S. Meng, S. Xu, R. Chen, Wearable thermoelectrics for personalized thermoregulation, Sci. Adv. 5 (5) (2019), https://doi.org/10.1126/sciadv.aaw0536.

[75] Y. Wang, Y. Shi, D. Mei, Z. Chen, Wearable thermoelectric generator to harvest body heat for powering a miniaturized accelerometer, Appl. Energy 215 (2018) 690-698, https://doi.org/10.1016/j.apenergy.2018.02.062.

[76] H. Liu, Y. Wang, D. Mei, Y. Shi, Z. Chen, Design of a wearable thermoelectric generator for harvesting human body energy, Wearable Sens. Robots 399 (2017) 55-66, https://doi.org/10.1007/978-981-10-2404-7_5.

[77] J. Yuan, R. Zhu, A fully self-powered wearable monitoring system with systematically optimized flexible thermoelectric generator, Appl. Energy 271 (2020) 115250, https://doi.org/10.1016/j.apenergy.2020.115250.

[78] Y. Eom, D. Wijethunge, H. Park, S.H. Park, W. Kim, Flexible thermoelectric power generation system based on rigid inorganic bulk materials, Appl. Energy 206 (2017) 649-656, https://doi.org/10.1016/j.apenergy.2017.08.231.

[79] A.R.M. Siddique, R. Rabari, S. Mahmud, B. Van Heyst, Thermal energy harvesting from the human body using flexible thermoelectric generator (FTEG) fabricated by a dispenser printing technique, Energy 115 (2016) 1081-1091, https://doi.org/10.1016/j.energy.2016.09.087.

[80] Z. Lu, H. Zhang, C. Mao, C.M. Li, Silk fabric-based wearable thermoelectric generator for energy harvesting from the human body, Appl. Energy 164 (2016) 57-63, https://doi.org/10.1016/j.apenergy.2015.11.038.

[81] H.E. Ahmed, B.H. Salman, A.S. Kherbeet, M.I. Ahmed, Optimization of thermal design of heat sinks: A review, International Journal of Heat and Mass Transfer, 118 (2018) 129-153, https://doi.org/10.1016/j.ijheatmasstransfer.2017.10.099.

[82] A. Elghool, F. Basrawi, T.K. Ibrahim, K. Habib, H. Ibrahim, D.M.N.D. Idris, A review on heat sink for thermo-electric power generation: Classifications and parameters affecting performance, Energy Convers. Manage. 134 (2017) 260-277, https://doi.org/10.1016/j.enconman.2016.12.046.

[83] A. Nozariasbmarz, R.A. Kishore, B. Poudel, U. Saparamadu, W. Li, R. Cruz, S. Priya, High power density body heat energy harvesting, ACS Appl. Mater. Interfaces 11 (43) (2019) 40107-40113, https://doi.org/10.1021/acsami.9b14823.

[84] Y. Shi, Y. Wang, D. Mei, Z. Chen, Wearable thermoelectric generator with copper foam as the heat sink for body heat harvesting, IEEE Access, 6 (2018) 43602-43611, https://doi.org/10.1109/ACCESS.2018.2863018.

[85] H. Park, Y. Eom, D. Lee, J. Kim, H. Kim, G. Park, W. Kim, High power output based on watch-strap-shaped body heat harvester using bulk thermoelectric materials, Energy 187 (2019) 115935, https://doi.org/10.1016/j.energy.2019.115935.

[86] K.T. Settaluri, H. Lo, R.J. Ram, Thin thermoelectric generator system for body energy harvesting, J. Electron. Mater. 41 (6) (2012) 984-988, https://doi.org/10.1007/s11664-011-1834-3.

[87] S.H. Jeong, F.J. Cruz, S. Chen, L. Gravier, J. Liu, Z. Wu, K. Hjort, S.L. Zhang, Z.B. Zhang, Stretchable thermoelectric generators metallized with liquid alloy, ACS Appl. Mater. Interfaces 9 (18) (2017) 15791-15797, https://doi.org/10.1021/acsami.7b04752.

[88] Y. Sargolzaeiaval, V.P. Ramesh, T.V. Neumann, V. Misra, D. Vashaee, M.D. Dickey, M.C. Öztürk, Flexible thermoelectric generators for body heat harvesting-Enhanced device performance using high thermal conductivity elastomer encapsulation on liquid metal interconnects, Appl. Energy 262 (2020) 114370, https://doi.org/10.1016/j.apenergy.2019.114370.

[89] B. Lee, H. Cho, K.T. Park, J.S. Kim, M. Park, H. Kim, Y. Hong, S. Chung, High-performance compliant thermoelectric generators with magnetically self-assembled soft heat conductors for self-powered wearable electronics, Nat. Commun. 11 (2020) 5948, https://doi.org/10.1038/s41467-020-19756-z.

[90] H. Park, D. Lee, D. Kim, H. Cho, Y. Eom, J. Hwang, H. Kim, J. Kim, S. Han, W. Kim, High power output from body heat harvesting based on flexible thermoelectric system with low thermal contact resistance, J. Phys. D Appl. Phys. 51 (36) (2018) 365501, https://doi.org/10.1088/1361-6463/aad270.

[91] M. Zamengo, J. Morikawa, Evaluation of cooling ability for a novel heat sink made of polyvinyl alcohol hydrogel, Int. J. Heat Mass Transfer 143 (2019) 118523, https://doi.org/10.1016/j.ijheatmasstransfer.2019.118523.

[92] L. Llanes, P. Dubessay, G. Pierre, C. Delattre, P. Michaud, Biosourced polysaccharide-based duperabsorbents, polysaccharides 1 (1) (2020) 51-79, https://doi.org/10.3390/polysaccharides1010005.

[93] D. Lee, H. Parka, G, Park, J. Kim, H. Kim, H. Cho, S. Han, W. Kim, Liquid-metal-electrode-based compact, flexible, and high-power thermoelectric device, Energy 188 (2019) 116019, https://doi.org/10.1016/j.energy.2019.116019.

[94] C.S. Kim, H.M. Yang, J. Lee, G.S. Lee, H. Choi, Y.J. Kim, S.H. Lim, S.H. Cho, B.J. Cho, Self-powered wearable electrocardiography using a wearable thermoelectric power generator, ACS Energy Lett. 3 (3) (2018) 501-507, https://doi.org/10.1021/acsenergylett.7b01237.

[95] G. Lee, C.S. Kim, S. Kim, Y.J. Kim, H. Choi, B.J. Cho, Flexible heatsink based on a phase-change material for a wearable thermoelectric generator, Energy 179 (2019) 12-18, https://doi.org/10.1016/j.energy.2019.05.018.

[96] T. Park, H. Lim, J.U. Hwang, J. Na, H. Lee, E. Kim, Roll type conducting polymer legs for rigid-flexible thermoelectric generator, APL Mater. 5 (7) (2017) 074106, https://doi.org/10.1063/1.4979873.

[97] M.S. Hossain, T. Li, Y. Yu, J. Yong, J.H. Bahk, E. Skafidas, Recent advances in printable thermoelectric devices: Materials, printing techniques, and applications, RSC Adv. 10 (14) (2020) 8421-8434, https://doi.org/10.1039/c9ra09801a.

[98] T. Varghese, C. Hollar, J. Richardson, N. Kempf, C. Han, P. Gamarachchi, D. Estrada, R.J. Mehta, Y. Zhang, High-performance and flexible thermoelectric films by screen printing solution-processed nanoplate crystals, Sci. Rep. 6 (1) (2016) 1-6, https://doi.org/10.1038/srep33135.

[99] M.S. Hossain, T. Li, Y. Yu, J. Yong, J.H. Bahk, E. Skafidas, Recent advances in printable thermoelectric devices: Materials, printing techniques, and applications, RSC Adv. 10 (14) (2020) 8421-8434, https://doi.org/10.1039/C9RA09801A.

[100] Y. Guo, C. Dun, J. Xu, P. Li, W. Huang, J. Mu, C. Hou, C.A. Hewitt, Q. Zhang, Y. Li, D.L. Carroll, H. Wang, Wearable thermoelectric devices based on Au-Decorated two-dimensional MoS_2, ACS Appl. Mater. Interfaces 10 (39) (2018) 33316-33321, https://doi.org/10.1021/acsami.8b10720.

[101] Z. Cao, E. Koukharenko, M.J. Tudor, R.N. Torah, S.P. Beeby, Flexible screen printed thermoelectric generator with enhanced processes and materials, Sens. Actuators, A 238 (2016) 196-206, https://doi.org/10.1016/j.sna.2015.12.016.

[102] K.S. Kwon, M.K. Rahman, T.H. Phung, S.D. Hoath, S. Jeong, J.S. Kim, Review of digital printing technologies for electronic materials, Flex. Print. Electron. 5 (2020) 043003, https://doi.org/10.1088/2058-8585/abc8ca.

[103] B. Chen, M. Kruse, B. Xu, R. Tutika, W. Zheng, M.D. Bartlett, Y. Wu J.C. Claussen, Flexible thermoelectric generators with inkjet-printed bismuth telluride nanowires and liquid metal contacts, Nanoscale 11 (12) (2019) 5222-5230, https://doi.org/10.1039/C8NR09101C.

[104] Y. Saberi, S.A. Sajjadi, H. Mansouri, Comparison of thermoelectric properties of Bi_2Te_3 and $Bi_2Se_{0\cdot3}Te_{2.7}$ thin film materials synthesized by hydrothermal process and thermal evaporation, Ceram. Int. 47 (8) (2021) 11547-11559, https://doi.org/10.1016/j.ceramint.2020.12.285.

[105] V. Karthikeyan, J.U. Surjadi. J.C.K. Wong, V. Kannan, K.H. Lam, X. Chen, Y. Lub, V.A.L. Roy, Wearable and flexible thin film thermoelectric module for multi-scale energy harvesting, J. Power Sources 455 (2020) 227983, https://doi.org/10.1016/j.jpowsour.2020.227983.

[106] W. Ren, Y. Sun, D. Zhao, A. Aili, S. Zhang, C. Shi, J. Zhang, H. Geng, J. Zhang, L. Zhang, J. Xiao, R. Yang, High-performance wearable thermoelectric generator with self-healing, recycling, and Lego-like

reconfiguring capabilities, Sci. Adv. 7 (7) (2021) eabe0586, https://doi.org/10.1126/sciadv.abe0586.

[107] D.L. Wen, H.T. Deng, X. Liu, G.K. Li, X.R. Zhang, X.S. Zhang, Wearable multi-sensing double-chain thermoelectric generator, Microsyst. Nanoeng. https://doi.org/10.1038/s41378-020-0179-6.

[108] G.M. Guttmann, Y. Gelbstein, Mechanical properties of thermoelectric materials for practical applications, InTech Open (2018), https://doi.org/10.5772/intechopen.75476.

[109] L. Wang, Y. Liu, Z. Zhang, B. Wang, J. Qiu, D. Hui, S. Wang, Polymer composites-based thermoelectric materials and devices, Composites Part B 122 (2017) 145-155, https://doi.org/10.1016/j.compositesb.2017.04.019.

[110] H.M. Elmoughni, A.K. Menon, R.M.W. Wolfe, S.K.Yee, A Textile-Integrated Polymer Thermoelectric Generator for Body Heat Harvesting, Adv. Mater. Technol. 4 (7) (2019) 1800708, https://doi.org/10.1002/admt.201800708.

[111] Z. Zhang, J. Qiu, S. Wang, Roll-to-roll printing of flexible thin-film organic thermoelectric devices, Manuf. Lett. 8 (2016) 6-10, https://doi.org/10.1016/j.mfglet.2016.04.002.

[112] Z. Zhang, B. Wang, J. Qiu, S. Wang, Roll-to-roll printing of spatial wearable thermoelectrics, Manuf. Lett. 21 (2019) 28-34, https://doi.org/10.1016/j.mfglet.2019.07.002.

[113] D. Yuan. Y. Guo, Y. Zeng, Q. Fan, J. Wang, Y. Yi, X. Zhu, Air-Stable n-type thermoelectric materials enabled by organic diradicaloids, Angew. Chem. Int. Ed. 58 (15) (2019) 4958-4962, https://doi.org/10.1002/anie.201814544.

[114] T. Chiba, Y. Seki, M. Takashiri, Correlation between the air stability of n-type thermoelectric properties and defects in single-walled carbon nanotubes with anionic surfactants, AIP Adv. 11 (1) (2021) 15332, https://doi.org/10.1063/5.0031344.

[115] W. Zhou, Q. Fan, Q. Zhang, Le Cai, K. Li, X. Gu, F. Yang, N. Zhang, Y. Wang, H. Liu, W. Zhou, S. Xie, High-performance and compact-designed flexible thermoelectric modules enabled by a reticulate carbon nanotube architecture, Nat. Commun. 8 (1) (2017) 1-9, https://doi.org/10.1038/ncomms14886.

[116] L. Wang, Q. Yao, J. Xiao, K. Zeng, S. Qu, W. Shi, Q. Wang, L. Chen, Engineered molecular chain ordering in single-walled carbon nanotubes/polyaniline composite films for high-performance organic thermoelectric materials, Chem. Asian J. 11 (12) (2016) 1804-1810, https://doi.org/10.1002/asia.201600212.

[117] L. Stepien, A. Roch , S. Schlaier, I. Dani , A. Kiriy, F. Simon, M.V. Lukowicz, C. Leyens, Investigation of the thermoelectric power factor of KOH-treated PEDOT:PSS dispersions for printing applications, Energy Harvesting Syst. 3 (1) (2015), https://doi.org/10.1515/ehs-2014-0060.

[118] L. Liu, Y. Sun, W. Li, J. Zhang, X. Huang, Z. Chen, Y. Sun, C. Di, W. Xu, D. Zhu, Flexible unipolar thermoelectric devices based on patterned poly[K: X(Ni-ethylenetetrathiolate)] thin films, Mater. Chem. Front. 1 (10) (2017) 2111-2116, https://doi.org/10.1039/c7qm00223h.

[119] K.T. Park, J. Choi, B. Lee, Y. Ko, K. Jo, Y.M. Lee, J.A. Lim, C.R. Park, H, Kim, High-performance thermoelectric bracelet based on carbon nanotube ink printed directly onto a flexible cable, J. Mater. Chem. A 6 (40) (2018) 19727-19734, https://doi.org/10.1039/c8ta08170k.

[120] W. Zeng, X.M. Tao, S. Lin, C. Lee, D. Shi, K.h. Lam, B. Huang, Q. Wang, Y. Zhao, Defect-engineered reduced graphene oxide sheets with high electric conductivity and controlled thermal conductivity for soft and flexible wearable thermoelectric generators, Nano Energy 54 (2018) 163-174, https://doi.org/10.1016/j.nanoen.2018.10.015.

[121] K. Liu, T. Ding, J. Li, Q. Chen, G. Xue. P. Yang, M. Xu. Z.L. Wang. J. Zhou, Thermal-electric nanogenerator based on the electrokinetic effect in porous carbon film, Adv. Energy Mater. 8 (13) (2018) 1702481, https://doi.org/10.1002/aenm.201702481.

[122] X. Wang, F. Meng, T. Wang, C. Li, H. Tang, Z, Gao. S. Li, F. Jiang, J. Xu, High performance of PEDOT:PSS/SiC-NWs hybrid thermoelectric thin film for energy harvesting, J. Alloys Compd. 734 (2018) 121-129, https://doi.org/10.1016/j.jallcom.2017.11.013.

[123] A. Sahu, B. Russ, N.C. Su, J.D. Forster, P. Zhou, E.S. Cho, P. Ercius, N.E. Coates, R.A. Segalman, J.J. Urban, Bottom-up design of de novo thermoelectric hybrid materials using chalcogenide resurfacing, J. Mater. Chem. A 5 (7) (2017) 3346-3357, https://doi.org/10.1039/C6TA09781B.

[124] L. Wang, Z. Zhang, Y. Liu, B. Wang, L. Fang, J. Qiu, K. Zhang, S. Wang, Exceptional thermoelectric properties of flexible organic-inorganic hybrids with monodispersed and periodic nanophase, Nat. Commun. 9 (2018) 3817, https://doi.org/10.1038/s41467-018-06251-9.

[125] H. An, M. Pusko, D. Chun, S. Park, J. Moon, In-situ synthesis of flexible hybrid composite films for improved thermoelectric performance, Chem. Eng. J. 357 (2019) 547–558, https://doi.org/10.1016/j.cej.2018.09.200.

[126] Y. Lu, Y. Ding, Y. Qiu, K. Cai, Q. Yao, H. Song, L. Tong, J. He, L. Chen, Good performance and flexible PEDOT:PSS/Cu 2 Se nanowire thermoelectric composite films, ACS Appl. Mater. Interfaces 11 (13) (2019) 12819-12829, https://doi.org/10.1021/acsami.9b01718.

[127] E.J. Bae, Y.H. Kang, K.S. Jang, S.Y. Cho, Enhancement of thermoelectric properties of PEDOT:PSS and tellurium-PEDOT:PSS hybrid composites by simple chemical treatment, Sci. Rep. 6 (1) (2016) 1-10, https://doi.org/10.1038/srep18805.

[128] E.J. Bae, Y.H. Kang, K.S. Jang, C. Lee, S.Y. Cho, Solution synthesis of telluride-based nano-barbell structures coated with PEDOT:PSS for spray-printed thermoelectric generators, Nanoscale 8 (21) (2016) 10885-10890, https://doi.org/10.1039/c5nr07032e.

[129] E.J. Bae, Y.H. Kang, C. Lee, S.Y. Cho, Engineered nanocarbon mixing for enhancing the thermoelectric properties of a telluride-PEDOT:PSS nanocomposite, J. Mater. Chem. A 5 (34) (2017) 17867-17873, https://doi.org/10.1039/c7ta04280a.

[130] Q. Guo, R. Ghadiri, T. Weigel, A. Aumann, E.L. Gurevich, C. Esen, O. Medenbach, W. Cheng, B. Chichkov, A. Ostendorf, Comparison of in situ and ex situ methods for synthesis of two-photon polymerization polymer nanocomposites, Polym. 6 (7) (2014) 2037-2050, https://doi.org/10.3390/polym6072037.

[131] Y. Du, X. Liu, J. Xu, S. Z. Shen, Flexible Bi-Te-based alloy nanosheet/PEDOT:PSS thermoelectric power generators, Mater. Chem. Front. 3 (7) (2019) 1328-1334 https://doi.org/10.1039/c9qm00087a.

[132] Y. Lu, Y. Qiu, K. Cai, X. Li, M. Gao, C. Jiang, J. He, Ultrahigh performance PEDOT/Ag2Se/CuAgSe composite film for wearable thermoelectric power generators, Mater. Today Phys. 14 (2020) 100223, https://doi.org/10.1016/j.mtphys.2020.100223.

[133] X. Zhao, C. Zhao, Y. Jiang, X. Ji, F. Kong, T. Lin, H. Shao, W. Han, Flexible cellulose nanofiber/Bi2Te3 composite film for wearable thermoelectric devices, J. Power Sources 479 (2020) 229044, https://doi.org/10.1016/j.jpowsour.2020.229044.

[134] S. Dutta, J. Kim, Y. Ide, J.H. Kim, M.S.A. Hossain, Y. Bando, Y. Yamauchi, K.C.W. Wu, 3D network of cellulose-based energy storage devices and related emerging applications, Mater. Horiz. 4 (2017) 522-545, https://doi.org/10.1039/C6MH00500D.

[135] B. Wu, Y. Guo, C. Hou, Q. Zhang, Y. Li, H. Wang, High-performance flexible thermoelectric devices based on all-inorganic hybrid films for harvesting low-grade heat, Adv. Funct. Mater. 29 (25) (2019) https://doi.org/10.1002/adfm.201900304.

[136] X. Xu. Y. Zuo, S. Cai, X. Tao, Z. Zhang, X. Zhou, S. He, X. Fang, H. Peng, Three-dimensional helical inorganic thermoelectric generators and photodetectors for stretchable and wearable electronic devices, J. Mater. Chem. C 6 (18) (2018) 4866-4872, https://doi.org/10.1039/C8TC01183D.

[137] J. Choi, Y. Jung, C. Dun, K.T. Park, M.P. Gordon, K. Haas, P. Yuan, H. Kim, C.R. Park, J.J. Urban, High-Performance, wearable thermoelectric generator based on a highly aligned carbon nanotube sheet, ACS Appl. Energy Mater. 3 (1) (2020) 1199-1206, https://doi.org/10.1021/acsaem.9b02255.

[138] J. Na, Y. Kim, T. Park, C. Park, E. Kim, Preparation of bismuth telluride films with high thermoelectric power factor, ACS Appl. Mater. Interfaces 8 (47) (2016) 32392-32400, https://doi.org/10.1021/acsami.6b10188.

[139] Y. Du, K.F. Cai, S.Z. Shen, R. Donelsonand, J.Y. Xu, H.X. Wang, T. Lin, Multifold enhancement of the output power of flexible thermoelectric generators made from cotton fabrics coated with conducting polymer, RSC Adv. 7 (69) (2017) 43737-43742, https://doi.org/10.1039/c7ra08663f.

[140] J.A. Lee, A.E. Aliev, J.S. Bykova, M.J. de Andrade, D. Kim, H.J. Sim, X. Lepró, A.A. Zakhidov, J.B. Lee, G.M. Spinks, S. Roth, S.J. Kim, R.H. Baughman, Woven-yarn thermoelectric textiles, Adv. Mater. 28 (25) (2016) 5038-5044, https://doi.org/10.1002/adma.201600709.

[141] J. Zhang, T. Zhang, H. Zhang, Z. Wang, C. Li, Z. Wang, K. Li, X. Huang, M. Chen, Z. Chen, Z. Tian, H. Chen, L.D. Zhao, L. Wei, Single-crystal SnSe thermoelectric fibers via laser-induced directional crystallization: from 1D fibers to multidimensional fabrics, Adv. Mater. 32 (36) (2020) 2002702, https://doi.org/10.1002/adma.202002702.

[142] Q. Wu J. Hu, A novel design for a wearable thermoelectric generator based on 3D fabric structure, Smart Mater. Struct. 26 (4) (2017) 045037, https://doi.org/10.1088/1361-665X/aa5694.

[143] A. Lund, Y. Tian, S. Darabi, C. Müller, A polymer-based textile thermoelectric generator for wearable energy harvesting, J. Power Sources 480 (2020) 228836, https://doi.org/10.1016/j.jpowsour.2020.228836.

[144] S. Qu, Y. Chen, W. Shi, M. Wang, Q. Yao, L. Chen, Cotton-based wearable poly(3-hexylthiophene) electronic device for thermoelectric application with cross-plane temperature gradient, Thin Solid Films 667 (2018) 59-63, https://doi.org/10.1016/j.tsf.2018.09.046.

[145] M. Ito, T. Koizumi, H. Kojima, T. Saito, M. Nakamura, From materials to device design of a thermoelectric fabric for wearable energy harvesters, J. Mater. Chem. A 5 (24) (2017) 12068-12072, https://doi.org/10.1039/c7ta00304h.

[146] Y. Lin, J. Liu, X. Wang, J. Xu, P. Liu, G. Nie, C. Liu, F. Jiang, An integral p-n connected all-graphene fiber boosting wearable thermoelectric energy harvesting, Compos. Commun. 16 (2019) 79-83, https://doi.org/10.1016/j.coco.2019.09.002.

[147] T. Sun, B. Zhou, Q. Zheng, L. Wang, W. Jiang, G.J. Snyder, Stretchable fabric generates electric power from woven thermoelectric fibers, Nat. Commun. 11 (2020) 572, https://doi.org/10.1038/s41467-020-14399-6.

[148] L.K. Allison T.L. Andrew, A Wearable all-fabric thermoelectric generator, Adv. Mater. Technol. 4 (5) (2019) 1800615, https://doi.org/10.1002/admt.201800615.

[149] S.J. Kim, J.H. We, B.J. Cho, A wearable thermoelectric generator fabricated on a glass fabric, Energy

Environ. Sci. 7 (2014) 1959-1965, https://doi.org/10.1039/C4EE00242C.

[150] X. Wang, H. Wang, B. Liu, Carbon nanotube-based organic thermoelectric materials for energy harvesting, Polym. 10 (11) (2018) 1196, https://doi.org/10.3390/polym10111196.

[151] X. Cheng, X. Wang, G. Chen, A convenient and highly tunable way to n-type carbon nanotube thermoelectric composite film using common alkylammonium cationic surfactant, J. Mater. Chem. A 6 (2018) 19030-19037, https://doi.org/10.1039/C8TA07746K.

[152] L. Brownlie J. Shapter, Advances in carbon nanotube n-type doping: Methods, analysis and applications, Carbon, 126 (2018) 257-270, https://doi.org/10.1016/j.carbon.2017.09.107.

[153] X. Lan, T. Wang, C. Liu, P. Liu, J. Xu, X. Liu, Y. Du, F. Jiang, A high performance all-organic thermoelectric fiber generator towards promising wearable electron, Compos. Sci. Technol. 182 (2019) 107767, https://doi.org/10.1016/j.compscitech.2019.107767.

[154] J.D. Ryan, A. Lund, A.I. Hofmann, R. Kroon, R. Sarabia-Riquelme, M.C. Weisenberger, C. Müller, All-organic textile thermoelectrics with carbon-nanotube-coated n-type yarns, ACS Appl. Energy Mater. 1 (6) (2018) 2934-2941, https://doi.org/10.1021/acsaem.8b00617.

[155] H. Hardianto, G. De Mey, B. Malengier, L. Van Langenhove, Textile-based thermoelectric generator fabricated from carbon fibers, J. Ind. Text. (2020), https://doi.org/10.1177/1528083720910686.

[156] G. Chen, W. Xu, D. Zhu, Recent advances in organic polymer thermoelectric composites, J. Mater. Chem. C, 5 (2017) 4350-4360, https://doi.org/10.1039/C6TC05488A.

[157] M.N. Gueye, A. Carella, J. Faure-Vincent, R. Demadrille, J.P. Simonato, Progress in understanding structure and transport properties of PEDOT-based materials: A critical review, Prog. Mater Sci. 108 (2020) 100616, https://doi.org/10.1016/j.pmatsci.2019.100616.

[158] N. Wen. Z. Fan, S. Yang, Y. Zhao, T. Cong, S. Xu, H. Zhang, J. Wang, H. Huang, C. Li, L. Pan, Highly conductive, ultra-flexible and continuously processable PEDOT:PSS fibers with high thermoelectric properties for wearable energy harvesting, Nano Energy 78 (2020) 105361, https://doi.org/10.1016/j.nanoen.2020.105361.

[159] J.Y. Kim, W. Lee, Y.H. Kang, S.Y. Cho, K.S. Jang, Wet-spinning and post-treatment of CNT/PEDOT:PSS composites for use in organic fiber-based thermoelectric generators, Carbon 133 (2018) 293-299, https://doi.org/10.1016/j.carbon.2018.03.041.

[160] H. Jin, J. Li, J. Iocozzia, X. Zeng, P.C. Wei, C. Yang, N. Li, Z. Liu, J.H. He, T. Zhu, J. Wang, Z. Lin, S. Wan, Hybrid Organic-Inorganic Thermoelectric Materials and Devices, Angew. Chem. Int. Ed. 58 (43) (2019) 15206-15226 https://doi.org/10.1002/anie.201901106.

[161] K. Chatterjee T.K. Ghosh, Thermoelectric Materials for Textile Applications, Mol. 26 (11) (2021) 3154, https://doi.org/10.3390/molecules26113154.

[162] H. Xu, Y. Guo, B. Wu, C. Hou, Q. Zhang, Y. Li, H. Wang, highly integrable thermoelectric fiber, ACS Appl. Mater. Interfaces 12 (29) (2020) 33297-33304, https://doi.org/10.1021/acsami.0c09446.

[163] J. Choi, Y. Jung, S.J. Yang, J.Y. Oh, J. Oh, K. Jo, J.G. Son, S.E. Moon, C.R. Park, H. Kim, Flexible and robust thermoelectric generators based on all-carbon nanotube yarn without metal electrodes, ACS Nano 11 (8) (2017) 7608-7614, https://doi.org/10.1021/acsnano.7b01771.

[164] C.L. Lim, Fundamental concepts of human thermoregulation and adaptation to heat: A review in the context of global warming, Int. J. Environ. Res. Public Health 17 (21) (2020) 7795, https://doi.org/10.3390/ijerph17217795.

[165] H. Liu, H. Fu, L. Sun, C. Lee, E.M. Yeatman, Hybrid energy harvesting technology: From materials, structural design, system integration to applications, Renewable Sustainable Energy Rev. 137 (2021) 110473, https://doi.org/10.1016/j.rser.2020.110473.

[166] Y. Wu, S. Kuang, H. Li, H. Wang, R. Yang, Y. Zhai, G. Zhu, Z.L. Wang, Triboelectric-thermoelectric hybrid nanogenerator for harvesting energy from ambient environments, Adv. Mater. Technol. 3 (11) (2018) 1800166, https://doi.org/10.1002/admt.201800166.

[167] X.Q. Wang, C.F. Tan, K.H. Chan, X. Lu, L. Zhu, S.W. Kim, G.W. Ho, In-built thermo-mechanical cooperative feedback mechanism for self-propelled multimodal locomotion and electricity generation, Nat. Commun. 9 (2018) 3438, https://doi.org/10.1038/s41467-018-06011-9.

[168] D.L. Wen, X. Liu, J.F. Bao, G.K. Li, T. Feng, F. Zhang, D. Liu, and X.S. Zhang, Flexible hybrid photo-thermoelectric generator based on single thermoelectric effect for simultaneously harvesting thermal and radiation energies, ACS Appl. Mater. Interfaces 13 (18) (2021) 21401-21410 https://doi.org/10.1021/acsami.1c03622.

[169] T.N. Huu, T.N. Van, O. Takahito, Flexible thermoelectric power generator with Y-type structure using electrochemical deposition process, Appl. Energy 210 (2018) 467-476, https://doi.org/10.1016/j.apenergy.2017.05.005.

[170] T. Sun, J.L. Peavey, M.D. Shelby, S. Ferguson, B.T. O'Connor, Heat shrink formation of a corrugated thin film thermoelectric generator, Energy Convers. Manag. 103 (2015) 674-680, https://doi.org/10.1016/j.enconman.2015.07.016.

[171] J.P. Rojas, D. Conchouso, A. Arevalo, D. Singh, I.G. Foulds, and M.M. Hussain, Paper-based origami flexible and foldable thermoelectric nanogenerator, Nano Energy 31 (2017) 296-301, https://doi.org/10.1016/j.nanoen.2016.11.012.

[172] H. Lv, L. Liang, Y. Zhang, L. Deng, Z. Chen, Z. Liu, H. Wang, G. Chen, A flexible spring-shaped architecture with optimized thermal design for wearable thermoelectric energy harvesting, Nano Energy (2021) 106260, https://doi.org/10.1016/j.nanoen.2021.106260.

[173] A. Patyk, Thermoelectric generators for efficiency improvement of power generation by motor generators-environmental and economic perspectives, Appl. Energy 102 (2013) 1448-1457, https://doi.org/10.1016/j.apenergy.2012.09.007.

[174] Y. Kishita, Y. Ohishi, M. Uwasu, M. Kuroda, H. Takeda, K. Hara, Evaluating the life cycle CO_2 emissions and costs of thermoelectric generators for passenger automobiles: A scenario analysis, J. Cleaner Prod. 126 (2016) 607-619, https://doi.org/10.1016/j.jclepro.2016.02.121.